THE BUCKLING OF CYLINDRICAL SHELLS WITH AN INITIAL IMPERFECTION UNDER AXIAL COMPRESSION LOADING

Thesis by

Charles D. Babcock, Jr.

In Partial Fulfillment of the Requirements

For the Degree of

Doctor of Philosophy

California Institute of Technology

Pasadena, California

1962

ABSTRACT

An experimental and theoretical investigation of the effect of a specific type of initial imperfection on the buckling load of a circular cylindrical shell under axial compression loading was carried out. The imperfection studied was axially symmetric in shape and had the form of a half sine wave in the length direction. Both inward and outward bowing imperfections were considered.

The experiments were carried out with shells fabricated by a copper electroforming process. The shells had no longitudinal seams and had unintended imperfections of the order of the wall thickness. The buckling stress for the intended imperfection studied was only slightly influenced over a considerable range of imperfection amplitudes.

The theoretical solution located the bifurcation points of the prebuckled axially symmetric state. The solution showed that outward bowing shells should have the same buckling stress as a perfect cylindrical shell and inward bowing shells should have a lower buckling stress than the perfect cylinder.

ACKNOWLEDGMENT

The author wishes to express his sincere appreciation to Dr. E. E. Sechler for his guidance of the work carried out in this investigation. The advice and suggestions of other members of the Department of Aeronautics is also appreciated.

Appreciation is expressed for the help received throughout the course of the experimental study from Mr. Carroll Bartsch of the Aeronautics Shop, Mr. Marvin Jessey of the Electronics Laboratory and Mr. Milton Wood of the Structures Laboratory. The help of Mrs. Martha Lamson of the Computing Center in carrying out the data reduction and numerical calculations is gratefully acknowledged. Very much appreciated was the help of Miss Helen Burrus for the typing and of Mrs. Betty Wood for the graphs and figures.

This study was supported by a National Aeronautics and Space Administration Research Grant and this aid is gratefully acknowledged.

TABLE OF CONTENTS

LIST OF TABLES

LIST OF FIGURES

LIST OF FIGURES (contd.)

LIST OF FIGURES (contd.)

LIST OF SYMBOLS

a_o	Amplitude of initial imperfection in inches
a_1	$a_o 2\sqrt{3(1-\nu^2)}/t$
A_j	Eigenvector of buckling problem
A_{ij}, B_{ij}	General coefficients of eigenvalue problem
a_{mj}, b_{ij}, c_{ij} d_{mj}, e_{mj}, f_{mj} g_{mj}, h_{mj} k_{mj+1}, k_{mj-1}	Constants defined on page 44
b_k	Constants in prebuckled solution
C_1, C_2, C_3, C_4	Constants defined on page 42
D	$Et^3/12(1-\nu^2)$
E	Young's modulus
F, F^*, $\bar{F}$	Stress function
L	Length of shell
m, $\bar{m}$	Circumferential wave number
N_x, N_y, N_{xy}	Membrane stresses for shallow shell equations
N_1, N_2	Membrane stresses for membrane equations
n	Axial wave number
R	Base Radius of shells
R_1, R_2	Principal radii of curvature of shell surface
t	Shell thickness
U	"Unevenness factor" of Donnell's theory

$u, \bar{u}$	Axial deflection of shell
$v, \bar{v}$	Circumferential deflection of shell
$w, w^*, \bar{w}$	Radial deflection of shell
w_o	Initial distance of shell from flat plate
x	Axial coordinate
y	Circumferential coordinate
$\Gamma_1, \Gamma_2, \Gamma_3, \Gamma_4$	Constants defined on page 42
δ_{ij}	Kronecker delta
$\xi, \bar{\xi}$	x variation of radial deflection
$\eta, \bar{\eta}$	x variation of stress function
θ	Angle between axis of shell and surface normal
λ	$-\frac{\sigma_o R}{Et} 2 \quad 3(1-\nu^2)$
ν	Poisson's ratio
ξ	$\pi x/L$
σ_o	Applied axial stress
∇^4	$(\frac{\partial^2}{\partial x^2} + \frac{\partial^2}{\partial y^2})^2$

I. INTRODUCTION

Problems of structural stability have been with the aeronautical engineer ever since the first flights. The Wright brothers, who accomplished the first successful human flight in a powered heavier-than-air machine, were concerned with this problem. In an entry in his diary of November 16, 1903, Orville Wright wrote:

> "We hung the machine on tips to test strength. The cloth wrinkled badly, necessitating a change in the trussing of the tips so that the strain be more evenly carried by front and rear spars and uprights. This requires a change in the controlling wires which will have to be operated at the rear. The uprights stood test of twice what will be required of them even though the wire connecting their centers had not been put in place."

Fortunately, for the Wright brothers and other early pioneers in aviation, the practical engineers of the day had a fairly good working knowledge of the strength and stability of columns as a result of investigations in other fields. But as the aircraft became more complicated and monocoque construction was introduced, the aeronautical engineer found that he had to build up his own body of working knowledge in regard to stability problems.

During this period of activity of the aeronautical engineer in stability investigations, shell problems received a great deal of attention. Outside of a few exceptions, the shell stability problems investigated were directed toward furnishing the designer with the information he needed to design airplanes. While this task was performed adequately, little heed was paid to carrying out experimental studies that could further increase the basic understanding of the problems.

The designer again required additional information concerning the stability of shells when he began to be concerned with missile and spacecraft. The previous work done for aircraft was not of sufficient accuracy or it was concerned with the wrong range of parameters. As shell stability problems again became actively investigated, more heed was paid to trying to understand the phenomenon. This has led us to an understanding of certain types of stability problems, but in some cases a complete understanding is far from attainment.

Of all the shell stability problems that have been the subject of intensive investigation, the one that seems the farthest from resolution is the case of a circular cylindrical shell under axial compression loading. It would seem that this case of simple geometry and loading would not be too complicated. However, at this time not a single explanation of the phenomenon can be put forth that is not open to debate and indeed is more than an untested hypothesis.

This is indeed a strange situation since this stability problem has probably been the subject of more investigation than any other facet of shell instability. Yet, the experimental and theoretical results are still widely varying, as will be shown in the following pages.

1. Historical Development

This section will attempt to give a summary of the progress made in the study of the stability of a thin cylindrical shell under axial compression loading. A great deal will be omitted for lack of space, but in some instances details will be included to help clarify the ideas.

Let us begin by developing what is called the classical buckling load for this shell and loading. First, we require a set of linearized differential equations governing the shell behavior. As in stability problems of this type, the equilibrium equations are written in the deformed state so that products of the constant membrane stresses (arising from the loading) and the deflections appear in the equations. The equations are, in general, referred to the shell after the axial load has been applied. Therefore, the boundary conditions become homogeneous. It should also be mentioned that the restraint of the ends due to any loading device or end plate is neglected during this loading so that the shell still has a circular cylindrical shape of slightly larger radius after the loading. The classical buckling load is then found by asking for the minimum eigenvalue (axial load) of this system of equations. It has been shown that if the shell is reasonably long ($L/R > 1$), but not so long that it can buckle as a strut, the minimum eigenvalue is given by:

$$\sigma_{C\ell} = \frac{1}{\sqrt{3(1-\nu^2)}} \frac{Et}{R}$$

This eigenvalue is the smallest value of the axial loading for which a non-trival solution of the governing differential equations exists.

A comparison of the experimental buckling stress, as given by several investigators, to that of the classical value is shown in Figure 1 (Ref. 2) as a function of R/t ratio. It is seen that the comparison is extremely poor especially toward the higher R/t values. The scatter in data is also quite large.

The question then arises as to why this discrepancy occurs and is so pronounced for axial compression loading. In general, it can be said that the analytical explanations of this behavior have progressed much farther than any experimental studies. This is largely due to the fact that a comprehensive experimental program is extremely difficult and expensive to carry out.

The way for further analytical progress was largely paved by Donnell in 1934 (Ref. 3) with the introduction of a simplified set of nonlinear differential equations. These equations are similar to the von Kármán large deflection plate equations, in that they use for dependent variables the stress function and the deflection in the radial direction.

Utilizing these equations of Donnell, von Kármán and Tsien made a very significant contribution in 1941 (Ref. 4). They were able to show that, for a cylinder under axial load, the equilibrium positions in the post-buckling state exhibit a very marked difference from other types of buckling. They showed that equilibrium positions existed at values as low as one-third of the classical buckling load. Figure 2 shows this phenomena as given by a later improvement of von Kármán and Tsien's work carried out by Kempner (Ref. 5). It should be mentioned that in von Kármán and Tsien's solution and similar solutions obtained after the original work, an energy method is used to obtain the load deflection curve shown in Figure 2.

Seeing this phenomenon, one is immediately led to saying that perhaps the classical criterion of infinitesimal disturbances is not sufficient in this case, since for loads much less than the classical load

there are equilibrium positions in the post-buckled state. This leads to the idea of a jump phenomenon in which the shell is subjected to a finite disturbance, as is true in the laboratory and field, which causes the shell to jump from the unbuckled state to the post-buckled state at some load less than the classical load. Up to this date this idea has not been expounded to any great extent. This is largely due to the difficulties of handling nonlinear differential equations. However, one exception should be noted.

In 1942 Tsien (Refs. 6 and 7), in an effort to explain the low values of buckling loads of spheres under external pressure and cylinders under axial compression, introduced what is now called the energy criterion of buckling. This states, in effect, that when the potential energy of the loaded structure in the unbuckled state first reaches the value of the potential energy of the structure in the buckled state for the same value of the loading parameter (load or deflection), the structure will jump from the unbuckled state to the buckled state, as the result of finite disturbances which are always present under laboratory and field conditions.

Perhaps this can be explained more clearly by a simple model introduced by M. Stein (Ref. 8). In his work Stein considers a column made up of three rigid links of equal length connected by linear springs with the middle link supported by 3 cubic hard springs. There exist 3 equilibrium configurations, other than straight, of this column as shown in Figure 3. The load deflection curve is shown in Figure 4. Considering the column loaded by an elastic spring of spring constant S, the potential energy can be easily calculated as a function of δ,

the displacement of the spring. This is shown in Figure 5 where the solid lines refer to the stable branches and the dotted lines to unstable ones.

The classical criterion of buckling states that the column will buckle from the symmetric mode to the antisymmetric mode when δ reaches δ_{Cl} indicated by the point A. It is easily seen from this plot that Tsien's energy criterion states that the column will buckle when δ reaches δ_{EC} indicated by point B. It is interesting to note that the energy barrier separating the two states is given by the ΔE shown in the figure. This is the difference between the potential energy of the unstable transitional mode and stable symmetric mode.

This energy criterion was rejected by most people since it lacked any theoretical basis and was substantiated only by buckling experiments made with columns with a nonlinear lateral support. This author believes that this criterion is not well founded in that it completely neglects the magnitude and method of application to the structure of the finite disturbance which takes the structure from the unbuckled state to the buckled one.

Tsien later saw that there was some inconsistency in his criterion in that it set a very arbitrary amplitude of disturbance that could cause the structure to buckle. He revised his criterion in a little referred to paper (Ref. 9) so as to remove this inconsistency. He states that the structure will buckle when the loading parameter first reaches the value where another buckled stable equilibrium state exists with the same value of the loading parameter. Referring again to the column model, this value is seen to be δ^*_{EC} indicated by point C.

Again this does not say anything about the amplitude of the disturbance, but it removes the arbitrariness of the original energy criterion. The energy barrier in this case is given by ΔE^*.

Another line of approach has been developed more fully. This is the consideration of the fact that any shell that is tested in the laboratory or used in the field is imperfect in its geometrical form to a greater or lesser degree. Therefore, when one determines the maximum load-carrying capacity, this initial imperfection must be taken into account.

The first attempts to do this were based on the linearized equations from which the classical buckling load was obtained. This was done by considering the initial imperfection to consist of a deviation in the radial direction and adding the appropriate term to the differential equations, thereby making them inhomogeneous. The solution of this problem shows that the deflection of the shell goes to infinity as the axial load approaches the eigenvalue of the homogeneous problem whose eigenfunction is of the same form as the initial imperfection in the radial direction. Therefore, if the shell remains elastic, the initial imperfection considered in this manner does not lower the maximum load-carrying capacity of the shell.

In 1934, Donnell (Ref. 3) considered the effect of initial imperfections, using the nonlinear equations which he had developed. In this work he assumed that the deflection of the shell in the radial direction and the initial imperfection maintain the same spacial dependence during the loading. He assumed a form of the radial deflection, solved a compatibility equation for the in-plane stresses and utilized an energy

theorem to approximate a solution of the radial equilibrium equation. The criterion of instability that was used was that a certain point of the shell surface enters into the yielding region of the material. Due to the complexity of the problem, the parameters in the assumed form of the radial deflection were held to a minimum.

In 1951 Donnell and Wan (Ref. 2) made a very significant improvement on Donnell's initial attempt to show the effect of initial imperfections. In this work the same assumption on the spacial dependence of the initial imperfection was retained. The major improvements were in the form of the radial deflection utilized and, in this case, the possibility of elastic buckling was included.

The form of the radial deflection assumed was the same as von Kármán and Tsien used in their paper on the post-buckled states of a shell under axial compression. The solution was obtained in the same manner as in the earlier work of Donnell. The number of constants to be determined by the energy theorem was five.

The buckling point determined in this work is a function of an "unevenness factor" U which is related to the initial imperfection in the following manner:

$$U = A_o \left(\frac{t}{R}\right)^2 n^{1.5} m^2$$

where A_o is the amplitude of the initial imperfection and n and m are the axial and circumferential wave numbers respectively. The effect of this imperfection on the equilibrium positions of the shell is shown in Figure 6.

Buckling as a result of yielding of the material can also be taken into account in the same manner as in Donnell's original paper. The comparison of this theory with some experimental results is shown in Figure 7. It is seen that, in general, the comparison is favorable. However, it must be remembered that the theory of initial imperfections as developed so far is unable to predict the buckling load for a specific type of initial imperfection as measured from experiments. However it has been felt to be very significant in that it shows the great sensitivity of a cylindrical shell subjected to axial compression to initial imperfections.

So we see that there are essentially two different schools of thought on the problem. The first one states that the great discrepancy between the experimental values of the buckling load and the classical load is due mostly to the fact that the classical criterion of buckling is not the proper criterion to be applied. What must be considered is the shell subjected to finite disturbances so that it can "jump" from the unbuckled state to the buckled state. Tsien's energy criterion is an outgrowth of this idea. To show that this is the correct answer by an analytical study one must study the nonlinear dynamical equations of a shell subjected to external forces. The problems inherent in an experimental program are likewise formidable.

The second line of reasoning on this problem is directed to the idea that the reason for the discrepancy between theory and experiment is that the cylinders tested are not the perfect shells that the theory assumes. The spirit of this school of thought is that very small initial deviations of the proper kind can cause large reductions in the maximum

load carrying capacity of the shell. To develop this theory from an analytical point of view, one can study the static nonlinear equations for a shell with a specific type of initial imperfection. This is a difficult task in most cases. The experimental approach would be to test shells with a known amount of initial imperfection.

2. Forward

The work that will be described in the main part of this thesis is an attempt to determine the effect of a specific type of initial imperfection on the buckling load of a circular cylindrical shell under axial compression loading. To determine this experimentally, a great deal of care must be exercised in order not to hide the results in the experimental inaccuracies. This immediately dictates that the test specimens must be within very close tolerances of the shape desired and requires the elimination of the seam common on most test specimens. It was decided that this could most easily be done by manufacturing the test shells by electroforming. In this manner a seamless cylinder can be produced that is essentially stress free and which has any form for which a mandrel can be produced.

The method of testing must also be such that repeated results can be obtained with identical test specimens. It was decided that a testing machine that controlled end displacement met this demand. In addition the load distribution must be monitored during the loading to assure that the load distribution is uniform. This must be done in such a manner that the shell is not disturbed.

Next a type of initial imperfection must be chosen. As stated earlier it must be such that a mandrel of this shape can be accurately produced. In this work a very simple type of imperfection is considered, consisting of an axial symmetric imperfection which has the shape of a half sine wave in the length direction. Both inward and outward deviations from a perfect cylindrical shape are considered. A few imperfections which are an arc of a circle are also considered.

II. EXPERIMENT

The experimental part of this work consists of the fabrication of the test specimens, measurement of the initial imperfection and carrying out the buckling tests.

1. Fabrication of the Test Specimens

The shells that were used for this testing program were fabricated by an electroforming process. In this manner a very uniform thickness shell without the complication of a seam can be obtained. In the following section the process will be described in detail.

Since it was necessary to fabricate shells of other than cylindrical shape, the form that was to be used had to be non-permanent in order to remove the finished shell. It was decided that a wax form would meet all the requirements. The wax used was a two to one mixture of refined paraffin and Mobile Cerese wax 2305. This wax was used since it had been shown (Ref. 10) to have the proper machining characteristics and could be cast free of air bubbles. A three-fourths inch layer of wax was first cast on a seven inch diameter water-cooled mandrel. After the wax had hardened it was machined to the shape of shell desired. Figure 8 shows the mandrel and a finished wax form. The plate at the top of the mandrel was used to carry the electrical current to the surface of the wax form.

As stated earlier, all the shells tested in this study were shells of revolution. A mandrel of this shape was obtained using a standard

lathe on which the in-and-out motion of the carriage was controlled while traversing the length of the mandrel. This was accomplished by utilizing the taper attachment and a follower. A ten-inch template was cut to the desired shape of the shell generator and attached rigidly to the taper attachment mounts. A ball bearing was attached to the tongue of the carriage and held against the template by weights. Enough weight was used so that the carriage followed the template quite accurately. Figure 9 shows the lathe set-up with a mandrel in place.

After the desired form was obtained, the wax was spray painted with a silver paint thinned with toluene. The electrical resistance of the paint was measured so as to assure that the paint was thick enough and was uniform over the mandrel. The paint must cover the current carrying plate at the top of the mandrel.

The plating was carried out in a Copper Fluoborate bath. A circular rolled copper anode 15 inches in diameter was used which extended in the bath to the bottom of the mandrel. Copper was chosen for several reasons. It has been found that of all the materials suited for this type of experimental work, copper has the lowest internal stresses developed during the plating process (Ref. 11). Other more desirable materials from a testing standpoint sometimes develop quite high internal stresses and are more difficult to electroform. Because of the limited experience with electroforming and simplicity of the copper process, copper was chosen as the plating material. Control consisted of a pH measurement with standard calorimetric paper to control the acid content and a density measurement to control the

copper concentration. During the plating, the bath was agitated both by the moving cathode and by forced air. The anode was bagged with a Dynel fabric to collect the anode sludge that would otherwise accumulate in the tank. Batch filtration was used after each cylinder was plated. The bath was also treated occasionally with activated charcoal to remove organic impurities that can cause a rough brittle plate if not removed. A standard transformer-rectifier and powerstat was used to give a uniformly varied current up to 130 amps. At full power the current density was about 55 amps per square foot. The plating time was approximately 20 minutes per 0.001 inches of plate. The plating was carried out at room temperature.

The mandrel was rotated during the plating so as to assure uniformity of thickness of the finished shell. Figure 10 shows the plating installation.

After the plating was completed, the mandrel was rinsed thoroughly and the shell then cut to the desired length while it was still on the mandrel. The shell was then removed from the mandrel by melting out the wax. Care had to be exercised so as not to damage the shell since the wax underwent a large expansion when it was heated to the melting point. This could cause a warping of the shell if it became trapped under the surface. The removal was accomplished by pouring hot wax over the shell so as to melt a thin layer of wax directly under the surface. Then the mandrel was immersed in a bath of hot wax. The excess wax and silver paint was removed from the shell with benzene. Figure 11 shows a completed test shell.

a. Wall Thickness

The plated shell was about three inches longer than the desired shell length. To assure uniformity of thickness, the finished shell was cut from the middle of the plated shell. This was done since the plate tended to build up to a greater thickness at the ends of the mandrel. It was found that this influence of the ends only extended about one inch from the ends of the mandrel therefore, by utilizing only the middle section of the shell, quite uniform thickness could be obtained.

The average thickness of the shell was determined before the buckling test by weighing the shell. The variation of thickness was determined after the buckling test by punching out discs from the shell and determining the weight of the discs. It was found that if a micrometer was used to measure the thickness, errors resulted since the outside surface of the shells was somewhat rough. The specific gravity used in the calculation of thickness was 8.9. The thickness of the shells was found to be quite uniform, the error being less than $\pm$ 3 per cent. Table I shows some typical measurements of thickness distribution.

b. Material Properties

The plated copper was somewhat soft in nature. This was undesirable from the buckling part of the experiment, but the advantages of copper stated in the preceding paragraphs were paramount in the decision to use copper. Another factor to be considered was that in the buckling of the shell, the post-buckled state was not of interest in this study and the stresses at the initiation of buckling were quite low.

Tests to determine the characteristics of the plated copper were carried out in uniaxial tension. This was done by utilizing long strips of the copper that were soldered into one-eighth inch thick plates that were in turn clamped into the jaws of an Instron testing machine. The strips had length to width ratios greater than 15. The head displacement of the testing machine was used as the measure of strain and the load read from the Instron load cell. A typical stress-strain curve is shown in Figure 12. The results of the tests are shown in Table II. The value of Young's modulus used in this work was 13.0×10^6 lb/in^2.

A determination of Poisson's ratio was not attempted since its influence in the reduction of the buckling data is of secondary importance. A value of 0.30 was used for this purpose.

2. Test Procedure

The buckling tests were carried out in the controlled displacement testing machine shown in Figure 13. This machine was designed to be rigid in comparison with the test specimen and capable of subjecting the test cylinder to very small increments of end displacement. The relative displacement of the two end plates of the testing machine was controlled by three screws. One complete turn of the screws gave a displacement of 0.025 inches. The screws could be operated independently to give the proper load distribution on the shell and then simultaneously to increase the load to the buckling point. The springs shown in the figure were used to preload the testing machine when mounting the test specimen in the machine and securing it to the

end plate of the testing machine. The testing was carried out when the machine was in the position shown in Figure 13. The end plate with the gear drive rested on pins and the opposite end rested on a set of rollers. Figure 14 shows the details of the displacement controlling screws.

The load distribution was monitored and total load was obtained on the load measuring cylinder shown in Figures 15 and 16. This consisted of a seamless brass cylinder which was 0.0107 inches thick, 2.5 inches long and 8.000 inches in diameter. Twenty-four foil-type strain gauges were mounted on the cylinder equally spaced around the circumference. The ones on the inside were directly opposite to those on the outside. The ring which acted as a mount for the test specimen was designed such that it was resistant to inplane motion but more flexible in out-of-plane motion. This was done so that the load would be reliably transmitted through the ring to the load measuring cylinder. This cylinder was secured to the end plate of the testing machine with a thin layer of Devcon. Devcon is a plastic-like material in a putty state which hardens in several hours after the addition of a hardening agent.

In order to see if the strain being measured in the load measuring cylinder corresponded to the strain in the test shell, the following test was carried out. A test cylinder was instrumented with strain gauges that were located at every other circumferential position as those on the load measuring cylinder. The test shell was mounted in the load measuring cylinder and both sets of gauges read as the shell was eccentrically loaded. Two typical readings showing the correspondence of the measured strains are shown in Figure 17.

When carrying out the buckling tests the gauges on the inside were connected in series with the ones directly opposite on the outside. This gave the compression in the load measuring cylinder directly. It was found that the bending strain occurring in the load measuring cylinder amounted to only one or two per cent of the compressional strain. Each set of gauges was connected into a Wheatstone bridge which has an initial balance. The output of the bridge was amplified by a factor of 5 using a Leeds and Northrup amplifier whose output was monitored on a Leeds and Northrup potentiometer.

The test cylinder was cast with a low melting temperature alloy into an end ring and the other end was secured to the load measuring cylinder in the same manner. After this operation was completed the the shell was measured to determine the initial imperfection.

a. Initial Imperfection Measurements

In this series of tests the initial imperfection that was measured was the deviation of the generators of the shell from a straight line. This measurement was carried out at nine stations around the circumference. The measurements were made with a reluctance type pick up consisting of an iron core coil through which passed a 100,000 cps signal. The impedance of the coil to this signal changed as the electromagnetic field of the coil was disturbed by the eddy currents generated in an external conducting surface. By determining the change in impedance of the coil the position of the external surface could be measured quite accurately. The signal was read on a standard dc voltmeter. The output of the pickup was about 25 volts per inch with a working range of approximately 0.200 inches. The noise level and

drift were such that deflection of 10^{-4} inches could be accurately read without ever making contact with the measured surface.

The measurements were carried out by mounting the sensing head of the pickup in a slide which traveled on a guide. The guide was carefully lapped to insure that it was as straight as possible. Figure 18 shows the pickup and guide. The guide was attached to the end rings of the shell to be measured and readings were taken at 32 stations along the generator. Figure 19 shows the initial imperfection measuring equipment in position on a cylinder.

b. Buckling Procedure

After the initial imperfections were measured, the end ring was then secured to the end plate of the testing machine with a thin layer of Devcon. After hardening of the Devcon was complete, the cylinder was ready for testing.

The buckling test was carried out in the following manner. The cylinder was initially loaded to about one-third of the expected buckling load, and the circumferential load distribution was made as uniform as possible by adjusting the three screws of the testing machine. The load was then gradually increased in small increments by turning the three screws simultaneously. After each increase the load distribution was adjusted again. This was carried out up to about two-thirds of the expected buckling load. After this point the load distribution was not adjusted so as to prevent buckling occurring during one of the adjustments. The load was increased in small increments and the strain gauges monitored until buckling occurred.

3. Test Results

As stated in the introduction, it was the purpose of the experimental study to investigate the effect of an axially symmetric imperfection on the buckling load under axial compression. Most of the imperfections had the shape of a half sine wave in the length direction. However, a few shells that had an imperfection that was part of a circular arc were also tested. A total of 34 shells were tested. Table III shows the intended imperfection of the shells and Figures 20 through 37 show the measured imperfection of these shells. These figures show the shell generator at nine locations equally spaced around the circumference. It will be noted that some of these figures show pronounced deviations from the intended imperfection. It is believed that these defects were caused during the removal of the shell from the wax mandrel. During this operation, the shell can become deformed since the wax has a much higher coefficient of expansion than the copper. Shells with an initial imperfection greater than 0.050 inches were not measured in detail since the initial imperfection measuring equipment was not designed to measure this large an imperfection. Table III also shows the wall thickness of the shells tested. All shells had a base diameter of 8 inches and a length of 10 inches.

Table III shows that some of the shells had an initial buckling. This initial buckling consisted of the formation of one wave on the surface of the shell. This would cause the load distribution to fall off in the neighborhood of the one wave without appreciably affecting the distribution over the rest of the circumference of the shell. After the initial buckling, the load was increased until general collapse occurred without attempting

to alter the load distribution. General collapse occurred in the same manner as for the shells that did not have an initial buckling.

General collapse consisted of a snap-through as characteristic of this type of testing. In all but a few cases the post-buckled state consisted of 2 to 3 rows of buckles that extended completely around the circumference. The number of circumferential waves is noted in Table III. All of the shells that had an initial imperfection amplitude greater than 0.010 inches buckled at one end or the other. This buckled state consisted of 2 to 3 rows of buckles that started quite close to one end and extended about one-third of the way up the shell. There did not seem to be a preferred end for this buckling to take place. The other shells with small positive imperfection, negative imperfection, and no intended imperfection buckled over the middle third of the shell. Again this consisted of 2 to 3 rows that extended completely around the circumference.

As stated in the previous section, the load distribution was adjusted to be as uniform as possible with the three testing machine screws. The adjustment was carried out by equalizing the strain in the load measuring cylinder at the 30°, 150° and 270° positions. This adjustment was not attempted after about 75 per cent of the expected buckling load was obtained. Table III gives the maximum variation in load distribution near buckling. The average maximum variation in load distribution for all the shells tested was 18.7 per cent. In most cases the average stress was nearer the maximum stress rather than the minimum. Figures 38 through 42 show typical load distributions as measured on the load measuring cylinder. Several distributions

are given in these figures as the load on the shell was increased. Figures 43 through 48 give the load distribution on the shells at the last reading before buckling. The position of the one wave formation is quite evident from the load distribution of shells X and 0 as given by Figures 39 and 41.

The results of the buckling tests are given in Table III and shown in Figure 49 as a function of initial imperfection amplitude a_o/t. The shells that underwent an initial buckling are so indicated in the figure. However, all the points shown are the general collapse points for the shells.

As Figure 49 shows, all of the shells tested that contained an intended imperfection of small amplitude buckled at a lower value of stress than the shells with no intended imperfection. However, it was noticed that the shells with large positive amplitude of initial imperfection show a definite trend to higher values of buckling stress. To investigate this trend further, two shells with an initial imperfection amplitude a_o/t of approximately 44 were tested. These imperfections were a part of a circular arc. From the results shown in Figure 49 one would be inclined to say that this upward trend with increasing a_o/t stops and the buckling stress approaches some constant value. Of course, this point would have to be further investigated to make a definite statement to this effect.

Figure 49 shows that all of the shells tested have a very high buckling stress as compared to other tests carried out in the past. Figure 1 shows that the maximum values of k obtained in the tests presented in Reference 2 for this range of R/t ratio is about 0.30.

The reason for the high values of buckling stress is not completely understood, however the following items could be influential.

(1) All of the shells tested had no seams. The effect of the seam on the buckling load is an uninvestigated effect. In the tests carried out in the past, it was usually assumed that if the buckling did not appear to initiate at the seam and the seam did not interfere with the post-buckled state then the seam had no effect. The validity of this assumption is not known.

(2) The influence of the testing machine is again an unknown parameter at this time. It has been assumed that this did not make a great deal of difference in most previous buckling tests. Certainly if the classical criterion of stability is believed this factor can not be of importance. Tsien's energy criterion of buckling accounts for this influence of the testing machine while the imperfection theory as developed by Donnell and Wan does not directly consider this effect but attempts to lump it into the "unevenness factor". The only experimental work that the author could find on this subject as applied to the testing of shells was carried out by N. J. Hoff (Ref. 20). However, the preliminary tests carried out in Hoff's work were inconclusive. The testing machine used in the tests presented here is nonlinear largely due to the ball bearings used in the screw assembly. The spring constant of the testing machine in the range of buckling loads is about 400,000 lb/in.

(3) The influence of load distribution is likewise an unknown factor. Very little data has been published on this aspect of buckling tests. The data that has been published by Ponsford (Ref. 21) and by Lo, Crate, and Schwarts (Ref. 22) show about the same order of magnitude of variation in load distribution as reported in the author's tests.

(4) Finally, there is the effect of the initial imperfections. A study of the data given here shows that the shells had an unintended initial imperfection of about the order of magnitude of the thickness. Not much can be said how this compares with the initial imperfection of other shells tested in axial compression due to the lack of this type of data. In shells tested by Goree and Nash (Ref. 23) that had longitudinal seams, the maximum imperfection varied from about 1/2 the wall thickness to 3 times the wall thickness.

III. THEORY

In an effort to determine the effect of the axial symmetric imperfection which has the shape of a half sine wave in the length direction, a theoretical solution of the buckling problem was carried out. The method of solution is as follows:

1. Determine the stresses and deflections in the shell that occur before buckling during the loading.

2. Consider the stresses and deflections occurring during the buckling as small perturbations about the solution of step 1 and linearize the equations.

3. Solve the eigenvalue problem obtained in 2 and determine the smallest eigenvalue.

1. Development of the Equations

The equations that will be used for the solution of this problem are the shallow shell equations of Marguerre (Ref. 12). While these equations might not be as accurate as one might desire, the complication inherent in more exact equations prohibits any simple solution. However, it should be mentioned that as the number of circumferential waves on the shell surface increases, the accuracy of the shallow shell equations increases.

Utilizing the coordinate system shown in Figure 50, the shallow shell equations of Marguarre are:

$$\nabla^4 F = Et \left[w_{xy}^2 - w_{xx} w_{yy} + 2w_{oxy} w_{xy} - w_{oxx} w_{yy} - w_{xx} w_{oyy} \right] \qquad (1a)$$

$$D\nabla^4 w = F_{yy}(w_{xx} + w_{oxx}) - 2F_{xy}(w_{xy} + w_{oxy}) + F_{xx}(w_{yy} + w_{oyy}) \qquad (1b)$$

where w_o is the initial deviation from the flat plate and F is the stress function defined as:

$$\frac{\partial^2 F}{\partial x^2} = N_y, \qquad \frac{\partial^2 F}{\partial y^2} = N_x, \qquad \frac{\partial^2 F}{\partial x \partial y} = -N_{xy}, \qquad (2)$$

and

$$w_{xx} = \frac{\partial^2 w}{\partial x^2}, \qquad F_{xx} = \frac{\partial^2 F}{\partial x^2} \quad \text{etc.}$$

Equation 1a is a compatibility relation and equation 1b is the equilibrium equation in the direction perpendicular to the xy plane.

For a circular cylindrical shell:

$$w_o = \frac{1}{2R} (y^2 - y_o^2). \qquad (3)$$

If this is substituted into equations 1a and 1b, the following set of equations is obtained:

$$\nabla^4 F = Et\left[w_{xy}^2 - w_{xx}w_{yy} - \frac{1}{R}w_{xx}\right] \tag{4}$$

$$D\nabla^4 w = F_{yy}w_{xx} - 2F_{xy}w_{xy} + F_{xx}w_{yy} + \frac{1}{R}F_{xx}.$$

This set of equations is the one which was originally derived by Donnell and utilized in his study of initial imperfections and by von Kármán and Tsien and other authors in the examination of the cylindrical shell in the post-buckled state.

In the case of interest here as shown in Figure 51:

$$w_o = \frac{1}{2R}(y^2 - y_o^2) - a_o \sin\frac{\pi x}{L}. \tag{5}$$

Substituting w_o into equations 1a and 1b, the following set of equations is obtained:

$$\nabla^4 F = Et\left[w_{xy}^2 - w_{xx}w_{yy} - a_o\left(\frac{\pi}{L}\right)^2 \sin\frac{\pi x}{L} w_{yy} - \frac{1}{R}w_{xx}\right], \tag{6}$$

$$D\nabla^4 w = F_{yy}\left(w_{xx} + a_o\left(\frac{\pi}{L}\right)^2 \sin\frac{\pi x}{L}\right) - 2F_{xy}w_{xy} + F_{xx}w_{yy} + \frac{1}{R}F_{xx}.$$

Let F^*, and w^* be the solutions of the axial symmetric problem before the buckling occurs. Let $\overline{F}$ and $\overline{w}$ be the perturbation stress function and radial deflection occurring during the buckling. Then

$$F = F^* + \overline{F} \qquad w = w^* + \overline{w}. \tag{7}$$

Substituting this into equation 6 and remembering that the * state is axially symmetric, one obtains:

$$\underline{\nabla^4 F^* + \frac{Et}{R} w^*_{xx}} + \nabla^4 \bar{F} + Et \left[\bar{w}_{yy}\left(w^*_{xx} + a_o \left(\frac{\pi}{L}\right)^2 \sin \frac{\pi x}{L}\right) + \right.$$

$$\left. + \frac{1}{R} \bar{w}_{xx} \right] + Et \left[\bar{w}_{xx}\bar{w}_{yy} - \bar{w}_{xy}^2 \right] = 0,$$

$$\underline{D \frac{d^4 w^*}{dx^4} - F^*_{yy}\left(w^*_{xx} + a_o \left(\frac{\pi}{L}\right)^2 \sin \frac{\pi x}{L}\right) - F^*_{xx} \frac{1}{R}} + D\nabla^4 \bar{w} + \qquad (8)$$

$$- \bar{F}_{yy}\left(w^*_{xx} + a_o \left(\frac{\pi}{L}\right)^2 \sin \frac{\pi x}{L}\right) - F^*_{yy} \bar{w}_{xx} - \bar{F}_{xx} \frac{1}{R} - F^*_{xx}\bar{w}_{yy} +$$

$$+ \left[- \bar{F}_{yy}\bar{w}_{xx} + 2\bar{F}_{xy}\bar{w}_{xy} - \bar{F}_{xx}\bar{w}_{yy} \right] = 0.$$

Since F^* and w^* are the solutions for the pre-buckled state, the terms that are underlined are equal to zero. Also, since we are only interested in the bifurcation points of the solutions, the perturbations may be considered arbitrarily small and all nonlinear terms in $\bar{F}$ and $\bar{w}$ can be dropped. This leaves us with the following set of equations:

$$\nabla^4 \bar{F} = Et \left[- \bar{w}_{yy}\left(w^*_{xx} + a_o \left(\frac{\pi}{L}\right)^2 \sin \frac{\pi x}{L}\right) - \frac{1}{R} \bar{w}_{xx} \right]$$

$$\qquad (9)$$

$$D\nabla^4 \bar{w} = \bar{F}_{yy}\left(w^*_{xx} + a_o \left(\frac{\pi}{L}\right)^2 \sin \frac{\pi x}{L}\right) + F^*_{yy} \bar{w}_{xx} + \bar{F}_{xx} \frac{1}{R} + F^*_{xx} \bar{w}_{yy}.$$

It is at once easily seen that the equations given above have a solution of the form:

$$\bar{w} = \bar{\zeta}(x) \sin \frac{\bar{m}y}{R}, \qquad \bar{F} = \bar{\eta}(x) \sin \frac{\bar{m}y}{R}. \tag{10}$$

This solution satisfies the necessary periodic conditions in the circumferential direction when $\bar{m}$ is a whole number. The governing equations then become:

$$\bar{\eta}^{IV} - 2\left(\frac{\bar{m}}{R}\right)^2 \bar{\eta}'' + \left(\frac{\bar{m}}{R}\right)^4 \bar{\eta} = Et\left[\left(\frac{\bar{m}}{R}\right)^2 \bar{\zeta}\left(w^*_{xx} + a_o\left(\frac{\pi}{L}\right)^2 \sin\frac{\pi x}{L}\right) - \frac{1}{R}\bar{\zeta}''\right]$$

$$D\left[\bar{\zeta}^{IV} - 2\left(\frac{\bar{m}}{R}\right)^2 \bar{\zeta}'' + \left(\frac{\bar{m}}{R}\right)^4 \bar{\zeta}\right] = -\bar{\eta}\left(\frac{\bar{m}}{R}\right)^2 \left(w^*_{xx} + a_o\left(\frac{\pi}{L}\right)^2 \sin\frac{\pi x}{L}\right) + \tag{11}$$

$$+ F^*_{yy}\bar{\zeta}'' + \frac{1}{R}\bar{\eta}'' - \left(\frac{\bar{m}}{R}\right)^2 F^*_{xx}\bar{\zeta}$$

where

$$\bar{\zeta}' = \frac{d\bar{\zeta}}{dx}, \qquad \bar{\eta}' = \frac{d\bar{\eta}}{dx}.$$

2. Solution Before Buckling

The axially symmetric solution must satisfy the following set of equations:

$$\nabla^4 F^* + \frac{Et}{R} w^*_{xx} = 0 \tag{12a}$$

$$D \frac{d^4 w^*}{dx^4} - F^*_{yy}(w^*_{xx} + a_o (\frac{\pi}{L})^2 \sin \frac{\pi x}{L}) - \frac{1}{R} F^*_{xx} = 0. \tag{12b}$$

a. Boundary Conditions

It will be assumed that the shell is free to expand radially at the ends during the loading and that the edges of the shell are supported in a pinned manner as the shell expands radially. This expansion is due to the Poisson ratio and is equal to $\frac{\nu R \sigma_o}{E}$, where σ_o is the applied stress.

Therefore, the boundary conditions on w^* are as follows:

$$w^* - \frac{\nu R \sigma_o}{E} = 0, \quad w^*_{xx} = 0 \qquad \text{at} \qquad x = 0, L \tag{13}$$

The boundary conditions on F are given by:

$$F_{yy} = N_x = \sigma_o t \qquad \text{at} \qquad x = 0, L \tag{14}$$

Obviously, these are not enough to completely define the problem, therefore other conditions must come from the symmetry of the problem. For the axially symmetric problem we know that u^* and w^* must be independent of y and that v^* must be identically zero.

b. Solution of the Equations

The problem will be solved in the following manner. Assume that w^* can be represented by the following expansion which satisfies the necessary boundary conditions on w^*:

$$w^* - \frac{\nu R\sigma_o}{E} = \sum_{k=1}^{\infty} b_k \sin \frac{k\pi x}{L}. \tag{15}$$

Substitute this into the equation for F^* and obtain a particular solution:

$$F_p^* = \sum_{k=1}^{\infty} \left(\frac{L}{k\pi}\right)^2 b_k \frac{Et}{R} \sin \frac{k\pi x}{L}. \tag{16}$$

For the homogeneous solution we will take the following in order to satisfy the boundary conditions:

$$F_h^* = \frac{1}{2} \sigma_o t y^2. \tag{17}$$

After the constants b_k are determined, it must be shown that this solution also satisfies the other conditions on u^* and v^*.

Substituting F^* and w^* into equation 12b, one obtains:

$$\left\{ \left[D\left(\frac{\pi}{L}\right)^4 + \sigma_o t\left(\frac{\pi}{L}\right)^2 + \frac{Et}{R^2} \right] b_1 - \sigma_o t\, a_o \left(\frac{\pi}{L}\right)^2 \right\} \sin \frac{\pi x}{L} +$$

$$+ \sum_{k=2}^{\infty} \left[D\left(\frac{k\pi}{L}\right)^4 + \sigma_o t \left(\frac{k\pi}{L}\right)^2 + \frac{Et}{R^2} \right] b_k \sin \frac{k\pi x}{L} = 0. \tag{18}$$

It is easily seen that this equation is satisfied if

$$b_k = 0, \quad k = 2, 3, 4, \ldots; \qquad b_1 = \frac{\sigma_o t\, a_o (\frac{\pi}{L})^2}{D(\frac{\pi}{L})^4 + \sigma_o t(\frac{\pi}{L})^2 + \frac{Et}{R^2}}. \tag{19}$$

Therefore, the solution of the axial symmetric problem is given by:

$$w^* = \frac{\nu R\sigma_o}{E} + \frac{\sigma_o t\, a_o (\frac{\pi}{L})^2}{D(\frac{\pi}{L})^4 + \sigma_o t(\frac{\pi}{L})^2 + \frac{Et}{R^2}} \sin\frac{\pi x}{L}.$$

$$F^* = \frac{1}{2}\sigma_o t\, y^2 + \frac{\sigma_o t\, a_o}{D(\frac{\pi}{L})^4 + \sigma_o t(\frac{\pi}{L})^2 + \frac{Et}{R^2}} \frac{Et}{R} \sin\frac{\pi x}{L}. \tag{20}$$

We must now look at u^* and v^*. Referring to Marguerre we find the strain displacement relations are given by:

$$\epsilon_x^* = \frac{\partial u^*}{\partial x} - \frac{\partial^2 w_o}{\partial x^2} w^* + \frac{1}{2}(\frac{\partial w^*}{\partial x})^2$$

$$\epsilon_y^* = \frac{\partial v^*}{\partial y} - \frac{\partial^2 w_o}{\partial y^2} w^* + \frac{1}{2}(\frac{\partial w^*}{\partial y})^2. \tag{21}$$

Utilizing the stress-strain relations,

$$\epsilon_x^* = \frac{1}{E}\left\{\sigma_x^* - \nu\,\sigma_y^*\right\}, \qquad \epsilon_y^* = \frac{1}{E}\left\{\sigma_y^* - \nu\,\sigma_x^*\right\}, \tag{22}$$

the definition of the stress function, and w_o one finds for u^* and v^*:

$$\frac{\partial u^*}{\partial x} = \frac{1}{Et}\left\{F^*_{yy} - \nu F^*_{xx}\right\} + a_o\left(\frac{\pi}{L}\right)^2 \sin\frac{\pi x}{L} w^* - \frac{1}{2}(w^*_x)^2,$$

$$\frac{\partial v^*}{\partial y} = \frac{1}{Et}\left\{F^*_{xx} - \nu F^*_{yy}\right\} + \frac{1}{R} w^* - \frac{1}{2}(w^*_y)^2. \tag{23}$$

Substituting in the solution for w^* and F^* one obtains:

$$\frac{\partial u^*}{\partial x} = \frac{\sigma_o}{E} + f(x)$$

$$\frac{\partial v^*}{\partial y} = 0 \tag{24}$$

where f is a function of x only. Therefore, we see that the solution for F^* and w^* satisfies the necessary symmetry conditions of the problem.

The quantities that are of interest that occur in the coefficients of the perturbation equations are the following:

$$w^*_{xx} = -\frac{\sigma_o t\, a_o \left(\frac{\pi}{L}\right)^4}{D\left(\frac{\pi}{L}\right)^4 + \sigma_o t\left(\frac{\pi}{L}\right)^2 + \frac{Et}{R^2}} \sin\frac{\pi x}{L},$$

$$F^*_{xx} = -\frac{\sigma_o t\, a_o}{D\left(\frac{\pi}{L}\right)^4 + \sigma_o t\left(\frac{\pi}{L}\right)^2 + \frac{Et}{R^2}} \frac{Et}{R}\left(\frac{\pi}{L}\right)^2 \sin\frac{\pi x}{L}, \tag{25a}$$

$$F^*_{yy} = \sigma_o t.$$

Let us now examine the denominator of b_1 which can be written in the following form:

$$\left(\frac{\pi}{L}\right)^2 \frac{Et^2}{2R\sqrt{3(1-\nu^2)}}\left\{\frac{Rt}{2\sqrt{3(1-\nu^2)}}\left(\frac{\pi}{L}\right)^2 + \frac{\sigma_o 2\sqrt{3(1-\nu^2)}R}{Et} + \frac{2\sqrt{3(1-\nu^2)}}{Rt}\left(\frac{L}{\pi}\right)^2\right\} \quad (26)$$

The middle term is equal to two when σ_o is the classical buckling stress and the first and last terms are reciprocals of each other. The value of the last term, for the shells that were tested in the experimental part of this work, is 1832. Since the σ_o of interest is always of the order of the classical buckling stress the denominator can be approximately rewritten as Et/R^2. Therefore, the quantities of interest can be written as:

$$w^*_{xx} = \frac{\sigma_o}{E} R^2 a_o \left(\frac{\pi}{L}\right)^4 \sin\frac{\pi x}{L},$$

$$F^*_{xx} = -\sigma_o Rt\, a_o \left(\frac{\pi}{L}\right)^2 \sin\frac{\pi x}{L}, \quad (25b)$$

$$F^*_{yy} = \sigma_o t.$$

It is noticed that w^*_{xx} occurs in the coefficient of the perturbation equations always in combination with $a_o(\pi/L)^2 \sin\frac{\pi x}{L}$. Therefore, this coefficient can be written as:

$$a_o \left(\frac{\pi}{L}\right)^2 \sin\frac{\pi x}{L}\left\{1 - \frac{\sigma_o}{E}\left(\frac{R\pi}{L}\right)^2\right\} \quad (27)$$

For the shells of concern here, R is of the order of L and σ_o is much less than E. Therefore, this second term in the brackets can be neglected in comparison with one. This amounts to neglecting the additional curvature of the shell in the x-direction caused by the loading in comparison with the initial curvature of the shell in this direction.

c. Membrane Solution

It would be interesting to compare the results calculated for the stresses in the preceding manner with those calculated from membrane theory. The appropriate equations for a membrane solution are:

$$\frac{N_1}{R_1} + \frac{N_2}{R_2} = 0 \tag{28a}$$

$$\frac{1}{R_1}\frac{dN_1}{d\theta} + \frac{\text{ctn } \theta}{R_2}(N_1 - N_2) = 0 \tag{28b}$$

$$R_1 = -\frac{(1 + r'^2)^{3/2}}{r''}$$

$$R_2 = r\sqrt{1 + r'^2} \tag{28c}$$

$$r = R\left(1 + \frac{a_o}{R}\sin\frac{\pi x}{L}\right), \quad r' = \frac{dr}{dx}$$

where N_1 and N_2 are the longitudinal and circumferential membrane stresses, R_1 and R_2 are the principal radii of curvature of the shell surface and θ is shown in Figure 52. Solving equations 28a for N_2 and substituting this into equation 28b one obtains:

$$\frac{1}{R_1}\frac{dN_1}{d\theta} + \frac{\text{ctn }\theta}{R_2}\left(1 + \frac{R_2}{R_1}\right)N_1 = 0. \tag{29}$$

Let us now make the following change of variables:

$$\frac{d}{d\theta} = \frac{d}{dx}\frac{dx}{d\theta} = -\frac{d}{dx}\frac{(1 + r'^2)}{r''} \tag{30}$$

This leaves us with the following equation for N_1:

$$\frac{dN_1}{d\theta} + \frac{r'}{r}N_1\left(1 + \frac{\frac{a_o}{R}\left(\frac{R\pi}{L}\right)^2 \sin\frac{\pi x}{L}}{1 + \frac{a_o}{R}\sin\frac{\pi x}{L}}\right). \tag{31}$$

In the range of parameters of concern here, the second term in the brackets can be neglected in comparison with one. The equation is then easily integrated and the proper boundary condition applied at $x = 0$. This gives the following results for N_1 and N_2:

$$N_1 = \sigma_o t \frac{1}{\left(1 + \frac{a_o}{R}\right)\sin\frac{\pi x}{L}}$$

$$N_2 = -\sigma_o t\, a_o R\left(\frac{\pi}{L}\right)^2 \sin\frac{\pi x}{L}. \tag{32}$$

Again, if the second term in the denominator of N_1 is neglected in comparison with unity, the results are the same as those obtained in the preceding manner.

3. Solution of the Perturbation Equations

Incorporating the results of the preceding section, the perturbation equations become:

$$\bar{\eta}'''' - 2\left(\frac{\bar{m}}{R}\right)^2\bar{\eta}'' + \left(\frac{\bar{m}}{R}\right)^4\bar{\eta} = Et\left\{\bar{\zeta}\left(\frac{\bar{m}}{R}\right)^2 a_o\left(\frac{\pi}{L}\right)^2 \sin\frac{\pi x}{L} - \frac{1}{R}\bar{\zeta}''\right\} \tag{33}$$

$$D\left\{\bar{\zeta}'''' - 2\left(\frac{\bar{m}}{R}\right)^2\bar{\zeta}'' + \left(\frac{\bar{m}}{R}\right)^4\bar{\zeta}\right\} = +\sigma_o t\bar{\zeta}'' + \frac{1}{R}\bar{\eta}'' + \sigma_o t\left(\frac{\bar{m}}{R}\right)^2\left(\frac{\pi}{L}\right)^2 a_o R\sin\frac{\pi x}{L}\bar{\zeta} +$$

$$- \left(\frac{\bar{m}}{R}\right)^2\left(\frac{\pi}{L}\right)^2 a_o \sin\frac{\pi x}{L}\ \bar{\eta}.$$

a. Boundary Conditions

As stated in the previous section, we have neglected the additional deflection of the shell caused by the loading. This will allow us to use the same strain displacement relations in order to find the relationship between the boundary conditions on the dependent variables $\bar{w}$ and $\bar{F}$ and the boundary conditions on the in-plane displacements $\bar{u}$ and $\bar{v}$. However, in this case we will neglect the quadratic terms involving the radial deflection since we are only interested in the bifurcation points of the solution. Referring to equation 23 we obtain the following:

$$\frac{\partial \bar{u}}{\partial x} = \frac{1}{Et}\left\{\bar{F}_{yy} - \nu \bar{F}_{xx}\right\} + a_o t\left(\frac{\pi}{L}\right)^2 \sin\frac{\pi x}{L}\,\bar{w} \tag{34a}$$

$$\frac{\partial \bar{v}}{\partial y} = \frac{1}{Et}\left\{\bar{F}_{xx} - \nu \bar{F}_{yy}\right\} + \frac{1}{R}\,\bar{w} \tag{34b}$$

After the initial load is applied, the ends of the shell are assumed to be pinned with respect to the radial direction. This implies

$$\bar{w} = \frac{\partial^2 \bar{w}}{\partial x^2} = 0 \qquad \text{at } x = 0, L$$

or since

$$\bar{w} = \bar{\xi} \sin\frac{\bar{m} y}{R} \tag{35}$$

$$\bar{\xi} = \bar{\xi}'' = 0 \qquad \text{at } x = 0, L$$

The boundary conditions that will be applied on $\bar{F}$ are as follows:

$$\bar{F} = \frac{\partial^2 \bar{F}}{\partial x^2} = 0, \qquad \text{at } x = 0, L$$

or since

$$\bar{F} = \bar{\eta} \sin\frac{\bar{m} y}{R} \tag{36}$$

$$\bar{\eta} = \bar{\eta}'' = 0 \qquad \text{at } x = 0, L$$

These conditions on $\bar{F}$ imply that at the ends of the shell the stress in the axial direction and $\bar{v}$ are equal to zero.

This is seen as follows:

$$\bar{N}_x = \bar{F}_{yy} = -\left(\frac{\bar{m}}{R}\right)^2 \sin\frac{\bar{m}y}{R}\bar{\eta} = 0 \qquad \text{at } x = 0, L. \tag{37}$$

To see that these conditions also make $\bar{v}$ equal to zero, we use equation 34b.

$$\bar{v} = \left\{\frac{1}{Et}\left[\bar{\eta}'' + \nu\left(\frac{\bar{m}}{R}\right)^2\bar{\eta}\right] + \frac{1}{R}\bar{\xi}\right\} \int^{y} \sin\frac{\bar{m}y}{R}dy + f(x) \tag{38}$$

The arbitrary function of x can be set equal to zero since it corresponds to a rigid rotation of each cross section. Since $\bar{\eta} = \bar{\eta}'' = \bar{\xi} = 0$ at $x = 0, L$, then also $\bar{v} = 0$ at $x = 0, L$. Equation 34a shows that in general $\bar{u}$ is not equal to zero at $x = 0, L$ but is a periodic function of y.

These boundary conditions are commonly used in shell stability analyses because of their simplicity. They can be looked upon as allowing the ends of the shell to warp freely in the axial direction, constraining the circumferential movement, and giving a pinned support with respect to the radial direction.

b. Solution of the Equations

Now let us introduce the nondimensional quantities as follows:

$$\xi = \bar{\xi}/t, \quad \eta = \bar{\eta}\,\frac{2\sqrt{3(1-\nu^2)}}{Et^3}, \quad \xi = x\frac{\pi}{L}, \quad m = \bar{m}\,\frac{L}{\pi R}$$

$$a_1 = \frac{a_o 2\sqrt{3(1-\nu^2)}}{t}, \; a = \frac{2\sqrt{3(1-\nu^2)}}{Rt}\left(\frac{L}{\pi}\right)^2, \; \lambda = -\frac{\sigma_o R}{Et}2\sqrt{3(1-\nu^2)}. \tag{39}$$

Using these, the differential equations for the perturbations become:

$$\eta'^{V} - 2m^2\,\eta'' + m^4\eta = -a\zeta'' + a_1 m^2 \zeta \sin\xi$$

$$\zeta'^{V} - 2m^2\zeta'' + m^4\zeta = -\lambda a\zeta'' + a\eta'' - \lambda a_1 m^2 \zeta \sin\xi - a_1 m^2 \eta \sin\xi. \tag{40}$$

For a cylindrical shell with no imperfection $a_1 = 0$. The resulting equations are:

$$\eta'^{V} - 2m^2\,\eta'' + m^4\eta = -a\zeta''$$

$$\zeta'^{V} - 2m^2\zeta'' + m^4\zeta = -\lambda a\zeta'' + a\eta''. \tag{41}$$

A solution to these equations which satisfies all the boundary conditions is given by:

$$\eta = A \sin n\xi, \quad \zeta = B \sin n\xi. \tag{42}$$

Substitution into equation 41 yields:

$$\begin{bmatrix} -an^2 & a_{mn} \\ a_{mn} - \lambda a n^2 & an^2 \end{bmatrix} \begin{Bmatrix} A \\ B \end{Bmatrix} = 0, \quad a_{mn} = (m^2 + n^2)^2. \tag{43}$$

For a non-trival solution to exist:

$$\lambda_{mn} = \frac{an^2}{a_{mn}} + \frac{a_{mn}}{an^2}, \qquad A = B\,\frac{a_{mn}}{an^2} \tag{44}$$

where n and m = $m\pi R/L$ must be integers.

$$(\lambda_{mn})_{\text{minimum}} = 2 \quad \text{when} \quad \frac{an^2}{a_{mn}} = 1$$

For a_1 not equal to zero the solution of the equations is somewhat more difficult. For this reason the solution given here will be an approximate one which satisfies the compatibility equation exactly and the equilibrium equation approximately. The procedure is as follows.

1. Assume a suitable form of $\mathcal{S}$ which contains a number of arbitrary constants and satisfies exactly the necessary boundary conditions.
2. Substitute $\mathcal{S}$ into the compatibility equation and solve for η making sure that η satisfies all the necessary boundary conditions.
3. Substitute $\mathcal{S}$ and η obtained in the first two steps in the equilibrium equation and determine the unknown constants in such a manner so as to minimize the error by the Galerkin method.

It is assumed that $\mathcal{S}$ can be represented by the following series which satisfies the necessary boundary conditions:

$$\mathcal{S} = \sum_{j=1}^{n} A_j \sin j\,\xi. \tag{45}$$

Solving the compatibility equation for η gives

$$\eta = \sum_{j=1}^{n} \frac{a_j^2}{a_{mj}} A_j \sin j\xi + \frac{a_1 m^2}{2} \sum_{j=1}^{n} A_j \left\{ \frac{\cos(j-1)\xi}{a_{mj-1}} - \frac{\cos(j+1)\xi}{a_{mj+1}} \right\} \tag{46}$$

$$+ C_1 \sinh m\xi + C_2 \cosh m\xi + C_3 \xi \sinh m\xi + C_4 \xi \cosh m\xi,$$

where C_1 to C_4 must be determined in such a manner that the boundary conditions are satisfied. This gives the following values for C_1 to C_4.

$$C_1 = \frac{1}{2m \sinh^2 m\pi} \left\{ \Gamma_1 \left(2m \cosh m\pi \sinh m\pi + m^2\pi \right) - \Gamma_2 \pi + \right.$$

$$\left. + \Gamma_3 \left(- 2m \sinh m\pi - m^2 \pi \cosh m\pi \right) + \Gamma_4 \pi \cosh m\pi \right\}$$

$$C_2 = - \Gamma_1$$

$$C_3 = \frac{1}{2m} \left\{ m^2 \Gamma_1 - \Gamma_2 \right\}$$

$$C_4 = \frac{1}{2m \sinh m\pi} \left\{ - \Gamma_1 m^2 \cosh m\pi + \Gamma_2 \cosh m\pi + \Gamma_3 m^2 - \Gamma_4 \right\} \tag{47}$$

$$\Gamma_1 = \frac{a_1 m^2}{2} \sum_{j=1}^{n} A_j \left\{ \frac{1}{a_{mj-1}} - \frac{1}{a_{mj+1}} \right\}, \quad \Gamma_2 = - \frac{a_1 m^2}{2} \sum_{j=1}^{n} A_j \left\{ \frac{(j-1)^2}{a_{mj-1}} - \frac{(j+1)^2}{a_{mj+1}} \right\}$$

$$\Gamma_3 = \frac{a_1 m^2}{2} \sum_{j=1}^{n} A_j (-1)^{j-1} \left\{ \frac{1}{a_{mj-1}} - \frac{1}{a_{mj+1}} \right\}, \quad \Gamma_4 = - \frac{a_1 m^2}{2} \sum_{j=1}^{n} A_j (-1)^{j-1} \left\{ \frac{(j-1)^2}{a_{mj-1}} - \frac{(j+1)^2}{a_{mj+1}} \right\}.$$

Next ζ and η are substituted in the equilibrium equation which is written in the following manner:

$$\zeta'^{v} - 2m^2\zeta'' + m^4\zeta + \lambda a\zeta'' - a\eta'' + \lambda a_1 m^2 \zeta \sin\xi + a_1 m^2 \eta \sin\xi = E \qquad (48)$$

E represents the error resulting from the fact that this equation is not identically satisfied. The unknown constants are determined so that this error is equal to zero "in the mean" in the following manner:

$$\int_0^{\pi} E \sin i\xi \, d\xi = 0, \quad i = 1, 2, \ldots n. \qquad (49)$$

The resulting equations for the A_j's then become:

$$\sum_{j=1}^{n} A_j \Bigg\{ \left[a_{mj} + \frac{a^2 j^4}{a_{mj}} - \lambda a j^2 + \frac{a_1^2 m^4}{4} \left(\frac{1}{a_{mj-1}} + \frac{1}{a_{mj+1}} \right) \right] \frac{\pi}{2} \delta_{ij} +$$

$$+ \left[-\frac{1}{4}\lambda a_1 m^2 - \frac{1}{4} a_1 a m^2 \frac{j^2}{a_{mj}} - \frac{1}{4} a_1 a m^2 \frac{(j+1)^2}{a_{mj+1}} \right] \left[\frac{1}{i+j+1} + \frac{1}{i-j-1} \right] \left[1 - (-1)^{i+j+1} \right] +$$

$$+ \left[\frac{1}{4}\lambda a_1 m^2 + \frac{1}{4} a_1 a m^2 \frac{j^2}{a_{mj}} + \frac{1}{4} a_1 a m^2 \frac{(j-1)^2}{a_{mj-1}} \right] \left[\frac{1}{i+j-1} + \frac{1}{i-j+1} \right] \left[1 - (-1)^{i+j+1} \right] +$$

$$- \frac{a_1^2 m^4 \pi}{8} \left[\delta_{i,j-2} \frac{1}{a_{mj-1}} - \delta_{i,2-j} \frac{1}{a_{mj-1}} + \delta_{i,j+2} \frac{1}{a_{mj+1}} \right] + \frac{a a_1 m^2 i}{2} \Bigg[- \left(\frac{(j-1)^2}{a_{mj-1}} + \right.$$

$$\left. - \frac{(j+1)^2}{a_{mj+1}} \right) \frac{1}{\sqrt{a_{mi}}} + \left(\frac{m^2}{a_{mj-1}} - \frac{m^2}{a_{mj+1}} + \frac{(j-1)^2}{a_{mj-1}} - \frac{(j+1)^2}{a_{mj+1}} \right) \frac{m^2}{a_{mi}} \Bigg] \left[1 - (-1)^{i+j+1} \right] + \frac{a_1^2 m^3}{8} \Bigg[- \frac{2m^2}{\sqrt{a_{mi-1}}} \cdot$$

$$\cdot \left(\frac{1}{a_{mj-1}} - \frac{1}{a_{mj+1}} \right) + \frac{(i-1)^2 - m^2}{a_{mi-1}} \left(\frac{m^2}{a_{mj-1}} - \frac{m^2}{a_{mj+1}} + \frac{(j-1)^2}{a_{mj-1}} - \frac{(j+1)^2}{a_{mj+1}} \right) \Bigg] \left[1 - (-1)^{i+j+1} \right]$$

$$- \frac{a_1^2 m^3}{8} \Bigg[- \frac{2m^2}{\sqrt{a_{mi+1}}} \left(\frac{1}{a_{mj-1}} - \frac{1}{a_{mj+1}} \right) + \frac{(i+1)^2 - m^2}{a_{mi+1}} \left(\frac{m^2}{a_{mj-1}} - \frac{m^2}{a_{mj+1}} + \right.$$

$$\left. + \frac{(j-1)^2}{a_{mj-1}} - \frac{(j+1)^2}{a_{mj+1}} \right) \Bigg] \left[1 - (-1)^{i+j+1} \right] \Bigg\}. \qquad (50)$$

This can also be written in the form:

$$\sum_{j=1}^{n} \left\{ \overline{A}_{ij} - \lambda \overline{B}_{ij} \right\} A_j = 0 \qquad i = 1, 2, \ldots n \tag{51}$$

If one looks closely, it is observed that every term of $\overline{A}_{ij}$ and $\overline{B}_{ij}$ is multiplied either by $\left[1 - (-1)^{i+j+1}\right]$ of by δ_{ij}. This means that every term in the $\overline{A}$ and $\overline{B}$ matrices whose sum of indices is odd is equal to zero. One, therefore, further observes that the even and odd problem can be separated, thereby greatly reducing the amount of necessary calculations. Therefore, the buckling problem reduces to finding the minimum eigenvalue of the following problem:

$$\sum_{j=1}^{n} (A_{ij} - \lambda B_{ij}) A_j = 0 \qquad i, j \text{ both even or odd,} \tag{52}$$

where

$$B_{ij} = \delta_{ij} - (b_{ij} - c_{ij}) \frac{a_1 m^2}{a \pi i^2}$$

$$A_{ij} = \left[\frac{a_{mj}}{aj^2} + \frac{aj^2}{a_{mj}} + \frac{a_1 m^4}{4aj^2} f_{mj} \right] \delta_{ij} + \frac{a_1 m^2}{\pi i^2} \left[b_{ij} k_{mj-1} - c_{ij} k_{mj+1} \right] +$$

$$- \frac{a_1^2 m^4}{4a i^2} \left[\delta_{i,j-2} \frac{1}{a_{mj-1}} - \delta_{i,2-j} \frac{1}{a_{mj-1}} + \delta_{i,j+2} \frac{1}{a_{mj+1}} \right] +$$

$$+ \frac{2a_1 m^2}{\pi i} \left[\frac{m^2 g_{mj}}{a_{mi}} - \frac{e_{mj}}{\sqrt{a_{mi}}} \right] + \frac{a_1^2 m^3}{2\pi a i^2} \left[g_{mj} h_{mi} - 2m^2 d_{mj} g_{mi} \right]$$

$$a_{mj} = (m^2 + j^2)^2, \quad b_{ij} = \frac{1}{i+j-1} + \frac{1}{i-j+1}, \quad c_{ij} = \frac{1}{i+j+1} + \frac{1}{i-j-1}$$

$$d_{mj} = \frac{1}{a_{mj-1}} - \frac{1}{a_{mj+1}}, \quad e_{mj} = \frac{(j-1)^2}{a_{mj-1}} - \frac{(j+1)^2}{a_{mj+1}}, \quad f_m = \frac{1}{a_{mj+1}} + \frac{1}{a_{mj-1}}$$

$$g_{mj} = \frac{1}{\sqrt{a_{mj-1}}} - \frac{1}{\sqrt{a_{mj+1}}}, \quad h_{mj} = e_{mj} - m^2 d_{mj}$$

$$k_{mj-1} = \frac{j^2}{a_{mj}} + \frac{(j-1)^2}{a_{mj-1}}, \quad k_{mj+1} = \frac{j^2}{a_{mj}} + \frac{(j+1)^2}{a_{mj+1}}$$

The minimum eigenvalue will be dependent on the number of circumferential waves n as well as the parameters of the problem a_1 and a which are the amplitude of the initial imperfection and the properties of the shell. The solutions of the eigenvalue problem were found by using an IBM 7090 digital computer. The results will be discussed in the following section.

4. Results

In all the calculations carried out the parameter containing the shell dimensions was fixed at the value corresponding to the experimental test cylinders. This value of a was 1832.

Let us first consider the case where the shell is bowed inward. This implies that $a_1 < 0$. The calculations were carried out in such a manner that the number of terms in the approximating function for the radial deflection was arbitrary. This was done so that throughout the calculations the convergence of the solution to the proper eigenvalue could be checked by increasing the number of terms holding all other parameters constant and determining the effect on the minimum eigenvalue. The maximum number of terms used was 20. It should be remembered that this corresponds to 40 terms in the expansion since the even and odd problems have been separated. It was found that for $a_1 < 0$ that the maximum number of terms needed was 10. The difference between this number and 20 terms affected the eigenvalue only in the 6th significant figure.

The computing procedure was to fix the value of the initial deflection parameter and calculate the minimum eigenvalue throughout

the whole range of circumferential wave number m. In all cases the number of approximating terms was adjusted so as to insure the correct minimum eigenvalue. Both the even and odd problems were computed. The results of this calculation for five values of $a_1 < 0$ are shown in Figure 53. The classical value for the perfect shell corresponds to 1. The numbers on the curves correspond to the predominant term in the eigenvector. It should be noted that as the circumferential wave number increases, the predominant term in the eigenvector increases. Another important point is that for a fixed a_1 the local minimums that occur for each predominant term in the eigenvector are always increasing as m increases.

The absolute minimum eigenvalue over the whole range of the circumferential wave number is easily found from these curves as well as the corresponding circumferential wave number. The mode shape of this minimum is seen to be the first mode. This means that the buckling shape for $a_1 < 0$ has the form $\sin \frac{\pi x}{L}$ in the axial direction. The higher modes contribute only about a 2 per cent correction to this pattern. The number of circumferential waves varies from 6 to 8 as a_1 varies from -100 to 0.

Let us now discuss the case where the shell bows outward which means a_1 is greater than zero. The computations were started in the same manner, but it was soon realized that this case was entirely different. It is seen from Figure 53 for the case of $a_1 < 0$, that the decrease of the eigenvalue below the classical value is accomplished by the lowering of the minimums of the curves that correspond to dominant terms of the eigenvector. As expected these minimums increase to

values above the classical value when a_1 becomes greater than zero. As in the previous case, the minimum corresponding to the eigenvector where the first term is dominant is affected the most and increases more than that where the second term is dominant and so forth. This means that as the circumferential wave number increases these minimums approach the classical value of 1 from above and exhibit no absolute minimum. As if this state of affairs were not enough another complication occurs.

In this case where $a_1 > 0$, the eigenvalues corresponding to eigenvectors whose predominant terms are of high axial wave number lie below the eigenvalues corresponding to eigenvectors of low axial wave number. This was not possible in the case $a_1 < 0$ since the local minimums shown in Figure 53 were always increasing with predominant terms in the eigenvectors. The result of this is that for any circumferential wave number an eigenvalue can be found arbitrarily close to the classical value of one, but it is always larger than one. Of course, this may correspond to an unreasonably high axial wave number, but the differential equations by themselves put no upper limit on this. Therefore, the conclusion for the calculations for the case of $a_1 > 0$ must be that the classical value of 1 is a lower bound of the eigenvalues for all values of $a_1 > 0$. The closeness to which one approaches this value is dependent on how hard one looks for the proper eigenvalue. Utilizing 20 terms in the approximating function for the case $a_1 = 20$, the value 1 can be approached to within 0.14 per cent.

The description of the eigenvector does not make too much sense in this case since convergence is not obtained. This is because

increasing the number of approximating terms only allows one to find an eigenvalue closer to 1 which was not found for the smaller problem since it corresponds to an axial wave number not included in the smaller problem.

Figure 54 shows the variation of the buckling stress with initial imperfection amplitude. The numbers on the curve correspond to the number of circumferential waves.

The theoretical solution as developed in the preceding section determines the effect of one specific type of initial imperfection. Any other initial imperfection that may occur is ignored in the solution. The value of the "unevenness factor" as given by Donnell for this specific initial imperfection is equal to zero.

The analysis is different from that of Donnell and Wan in that the imperfection considered does not have the same spacial variation as the final buckled form. Donnell and Wan did not attempt to determine the effect of this type of imperfection. The contention of their analysis is that the initial imperfection that has the form of the final buckling deflection is the most important imperfection in the reduction of the buckling load from the classical result. They do not say that all other imperfections can not cause a reduction in the buckling load. However, if it could be shown that there are imperfections quite different from the final buckling form that are just as influential in the reduction of the buckling load as that which does have this form the analysis of Donnell and Wan would be in doubt.

The theoretical solution given here also contains other assumptions that should be discussed. The effect of the assumptions on the

boundary conditions of the axially symmetric solution is not completely understood at this time. In most cylindrical shell stability analysis the expansion due to Poisson's ratio or to other loading was usually ignored when computing the membrane stress state. This was done on the basis of a solution of the restraint problem given by Flugge (Ref. 1). However, there is some evidence that the restraint caused by the end plates of the shell may be more important than has usually been assumed.

The boundary conditions on the perturbations are also cause for concern. For a shell without imperfections having the dimensions of concern here, it has been shown that the boundary conditions (simple support or clamped) are not important in the calculation of the buckling stress. However, in these solutions the number of waves in the axial direction is usually large. For the solution given here for $a_o < 0$, the buckling mode has a half wave in the axial direction. Therefore, the influence of the boundary conditions may be more important than was anticipated.

IV. CONCLUSION

The comparison between the theory and experiment is shown in Figure 55. For $a_o < 0$ the trend is the same but the reduction in buckling stress given by the theory is much greater than that of the buckling tests. The mode shape given by the theory contains roughly one half the number of circumferential waves observed in the post-buckling state of the shells that were tested. The axial variation is in disagreement in that the theory predicts one long wave from top to bottom while the tests show that in the post-buckled state the waves are roughly of aspect ratio one.

Since the difference between the theory and experiment is so pronounced for the case of $a_o < 0$, the following comparison was made. The value of the buckling stress was found that corresponded to approximately the same number of waves in the circumferential direction as that found in the tests. The comparison for $a_o < 0$ is shown in Figure 56. The numbers on the curves correspond to the predominant term in the eigenfunction expansion, and those at the ends of the curves to the number of circumferential waves. It is seen that the decrease in buckling stress with increasing negative imperfection amplitude is less as the circumferential wave number increases. The buckling mode shape is also more in line with the experimental results. The eigenfunction has more axial waves as the number of circumferential waves increases and the amplitude of the waves at the center of the shell is greater than the amplitude of the waves at the edges. Again, this is nearer the experimental results.

For $a_o > 0$ the theory predicts that the buckling stress should be independent of a_o. The tests show that there is a definite decrease of the buckling stress for small positive a_o. However, there is some indication that this buckling stress for large positive a_o would increase to about the same value as that for no intended imperfection.

The discrepancy between the theory and experiment can be traced to several sources. One source of error in the theory is the neglect of the end constraint during the loading. The effect of this constraint is not completely understood but there is some evidence that it may be more important than previously anticipated.

Another source of error in the theory is the assumption on the boundary conditions of the perturbations. This may be particularly true since the boundary conditions chosen allow the eigenfunction of the minimum eigenvalue to have almost the same axial variation as the initial imperfection. If other boundary conditions were adopted, the minimum eigenvalue might be found corresponding to a higher axial and circumferential wave number.

The most important experimental errors were the unintended initial imperfection and the nonuniformity of loading. In most of the shells tested the unintended imperfection was of the order of magnitude of the thickness of the shell. This imperfection was usually not of axially symmetric shape but a deviation of the cross section from a true circle. The influence of this imperfection and the nonuniform loading is not known.

The two imperfections studied did not have a very great influence on the buckling load of the shells tested. For all of the shells the value of k varied from 0.460 to 0.267. This amount of spread for even supposedly identical test specimens is not uncommon in shell stability studies. While there are definite trends established with increasing and decreasing a_o for this specific type of imperfection, the overall effect of the imperfection is small for imperfection amplitudes of the order of the wall thickness. This tends to lend support to Donnell's contention that imperfections that do not have the shape of the buckled form are unimportant. However, the buckling tests carried out for the shells with no intended imperfection also demonstrate that a substantial percentage of the classical buckling load can be achieved with test specimens that are quite imperfect.

REFERENCES

1. Flugge, W.: Stresses in Shells. Julius Springer, Berlin (1960).

2. Donnell, L. H., and Wan, C. C.: Effect of Imperfections on Buckling of Thin Cylinders and Columns under Axial Compression. Journal Appl. Mech., Vol. 17, No. 1, p. 73 (1950).

3. Donnell, L. H.: A New Theory for the Buckling of Thin Cylinders under Axial Compression and Bending. Trans. of the American Soc. of Mech. Eng., Vol. 56, p. 795 (November 1934).

4. Kármán, T., von, and Tsien, H. S.: The Buckling of Thin Cylindrical Shells under Axial Compression. Journal Aero. Sciences, Vol. 8, No. 8, p. 302 (June 1941).

5. Kempner, J.: Postbuckling Behavior of Axially Compressed Circular Cylindrical Shells. Journal Aeronautical Sciences, Vol. 21, No. 5, p. 329 (May 1954).

6. Tsien, H. S.: Buckling of a Column with Nonlinear Lateral Supports. Journal Aeronautical Sciences, Vol. 9, No. 4, p. 119, (February 1942).

7. Tsien, H. S.: A Theory for the Buckling of Thin Shells. Journal Aeronautical Sciences, Vol. 9, No. 10, p. 373 (August 1942).

8. Stein, M.: The Phenomenon of Change in Buckle Pattern in Elastic Structures. NASA TR R-39 (1959).

9. Tsien, H. S.: Lower Buckling Load in the Non-linear Buckling Theory for Thin Shells. Quart. Appl. Math., Vol. 5, p. 236, (1947).

10. Thompson, J. M. T.: Making of Thin Metal Shells for Model Stress Analysis. Journal Mech. Eng. Sciences, Vol. 2, No. 2, (1960).

11. Gray, A. G.: Modern Electroplating. John Wiley and Sons, New York (1953).

12. Marguerre, K.: Zur Theorie der gekrummten Platte grosser Formanderung. Proc. 5th International Congress Appl. Mech., p. 93 (1938).

13. Donnell, L. H.: Stability of Thin-Walled Tubes under Torsion. NACA Rep. No. 479 (1933).

14. Hoff, N. J.: Buckling and Stability. The Forty-first Wilbur Wright Memorial Lecture. Journal Royal Aeronautical Society, Vol. 58, p. 3 (January 1954).

15. Leggett, D. M. A., and Jones, R. P. N.: The Behavior of a Cylindrical Shell under Axial Compression when the Buckling Load has been Exceeded. British Aeronautical Research Committee Rand M 2190 (August 1942).

16. Michielsen, H. F.: The Behavior of Thin Cylindrical Shells After Buckling under Axial Compression. Journal Aeronautical Sciences, Vol. 15, p. 738 (1948).

17. Timoshenko, S.: Theory of Elastic Stability. McGraw-Hill Book Co., New York (1936).

18. Mushtari, Kn. M., and Galimev, K. Z.: Non-Linear Theory of Thin Elastic Shell. Translated by Morgenstern, J., and Schorr-Kon, J. J., Israel Program for Scientific Translations.

19. Fung, Y. C., and Sechler, E. E.: Instability of Thin Elastic Shells. Structural Mechanics, Proc. of First Symposium on Naval Structural Mechanics, Pergamon Press (1960).

20. Hoff, N. J.: Buckling of Thin Shells. Stanford University SUDAER No. 114 (August 1961)

21. Ponsford, H. T.: The Effects of Stiffeners on the Buckling of Cylinders with Moderate Wall Thickness. Doctoral Thesis, California Institute of Technology (1953).

22. Lo, Hsu, Crate, H., Schwartz, E. B.: Buckling of Thin Walled Cylinder under Axial Compression and Internal Pressure. NACA Report 1027 (1951).

23. Goree, W. S., and Nash, W. A.: Elastic Stability of Circular Cylindrical Shells Stabilized by a Soft Elastic Core. University of Florida Tech. Rep. No. 4 (May 1960).

TABLE I

THICKNESS VARIATION OF SHELLS

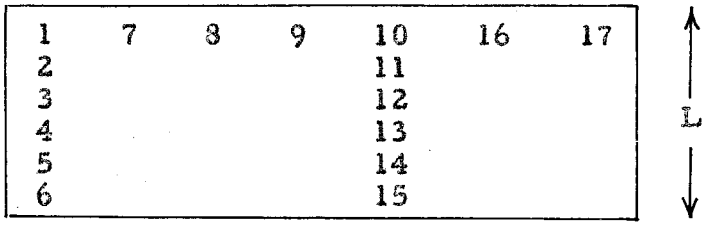

Thickness measured at the positions on the shell surface indicated above.

Position	Thickness inches x 10^3				
	Shell no. X	Shell no. 3	Shell no. 4	Shell no. A	Shell no. J
1	4.32	4.58	4.58	4.65	4.38
2	4.30	4.59	4.55	4.64	4.32
3	4.29	4.62	4.53	4.64	4.30
4	4.26	4.61	4.46	4.62	4.20
5	4.33	4.60	4.44	4.62	4.15
6	4.32	4.60	4.47	4.61	4.16
7	4.29	4.56	4.55	4.64	4.32
8	4.31	4.52	4.54	4.61	4.31
9		4.55	4.64	4.61	4.28
10	4.32	4.57	4.55	4.59	4.37
11	4.35	4.53	4.56	4.62	4.31
12	4.34	4.58	4.54	4.62	4.16
13	4.35	4.50	4.46	4.62	4.16
14	4.35	4.50	4.45	4.62	4.27
15	4.35		4.51	4.59	4.20
16	4.32	4.55	4.61	4.65	4.38
17	4.31	4.55	4.62		
Average	4.32	4.56	4.53	4.62	4.27

TABLE II

YOUNG'S MODULUS TESTS FOR PLATED COPPER

Test	Thickness inches x 10^3	Orientation	E lb/in^2 x 10^{-6}
1	4.54	Axial	12.7
2	4.54	Axial	12.8
3	4.54	Axial	12.4
4	4.54	Circumferential	12.7
5	4.54	Circumferential	12.8
6	4.54	Circumferential	13.2
7	4.21	Circumferential	12.9
8	4.14	Circumferential	13.0
9	4.16	Circumferential	13.1
10	4.84	Circumferential	13.2
11	4.86	Circumferential	13.7
12	4.90	Circumferential	13.7
13	4.90	Circumferential	12.8
14	4.83	Circumferential	12.7
		Average	13.0

TABLE III

SUMMARY OF BUCKLING TESTS

III = Intended Initial Imperfection, $k = \frac{\sigma_o R}{Et}$, m = Number of Circumferential Waves

Shell	III inches	$t \times 10^3$ inches	a_o/t	k initial	k collapse	$\frac{\sigma \text{ max} - \sigma \text{ min}}{\sigma \text{ ave}}$ %	m
A	0	4.62	0	-	0.460	19.4	16-18
B	0	4.45	0	-	0.438	16.1	14-15
C	0	4.50	0.5	-	0.435	23.7	15-17
Y	0.010S in x/L	4.82	2.1	-	0.429	14.4	15-17
Z	0.010S in x/L	4.61	2.2	-	0.359	17.1	15
AA	0.010S in x/L	4.50	2.2	0.305	0.362	15.4	16-17
7	0.010S in x/L	4.57	4.5	-	0.407	13.0	14-18
V	0.020S in x/L	4.49	4.5	-	0.326	55.4	16-17
U	0.020S in x/L	4.49	4.5	-	0.352	26.1	14-15
X	0.020S in x/L	4.32	4.6	0.258	0.337	9.7	15
8	0.020S in x/L	4.60	4.4	-	0.423	19.2	15-17
M	0.030S in x/L	4.52	6.6	-	0.369	15.5	19-20

TABLE III (contd.)

SUMMARY OF BUCKLING TESTS

III = Intended Initial Imperfection, $k = \frac{\sigma_o R}{Et}$, m = Number of Circumferential Waves

Shell	III inches	$t \times 10^3$ inches	a_o/t	k initial	k collapse	$\frac{\sigma \max - \sigma \min}{\sigma \text{ ave}}$ %	m
N	0.030S in x/L	4.57	6.6	-	0.342	18.0	16-17
O	0.030S in x/L	4.46	6.7	0.351	0.377	10.0	21
J	0.040S in x/L	4.27	9.4	-	0.366	21.3	17
K	0.040S in x/L	4.57	8.8	-	0.346	9.7	16-17
L	0.040S in x/L	4.46	9.0	0.272	0.321	16.7	13-15
G	0.050S in x/L	4.60	11.1	-	0.297	19.7	21
H	0.050S in x/L	4.46	10.7	-	0.385	17.3	21-22
I	0.050S in x/L	4.68	10.7	-	0.312	10.9	18-20
2	0.100S in x/L	4.36	22.9	0.361	0.369	15.8	18-20
3	0.100S in x/L	4.56	21.9	-	0.416	12.7	19-20
AB	-0.010S in x/L	4.59	-2.2	-	0.398	9.2	14-15
AD	-0.010S in x/L	4.57	-2.2	-	0.333	28.6	16-18

TABLE III (contd.)

SUMMARY OF BUCKLING TESTS

III = Intended Initial Imperfection, $k = \frac{\sigma_o R}{Et}$, m = Number of Circumferential Waves

Shell	III inches	$t \times 10^3$ inches	a_o/t	k initial	k collapse	$\frac{\sigma max - \sigma min}{\sigma ave}$ %	m
S	-0.040S in x/L	4.50	-8.9	-	0.331	19.7	15
T	-0.040S in x/L	4.50	-8.9	0.271	0.283	32.5	13-14
4	-0.040S in x/L	4.53	-8.8	-	0.373	19.9	14-16
P	-0.050S in x/L	4.45	-10.7	-	0.267	11.7	14
O	-0.050S in x/L	4.51	-11.1	0.258	0.268	20.0	14
R	-0.050S in x/L	4.42	-10.9	0.231	0.308	14.5	15-16
1	-0.050S in x/L	4.52	-11.1	-	0.361	41.9	15
11	$0.100\ 2(\frac{x}{L/2})-(\frac{x}{L/2})^2$	4.49	22.3	-	0.430	9.7	17-18
12	$0.200\ 2(\frac{x}{L/2})-(\frac{x}{L/2})^2$	4.56	43.8	-	0.437	12.0	18-19
13	$0.200\ 2(\frac{x}{L/2})-(\frac{x}{L/2})^2$	4.47	44.7	-	0.355	17.5	19

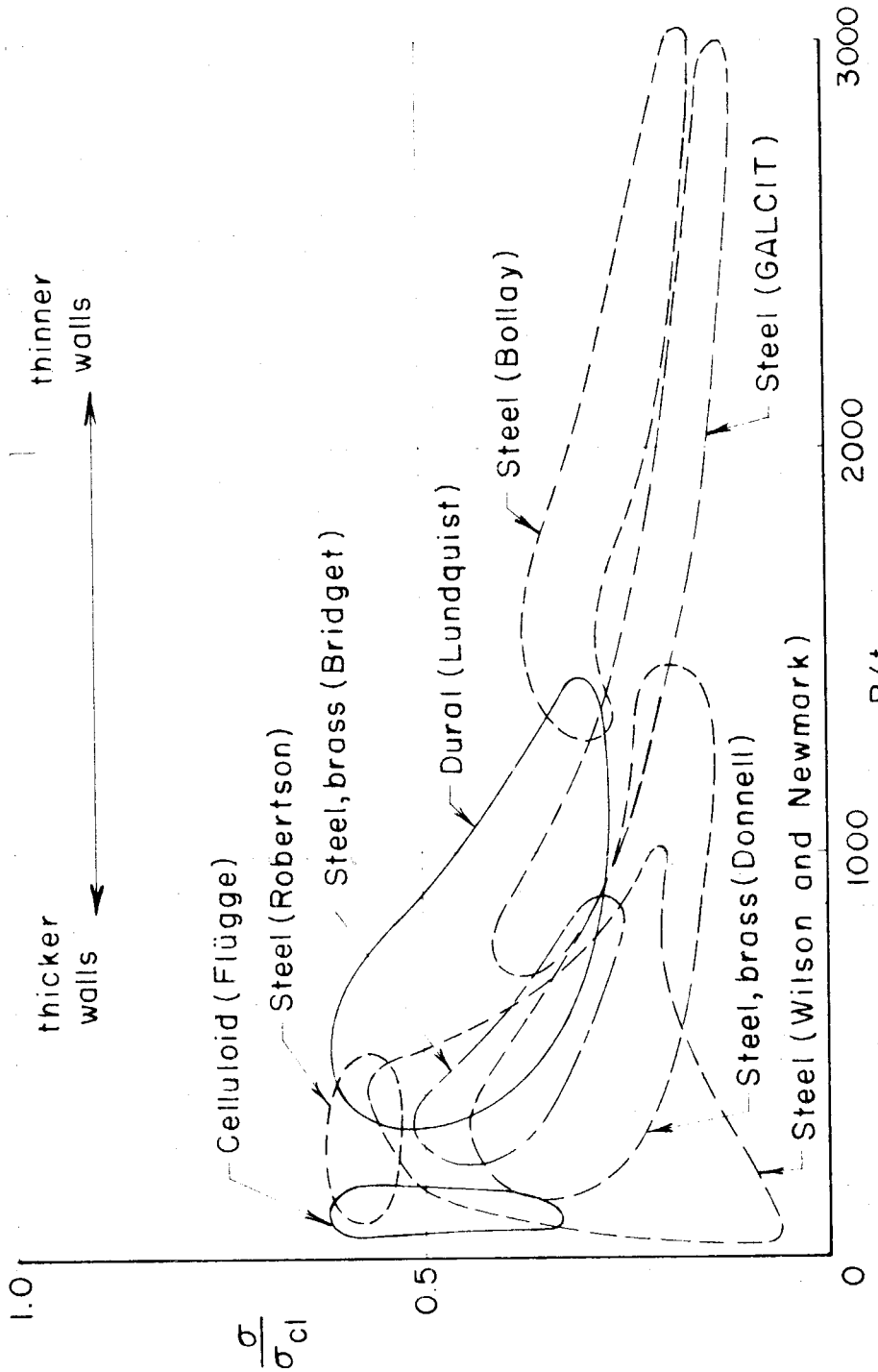

FIG. 1 – COMPARISON OF EXPERIMENTAL BUCKLING STRESS FOR A CYLINDER UNDER AXIAL COMPRESSION WITH THAT GIVEN BY THE CLASSICAL VALUE (FROM DONNELL AND WAN, REF. 2)

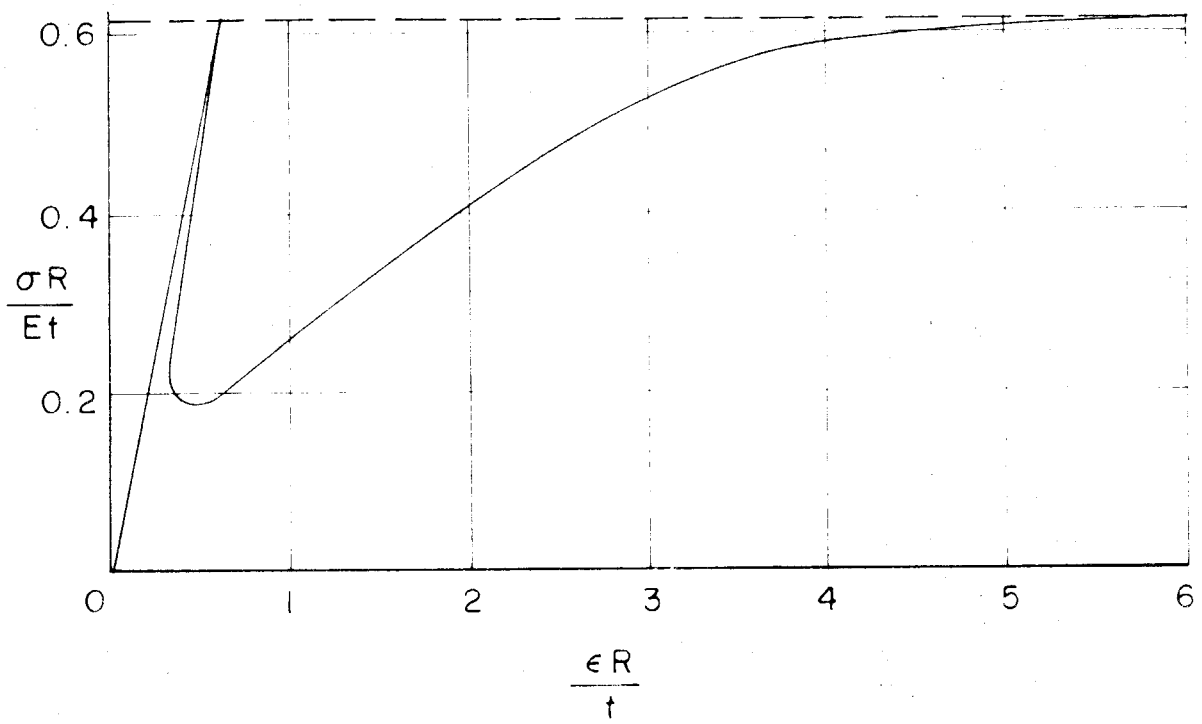

FIG. 2 - VARIATION OF AVERAGE STRESS WITH UNIT END SHORTENING FOR A CYLINDER UNDER AXIAL COMPRESSION (KEMPNER, REF. 5)

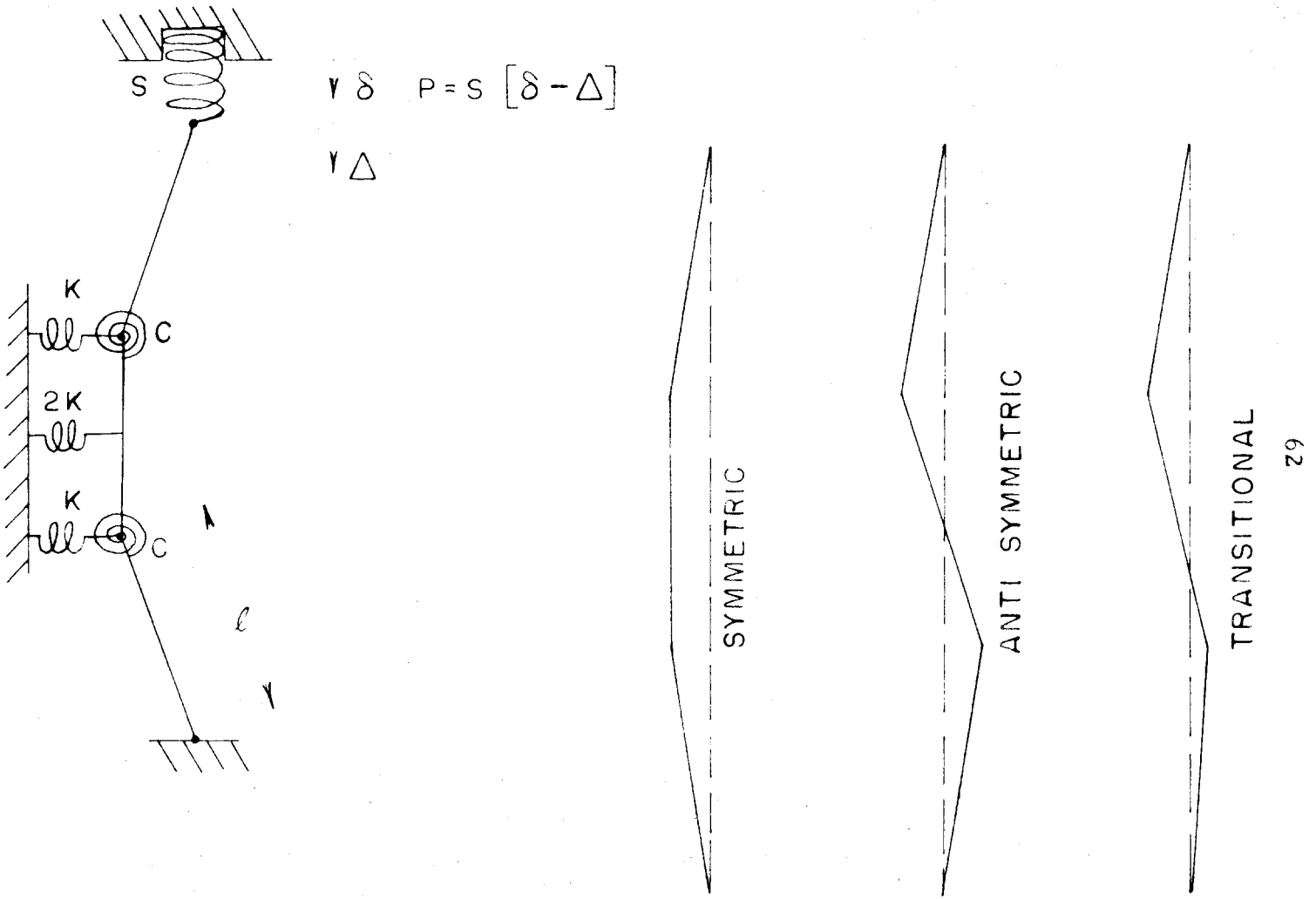

FIG. 3 - EQUILIBRIUM CONFIGURATION OF THREE PART COLUMN

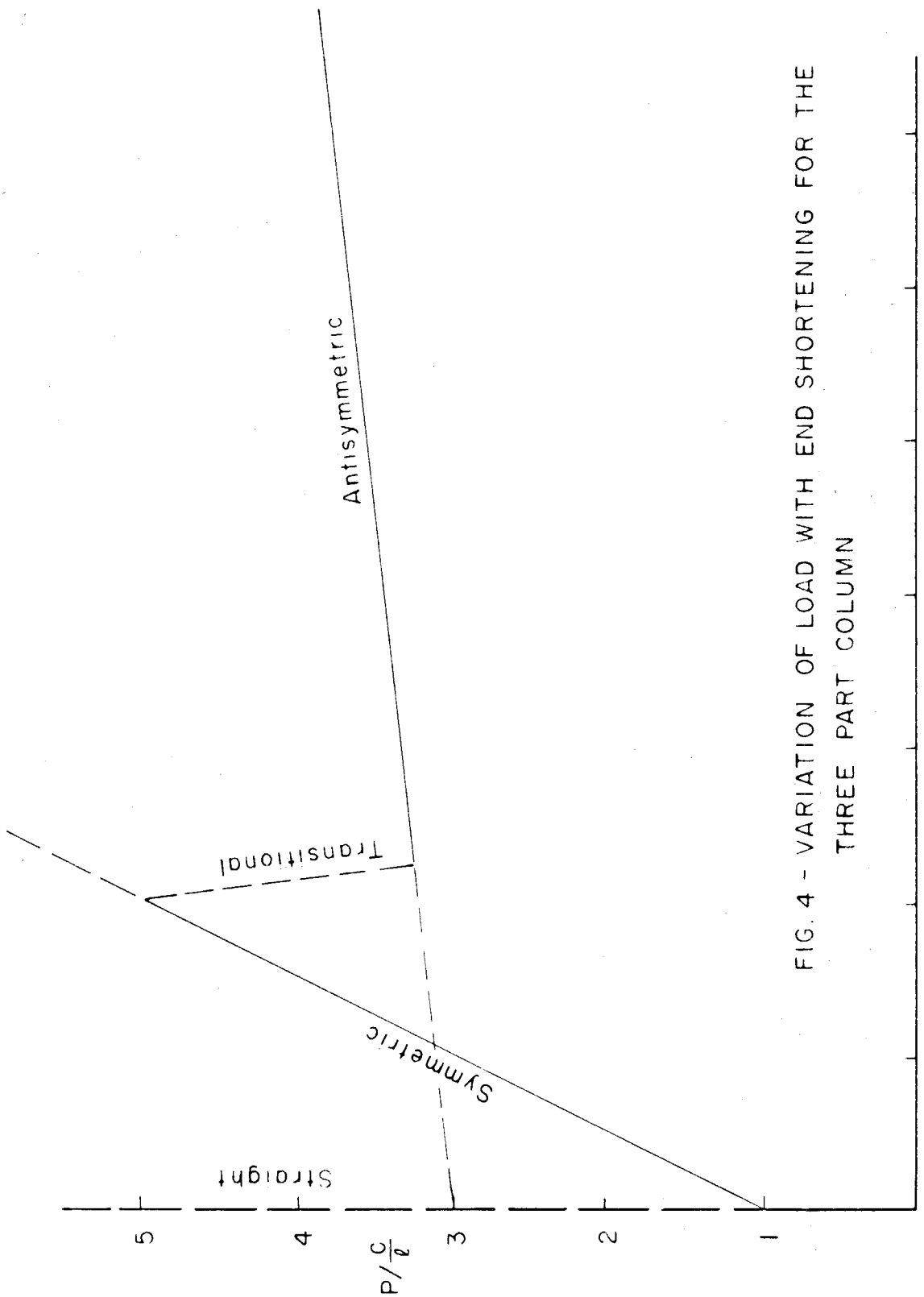

FIG. 4 - VARIATION OF LOAD WITH END SHORTENING FOR THE THREE PART COLUMN

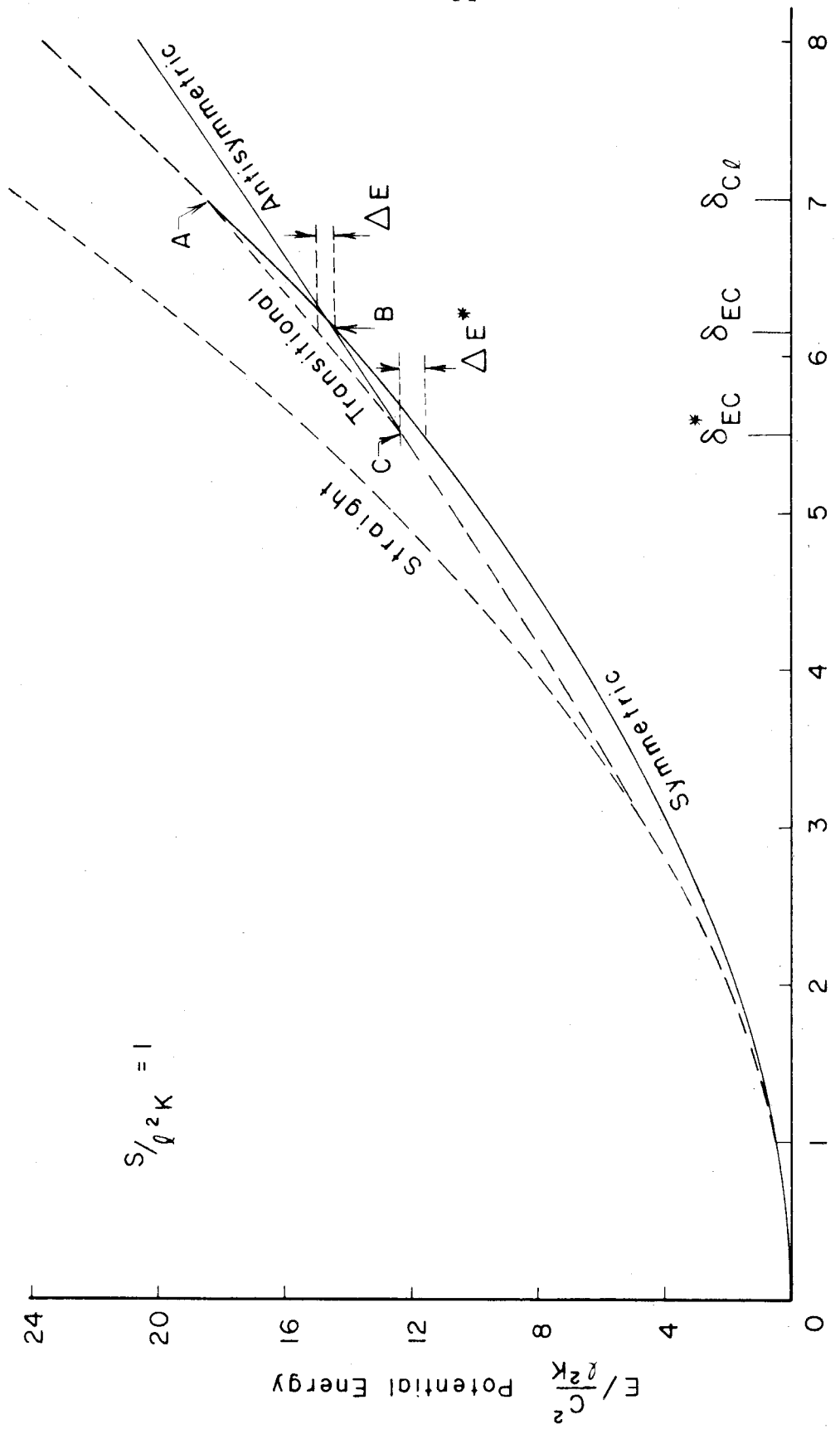

FIG. 5 - VARIATION OF POTENTIAL ENERGY WITH LOADING PARAMETER δ FOR THE THREE PART COLUMN

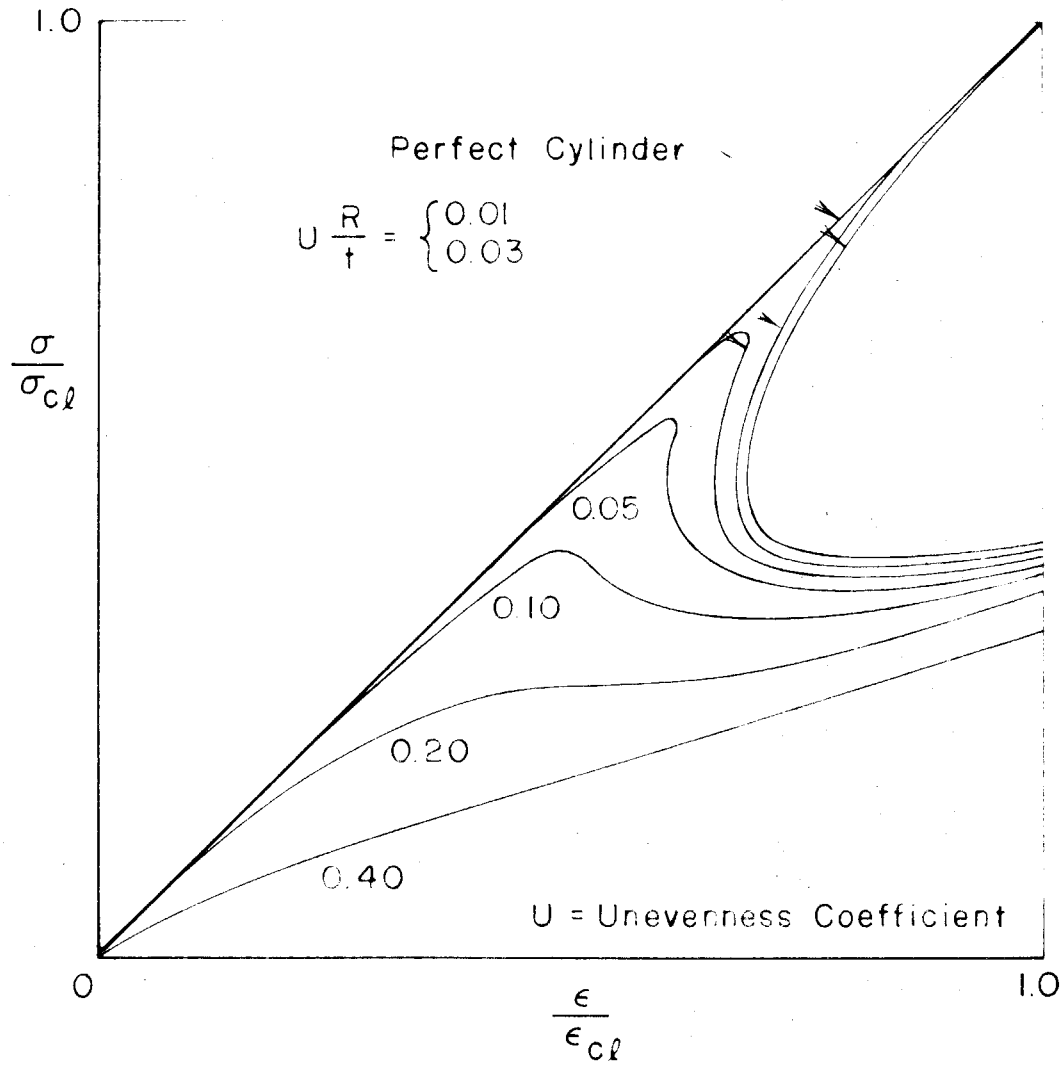

FIG. 6 - DONNELL'S SOLUTION OF AVERAGE STRESS VS. UNIT END SHORTENING FOR IMPERFECT CYLINDERS UNDER AXIAL COMPRESSION (FROM DONNELL AND WAN, REF. 2)

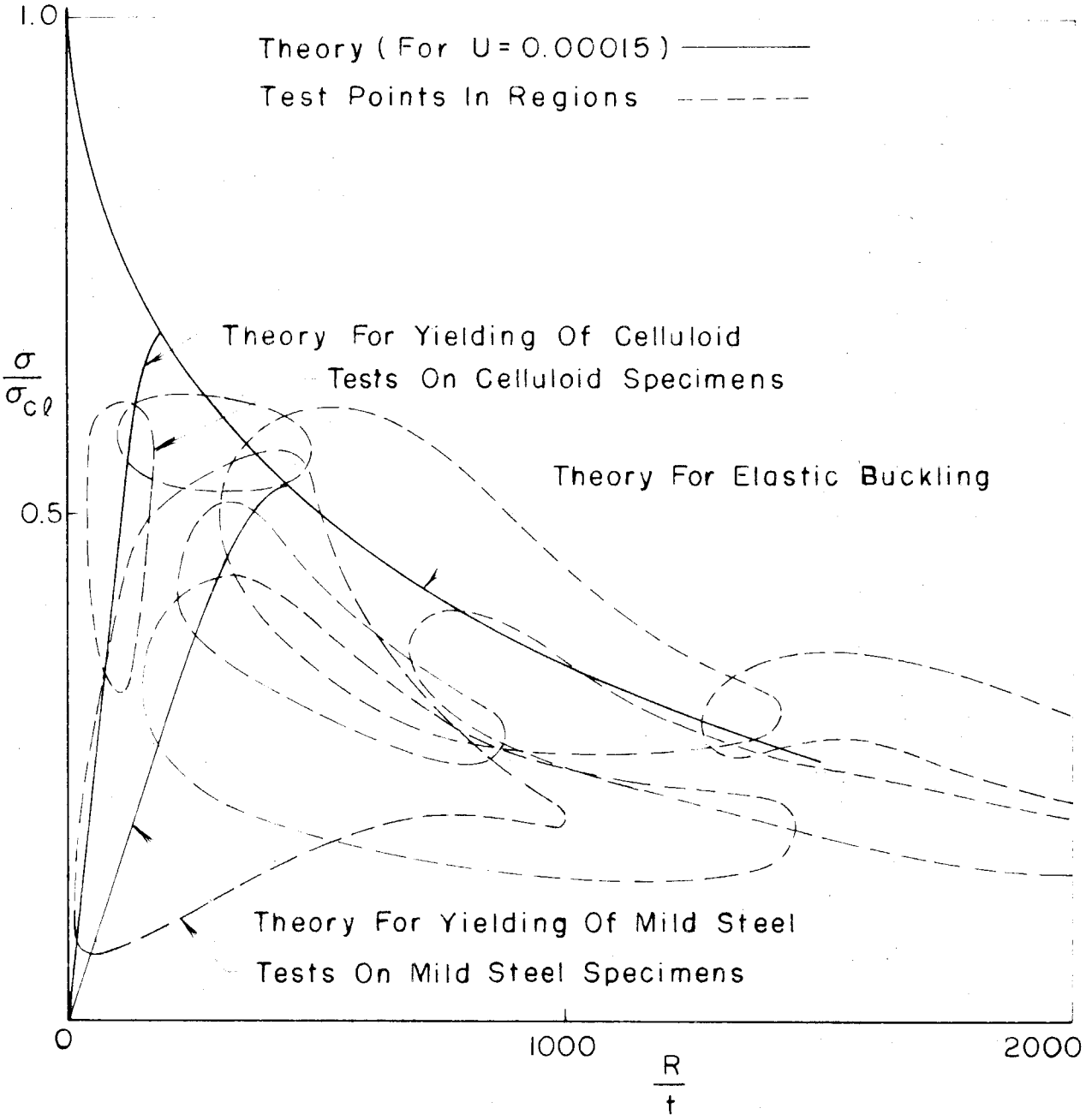

FIG. 7 - COMPARISON OF EXPERIMENTS WITH DONNELL AND WAN'S IMPERFECTION THEORY (FROM DONNELL AND WAN, REF. 2)

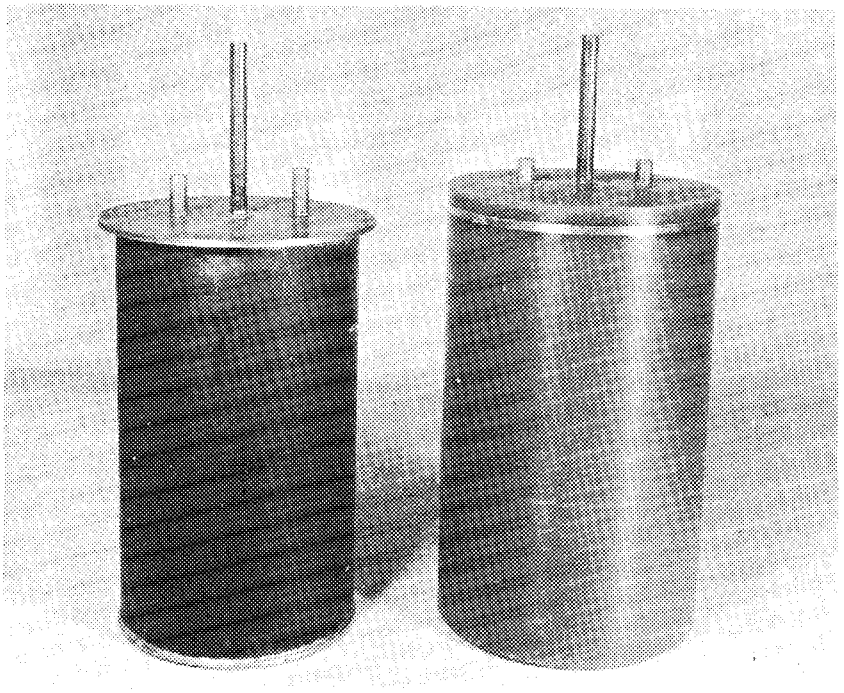

Fig. 8. Mandrel and Finished Wax Form

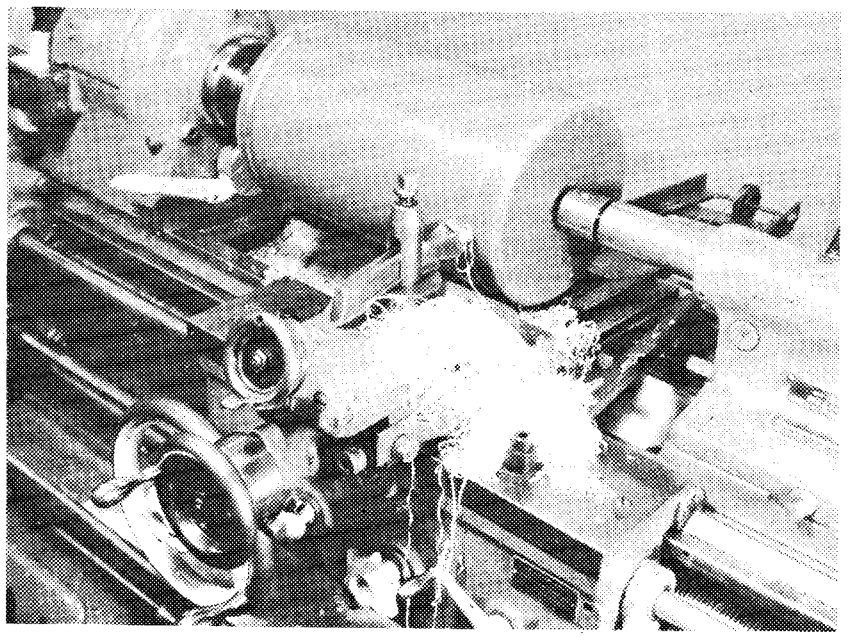

Fig. 9. Lathe Setup

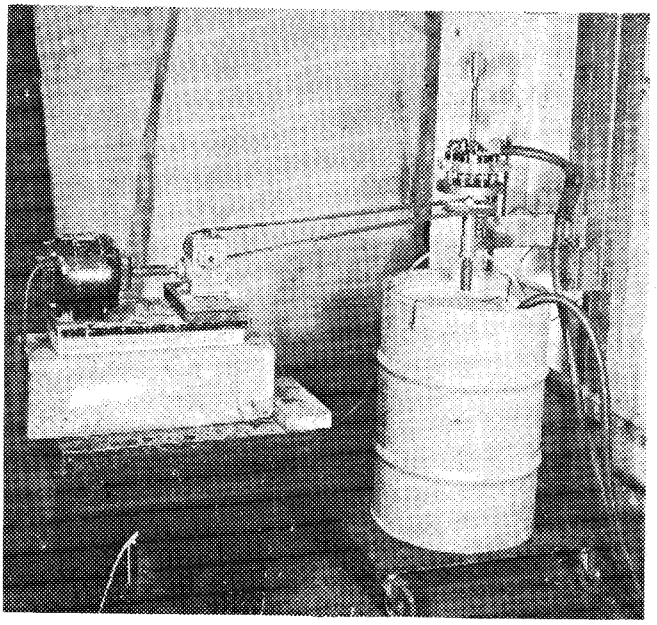

Fig. 10. Plating Installation

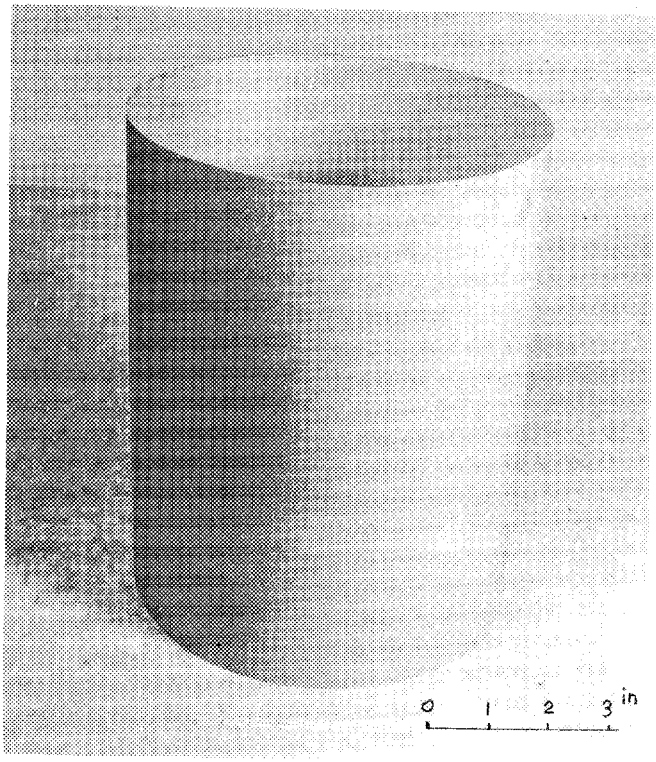

Fig. 11. Test Shell

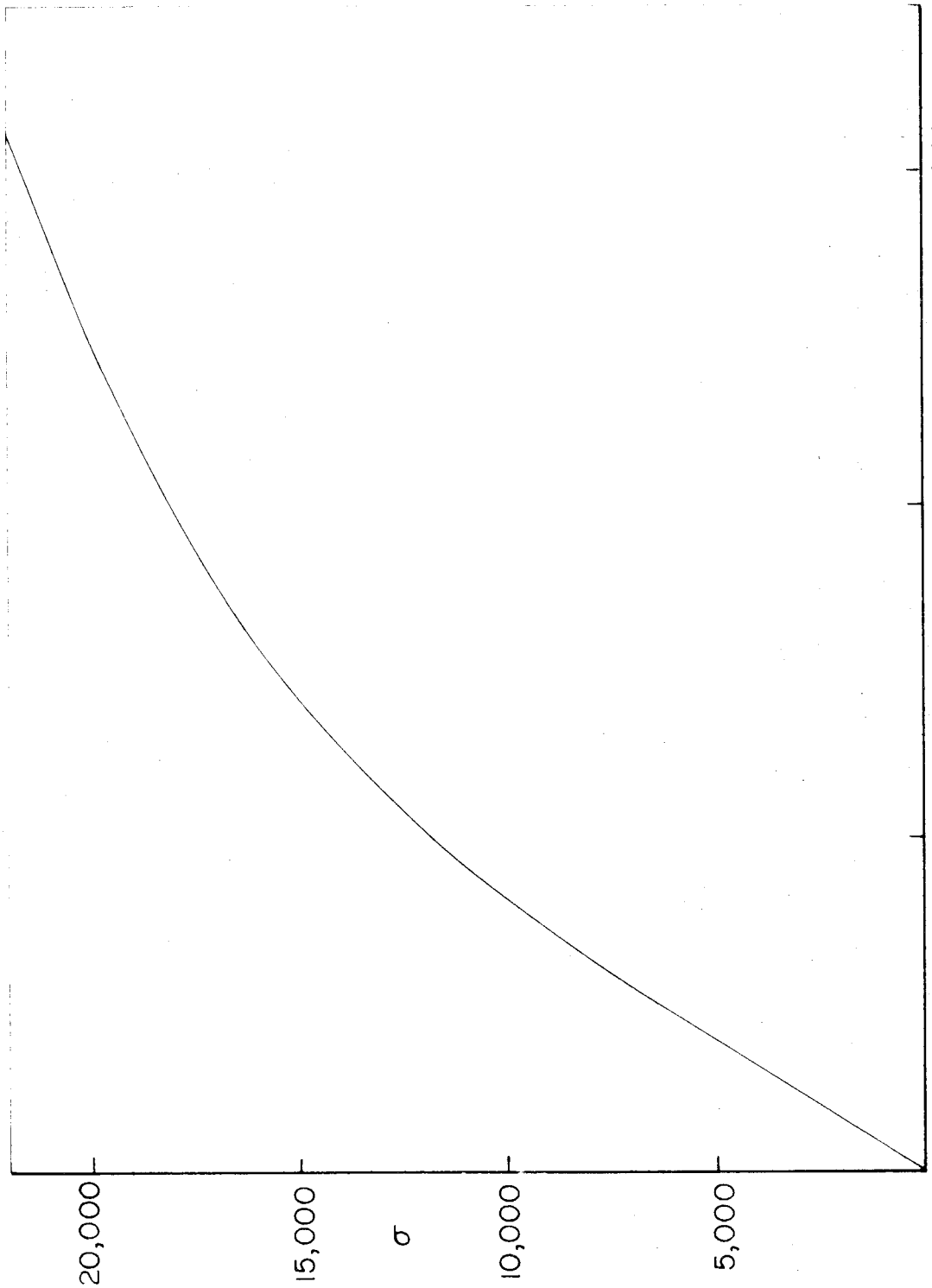

FIG. 12 - STRESS STRAIN CURVE FOR PLATED COPPER

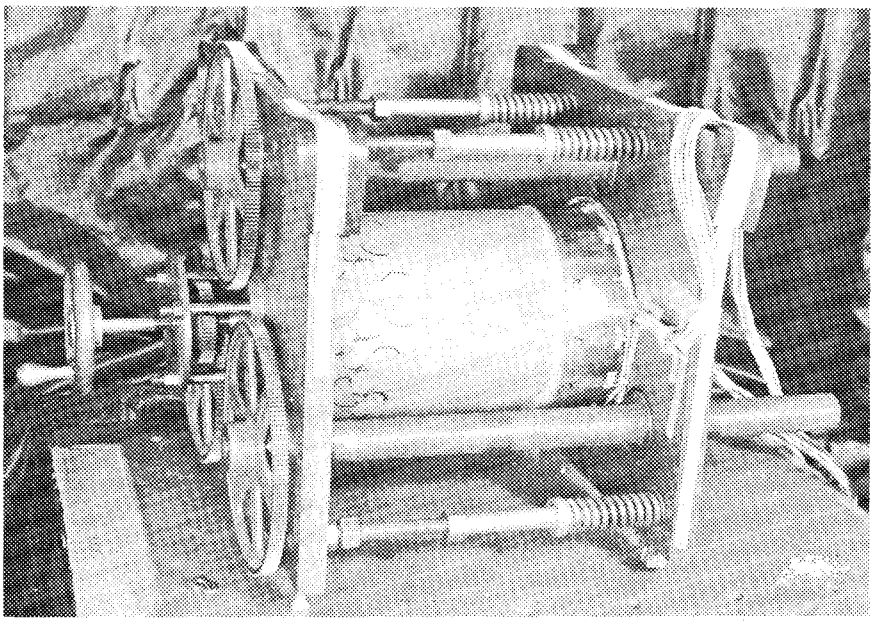

Fig. 13. Testing Machine

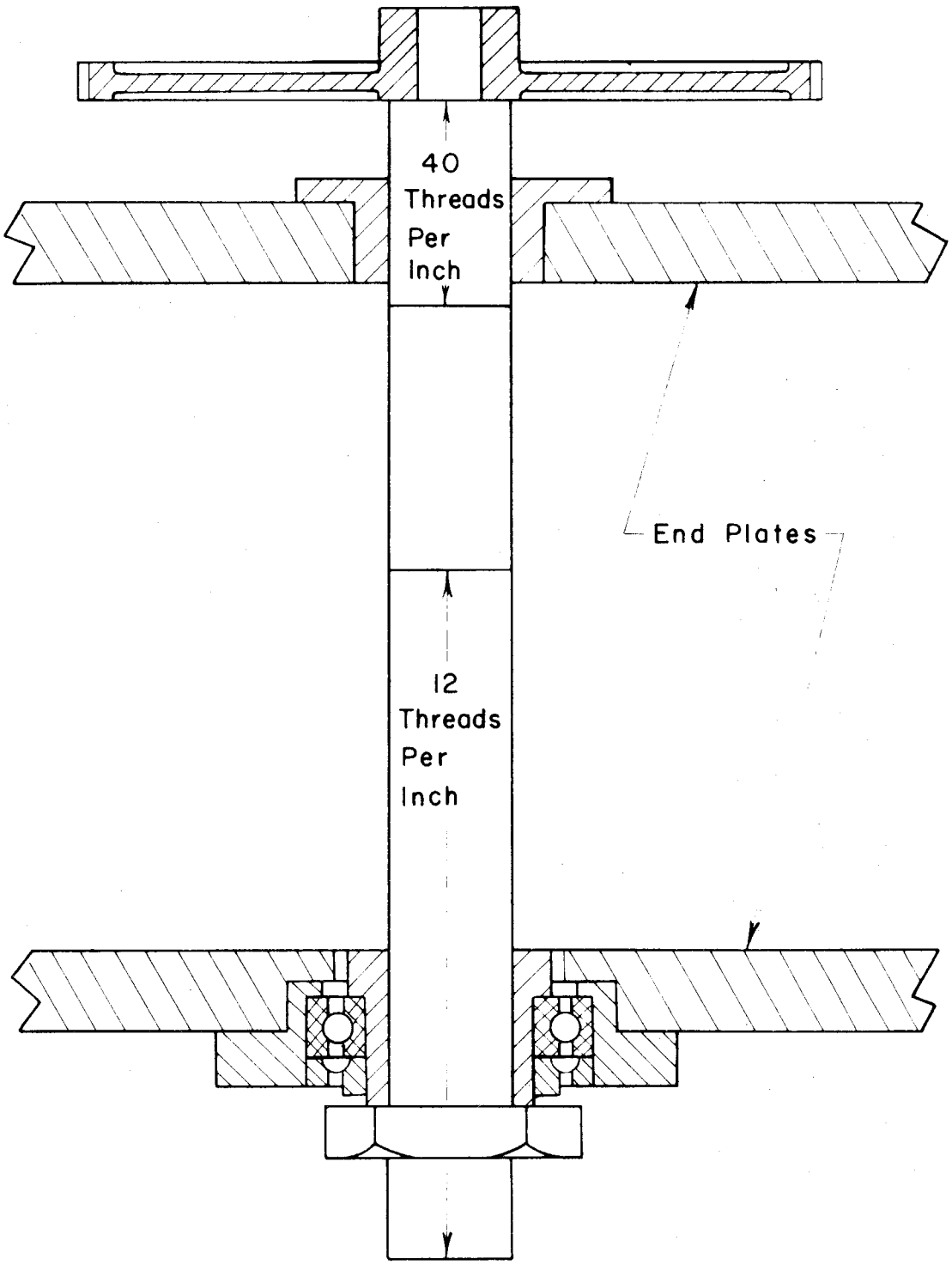

FIG. 14 – DETAILS OF TESTING MACHINE SCREW

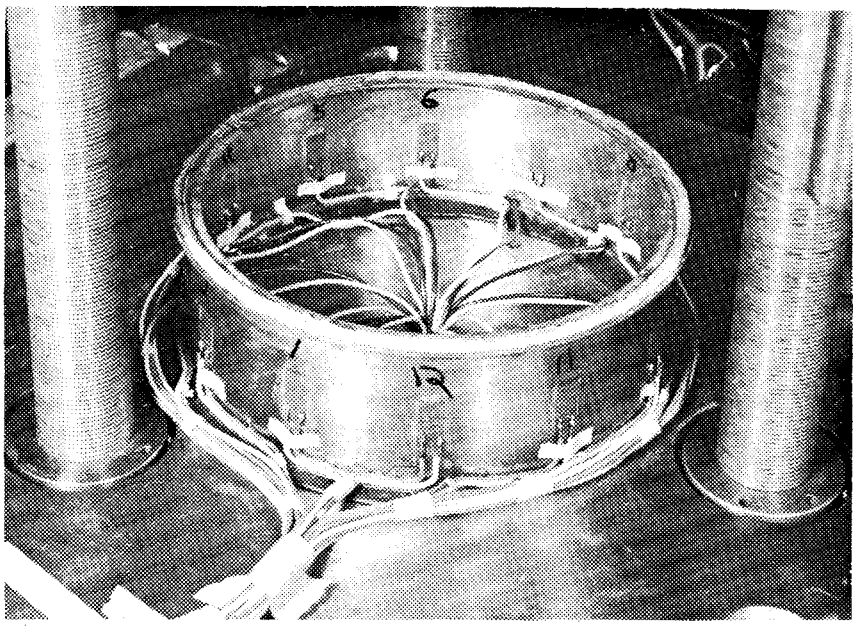

Fig. 15. Load Measuring Cylinder

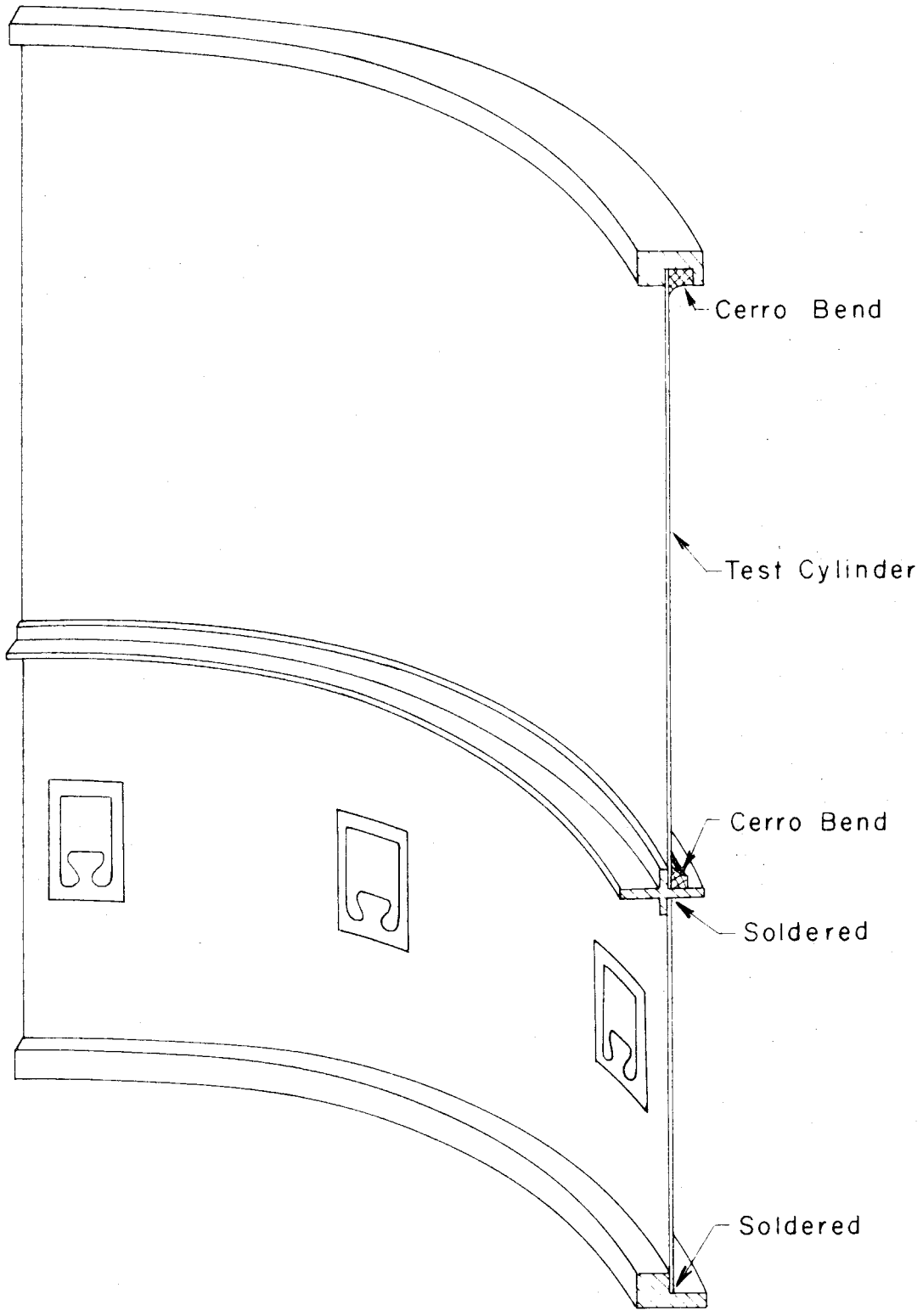

FIG. 16 — DETAILS OF LOAD MEASURING CYLINDER

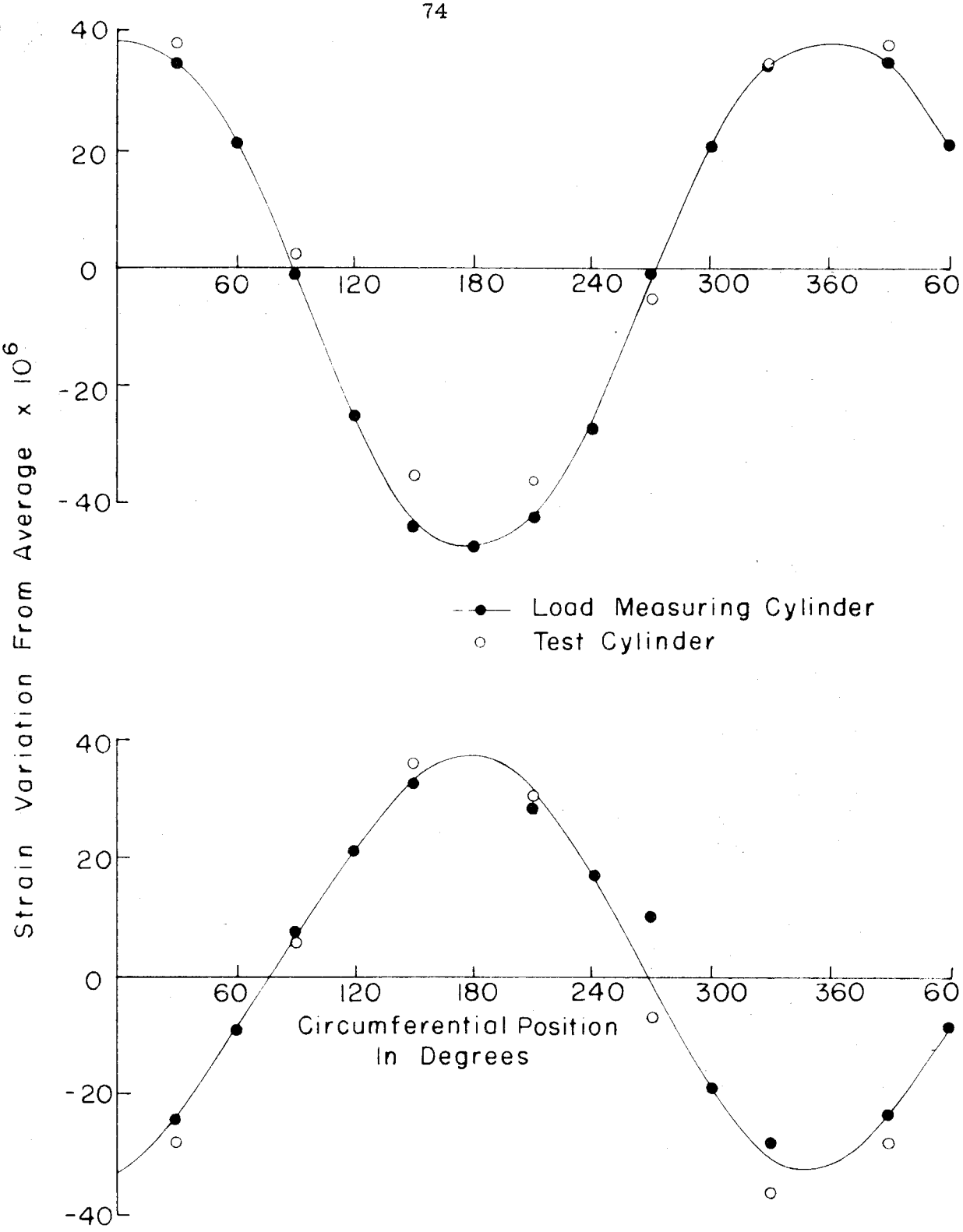

FIG. 17- COMPARISON OF STRAIN IN TEST CYLINDER AND IN LOAD MEASURING CYLINDER

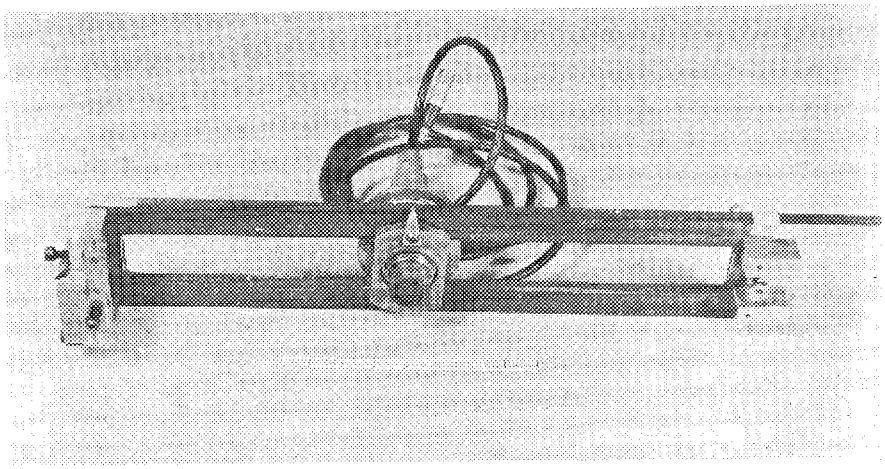

Fig. 18. Initial Imperfection Measuring Equipment

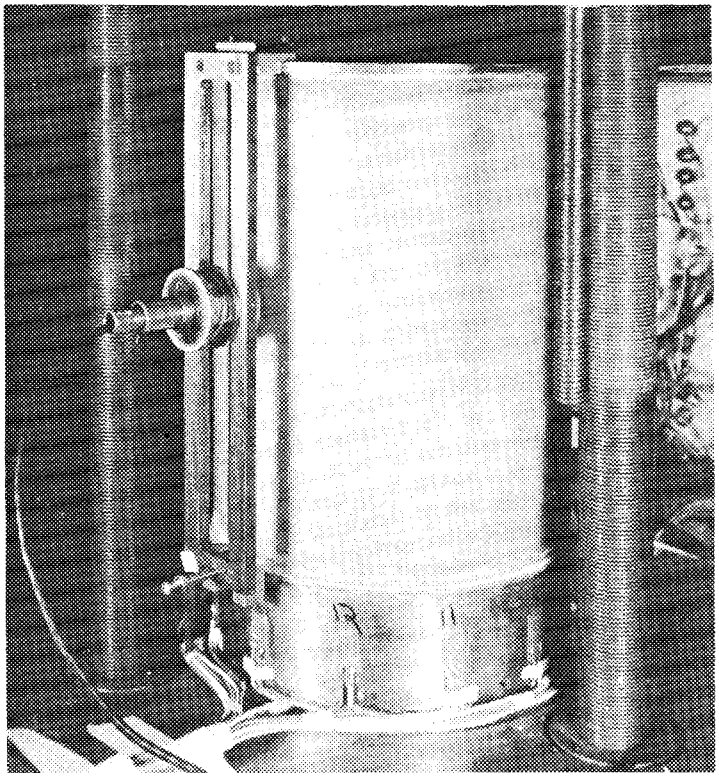

Fig. 19. Initial Imperfection Measuring Equipment in Position on a Cylinder

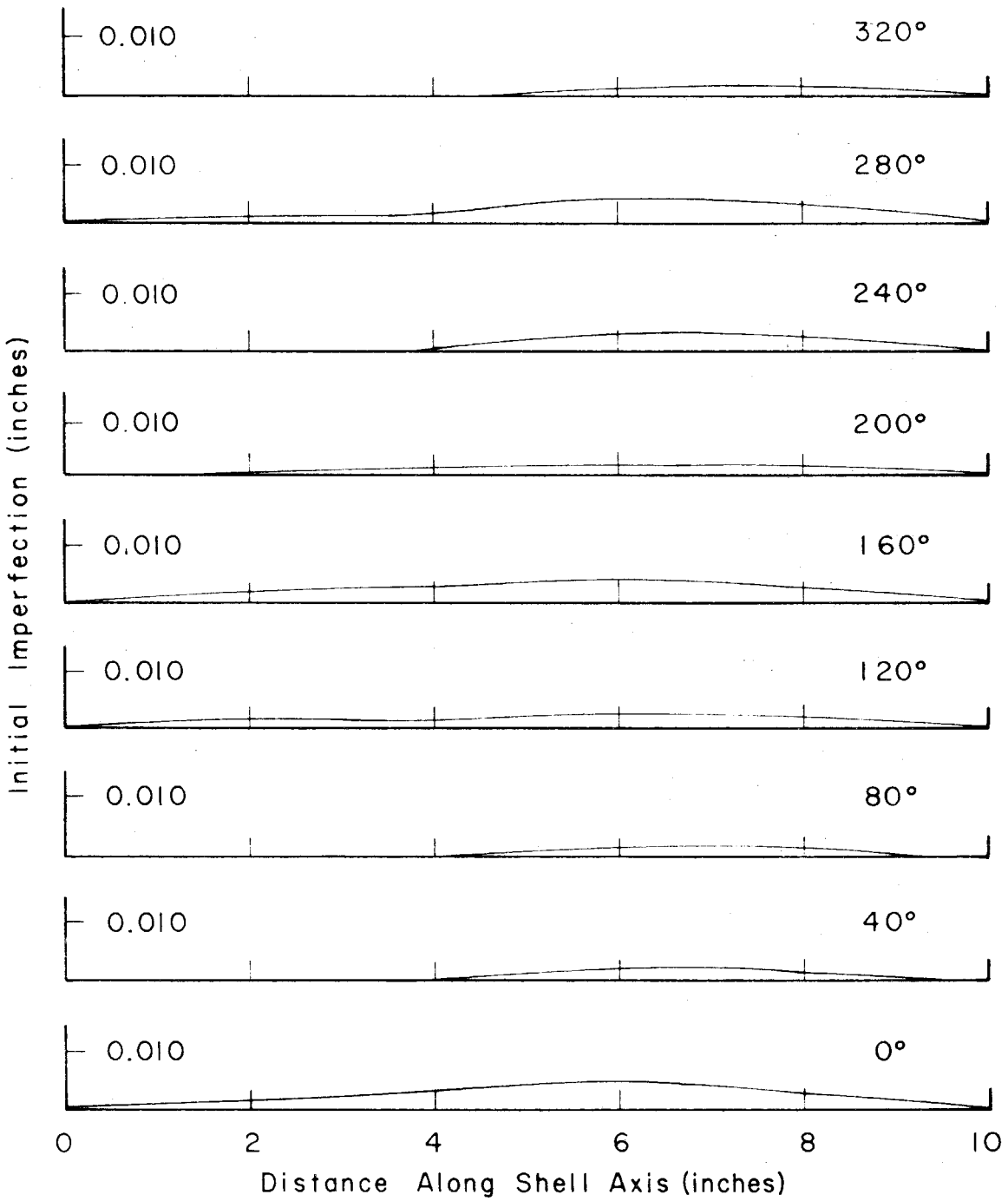

FIG. 20 SHELL C INITIAL IMPERFECTION

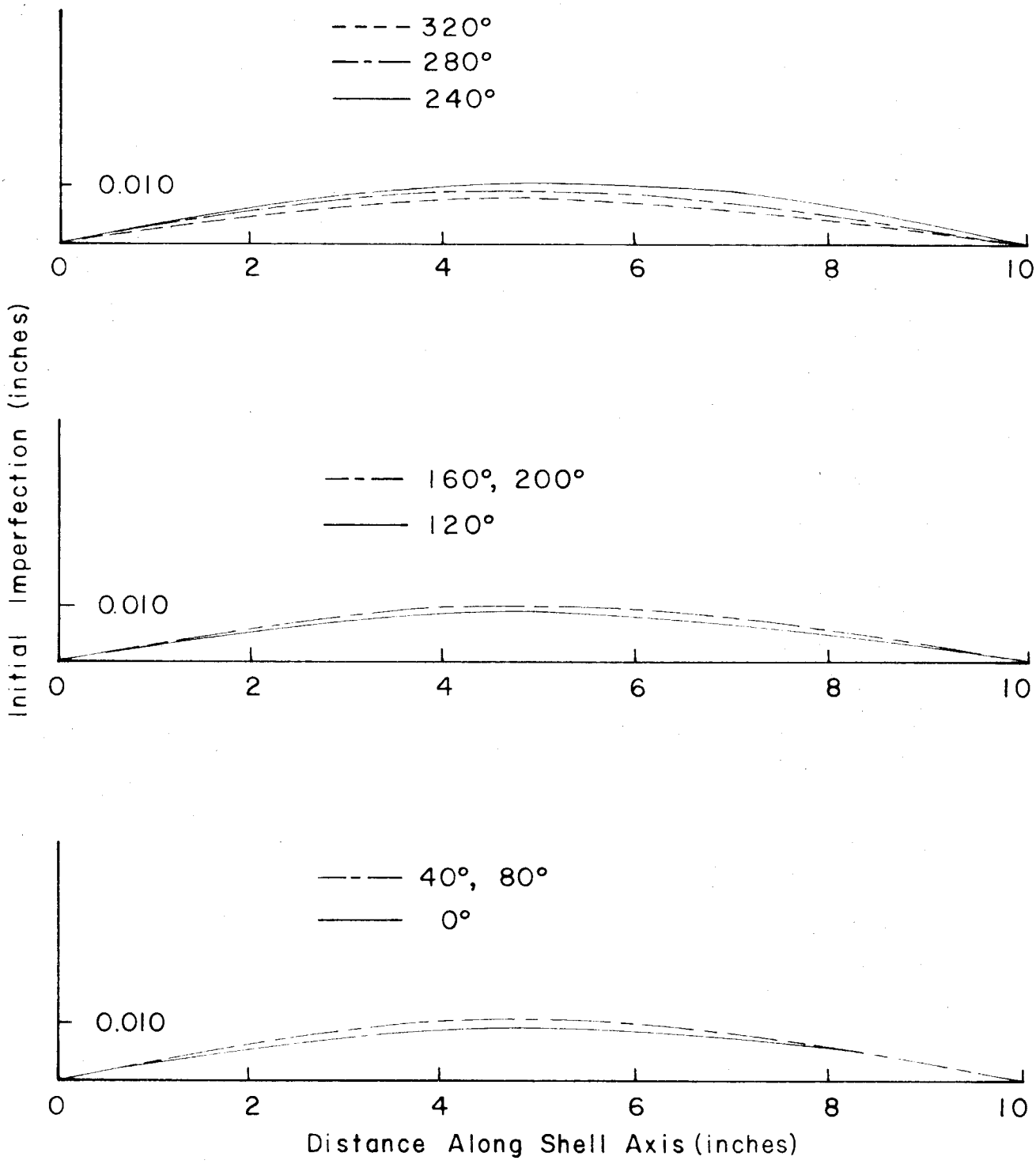

FIG. 21 SHELL 7 INITIAL IMPERFECTION

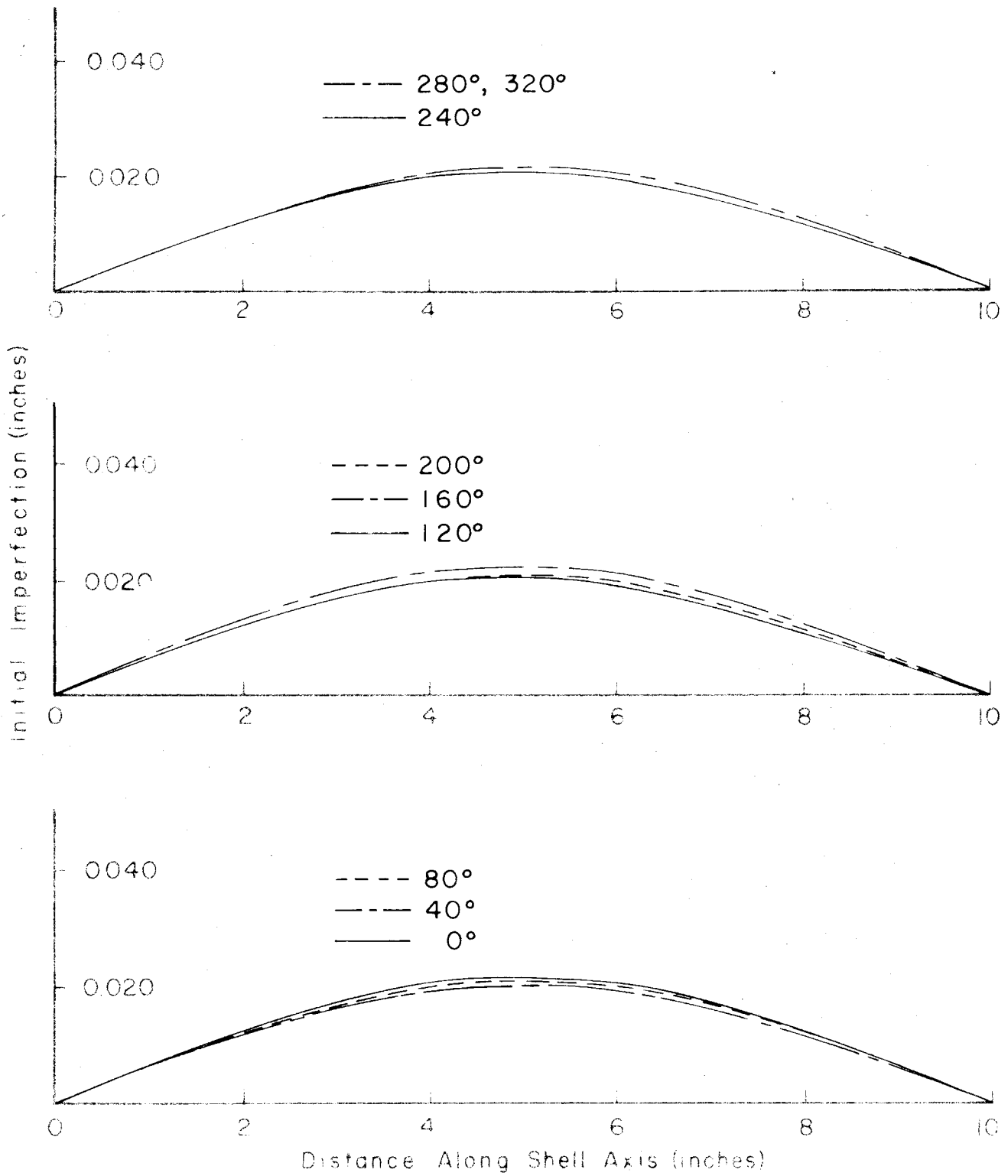

FIG. 22 SHELL V INITIAL IMPERFECTION

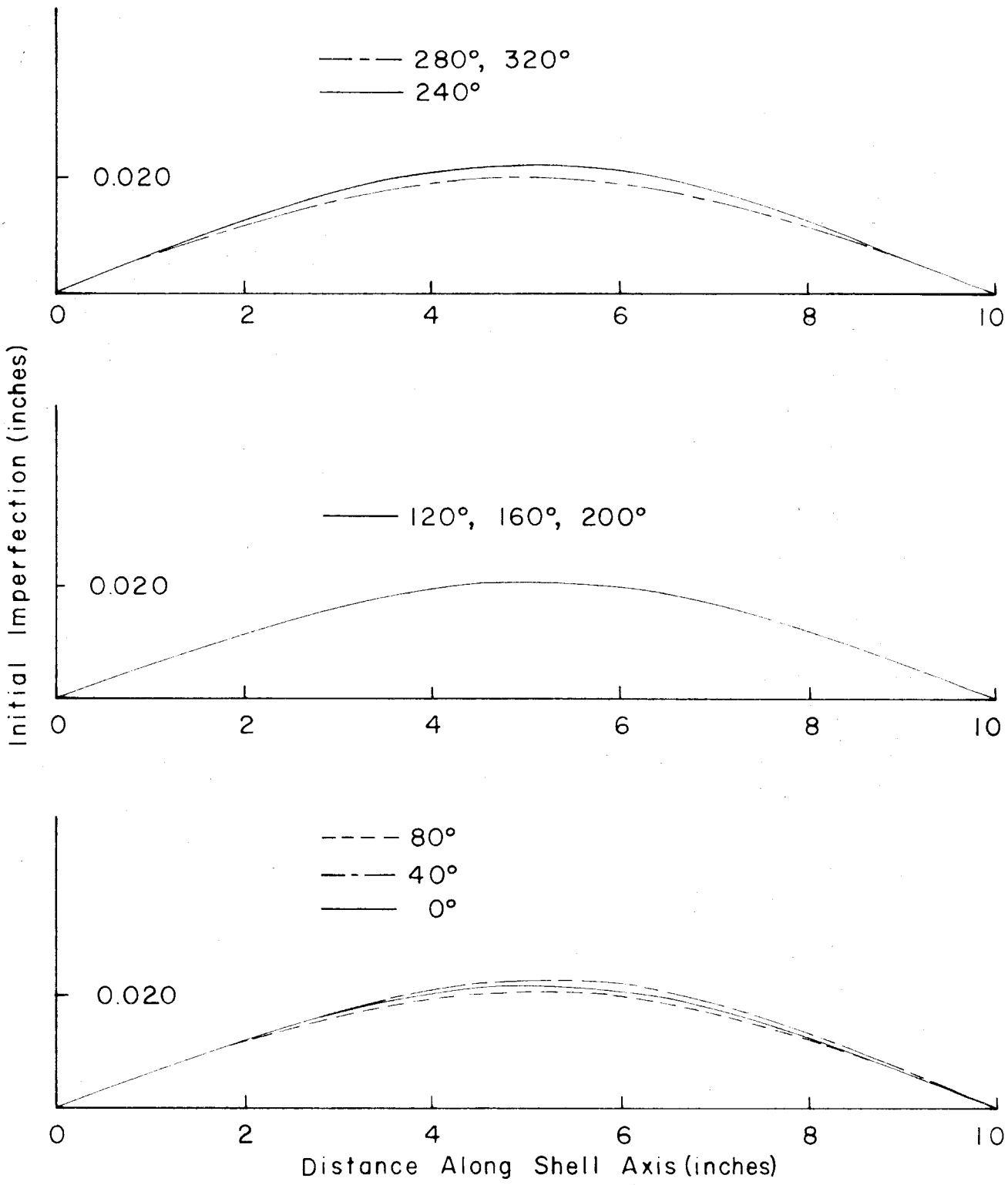

FIG. 23 SHELL X INITIAL IMPERFECTION

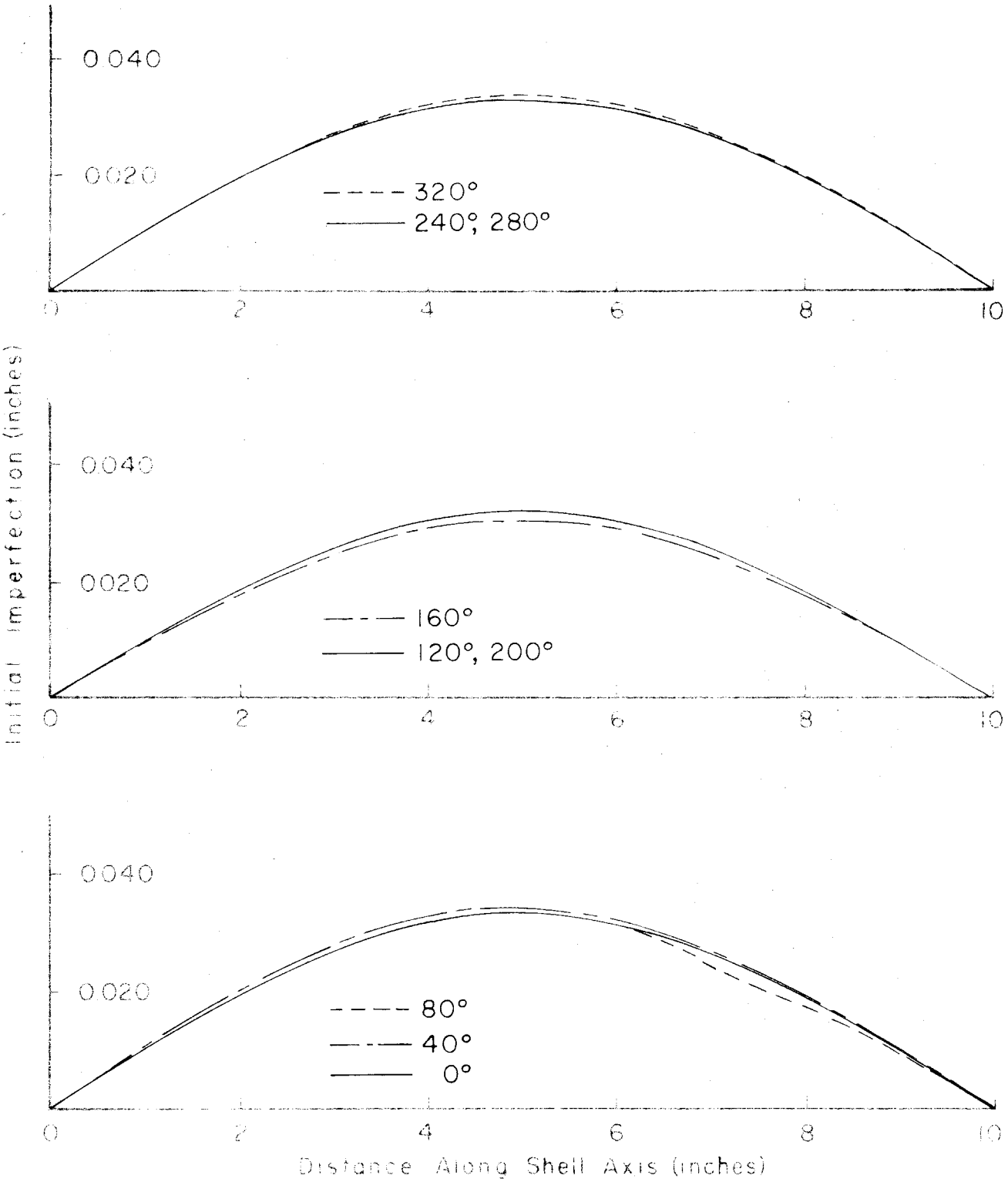

FIG. 24 SHELL M INITIAL IMPERFECTION

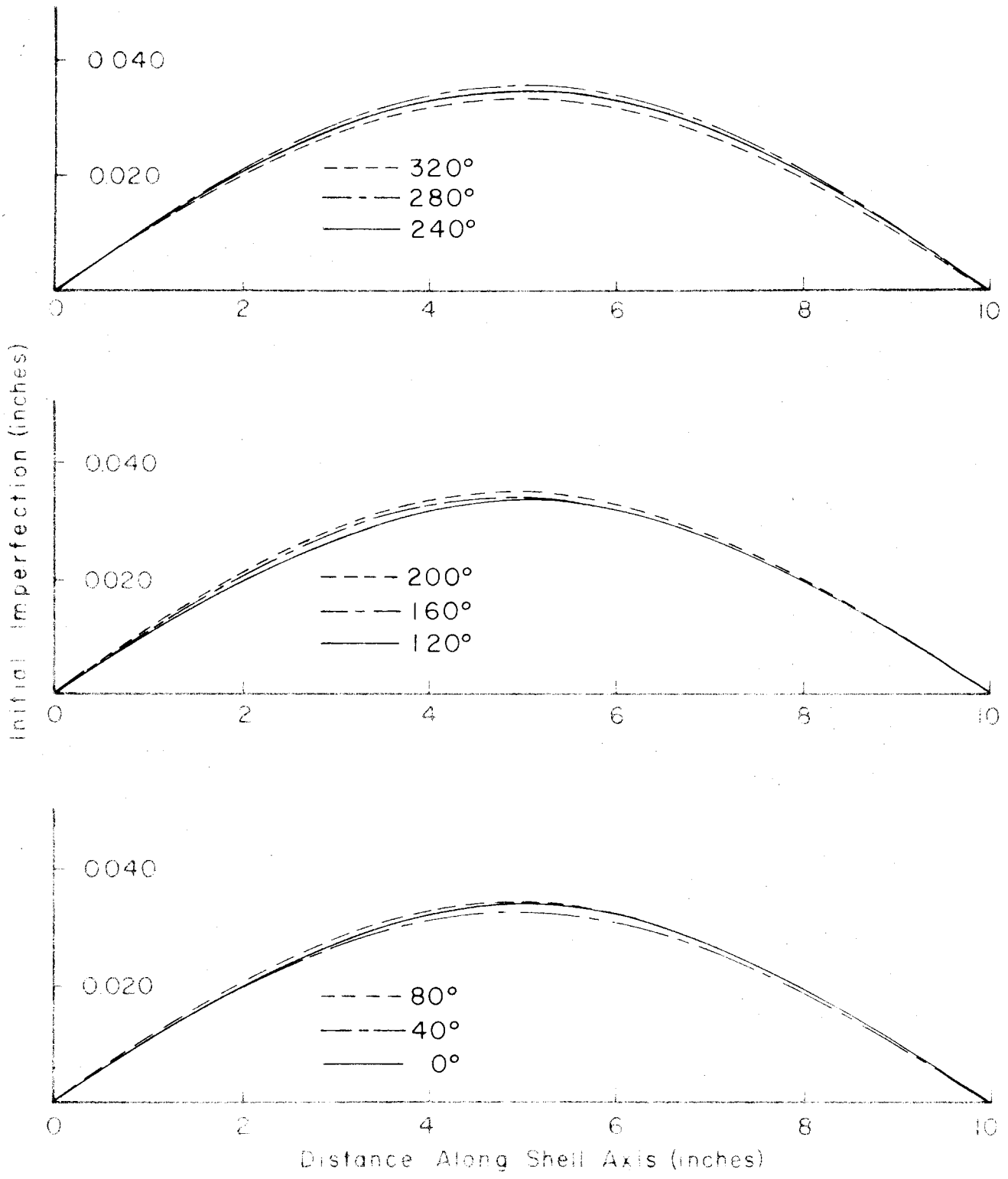

FIG. 25 SHELL N INITIAL IMPERFECTION

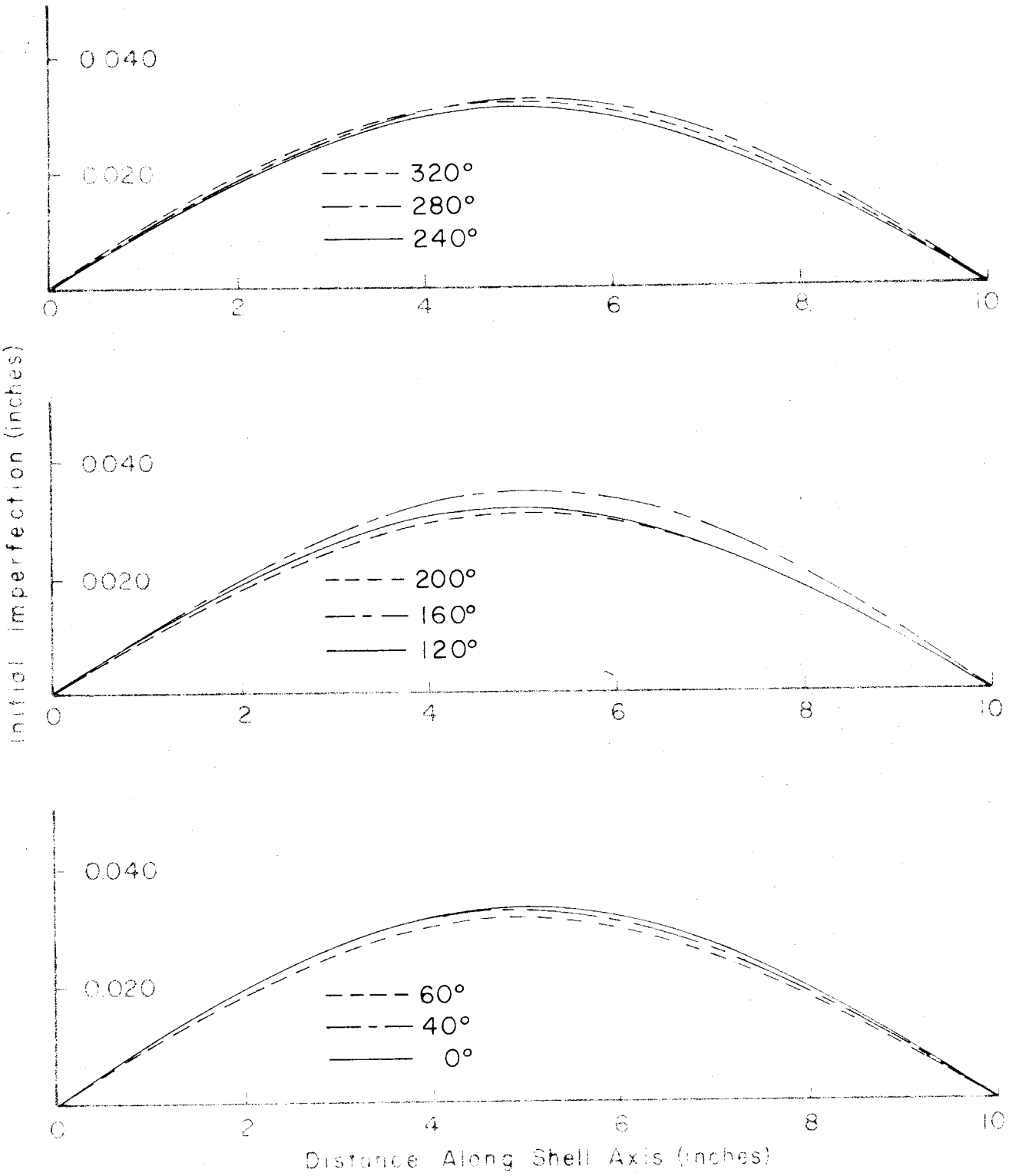

FIG. 26 SHELL 0 INITIAL IMPERFECTION

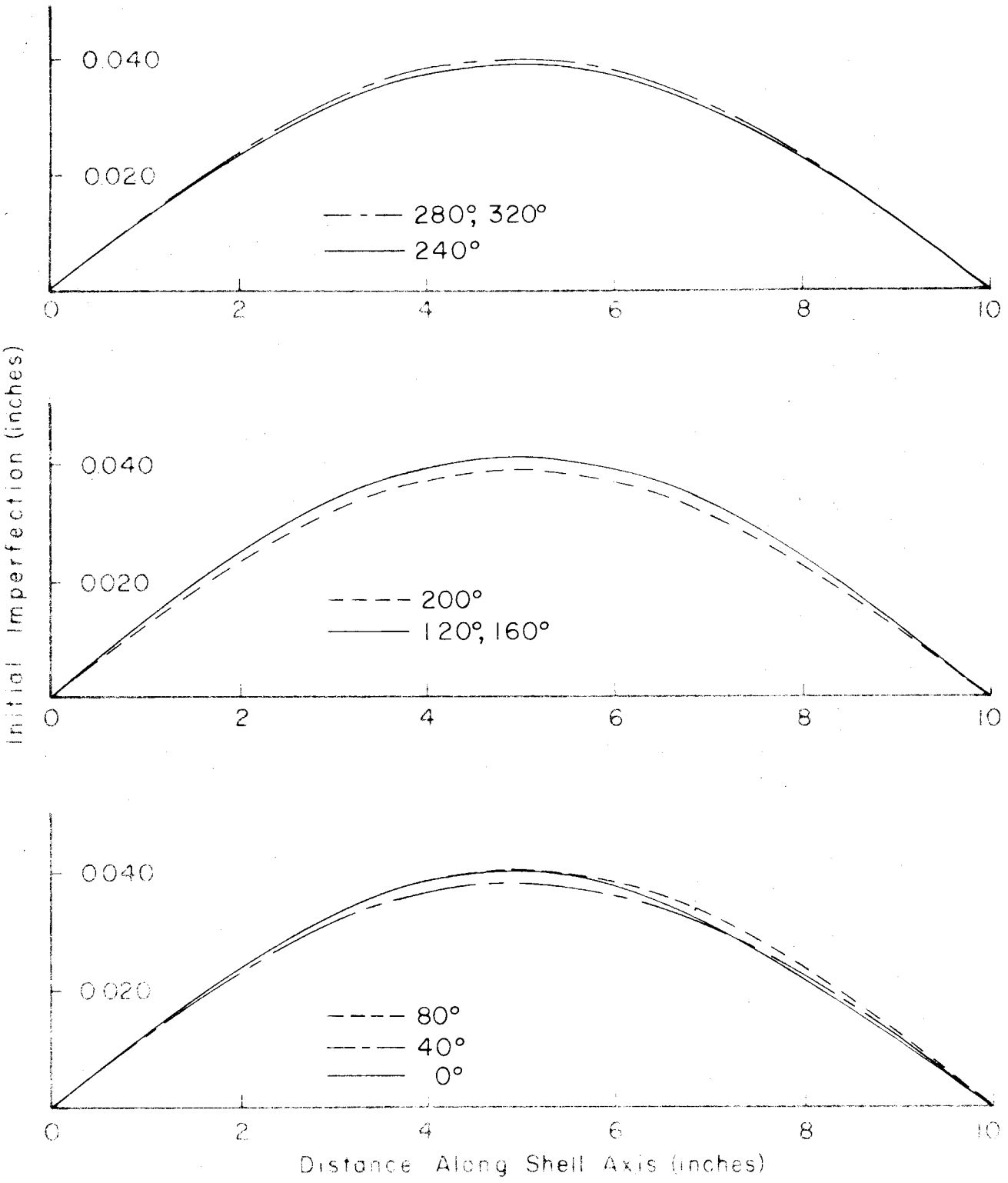

FIG. 27 SHELL J INITIAL IMPERFECTION

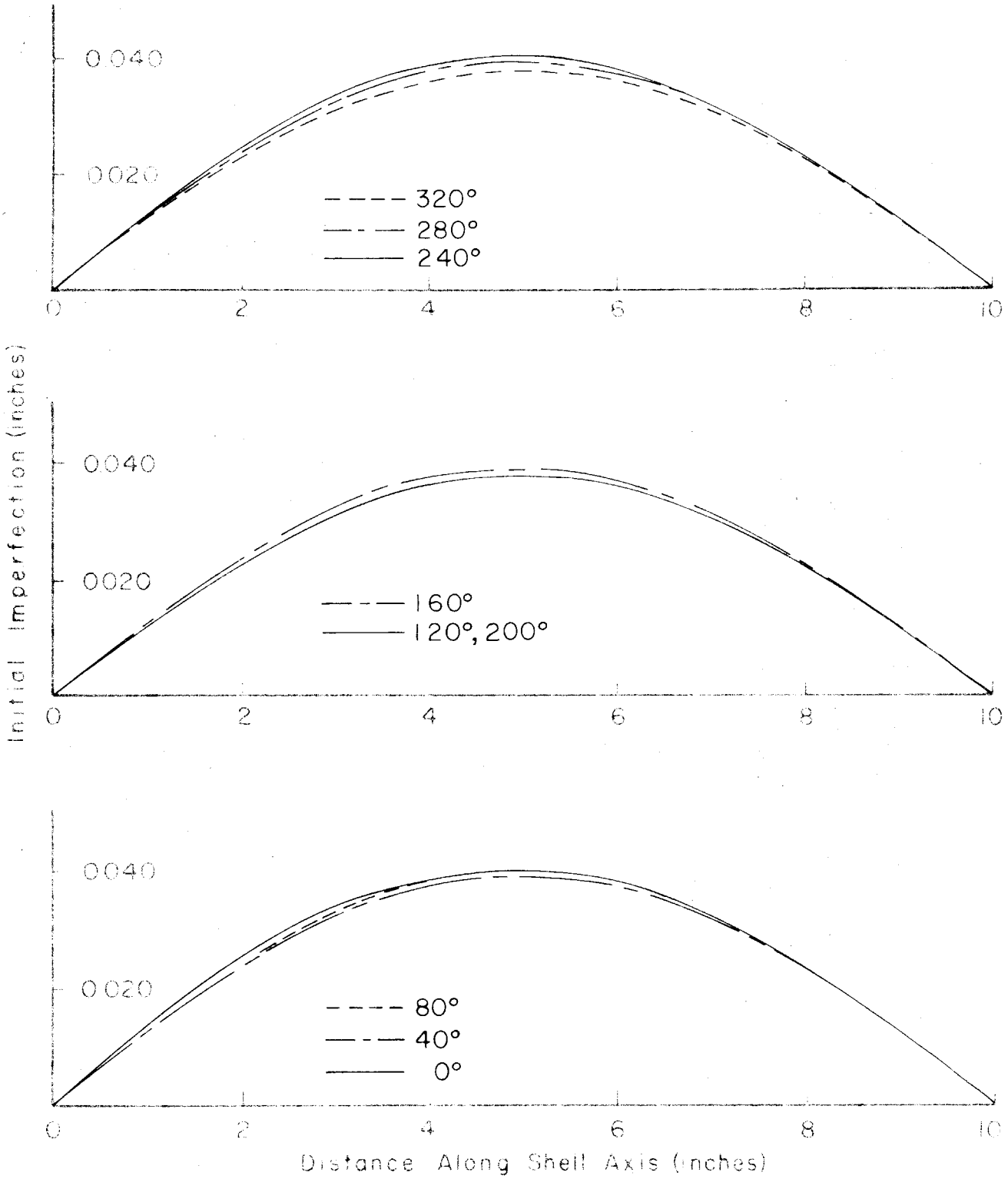

FIG. 28 SHELL K INITIAL IMPERFECTION

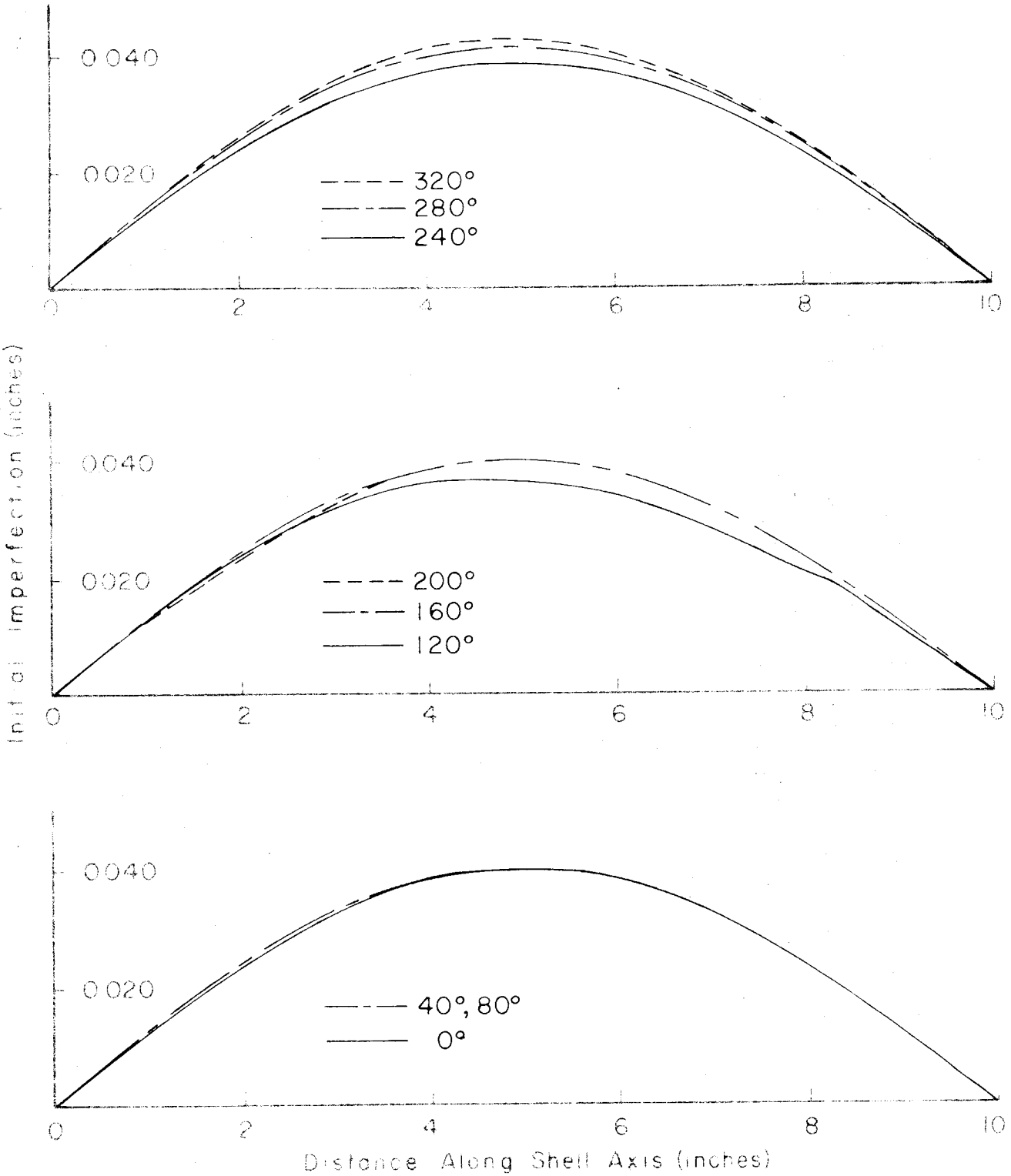

FIG. 29 SHELL L INITIAL IMPERFECTION

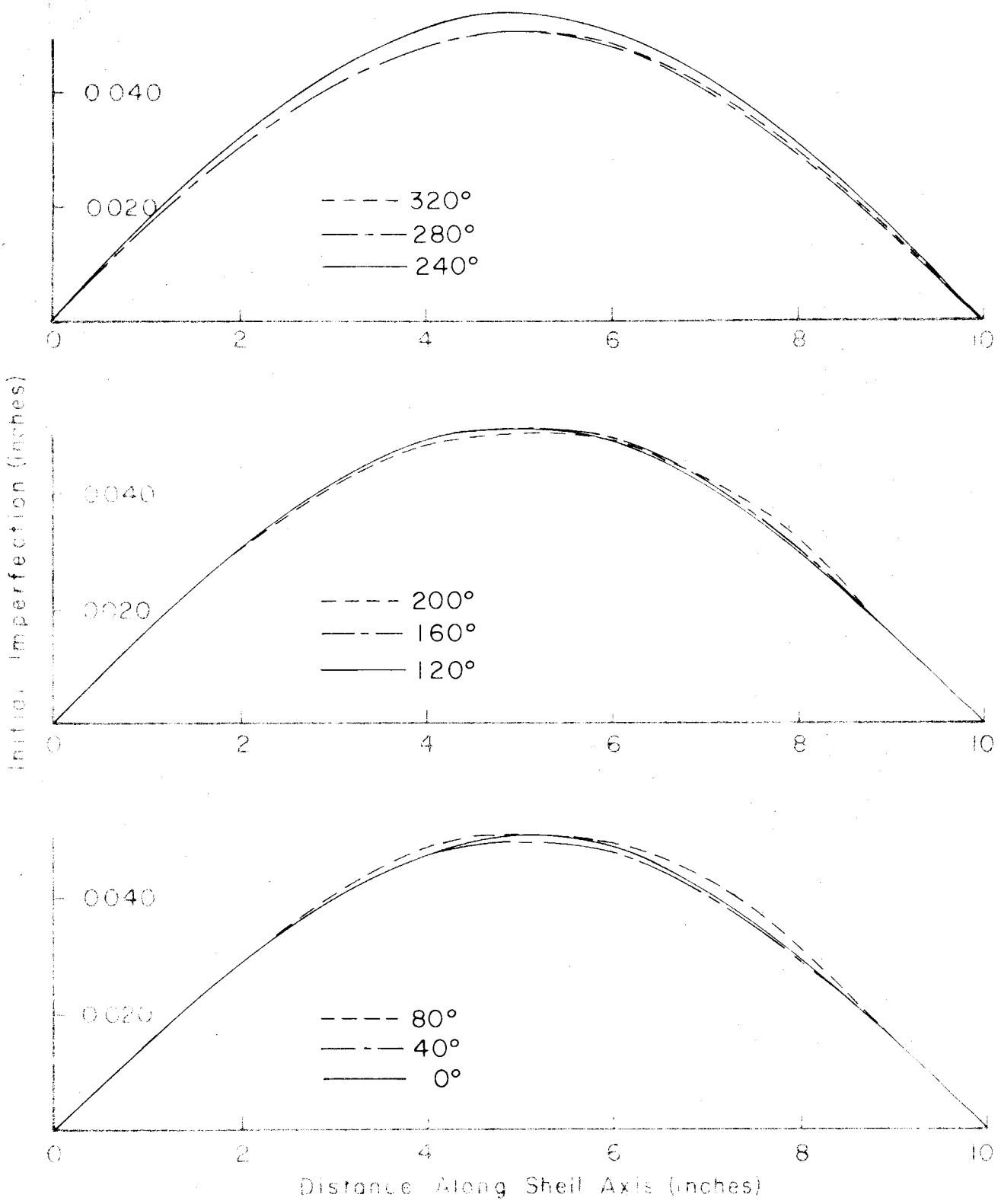

FIG. 30 SHELL G INITIAL IMPERFECTION

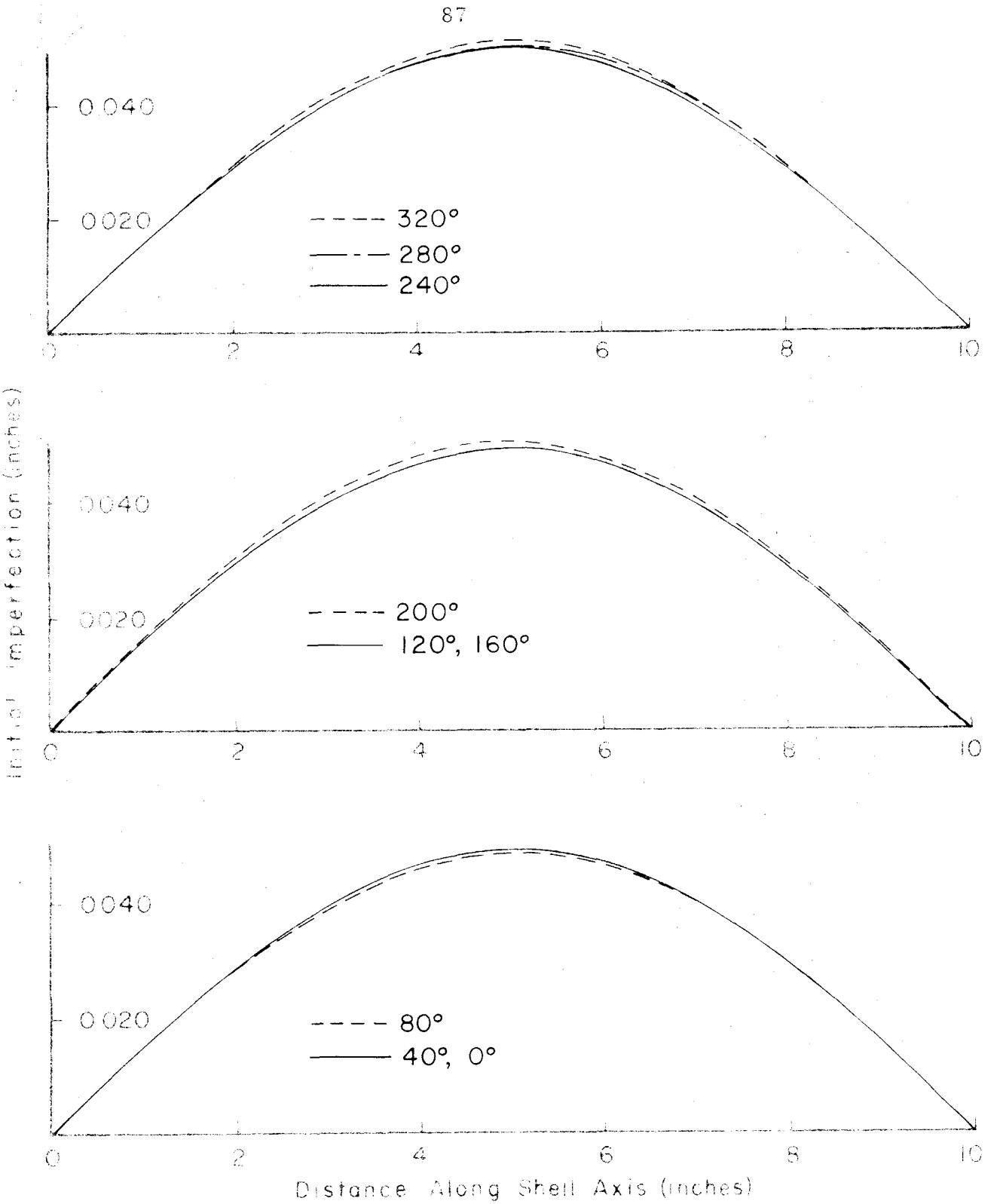

FIG. 31 SHELL H INITIAL IMPERFECTION

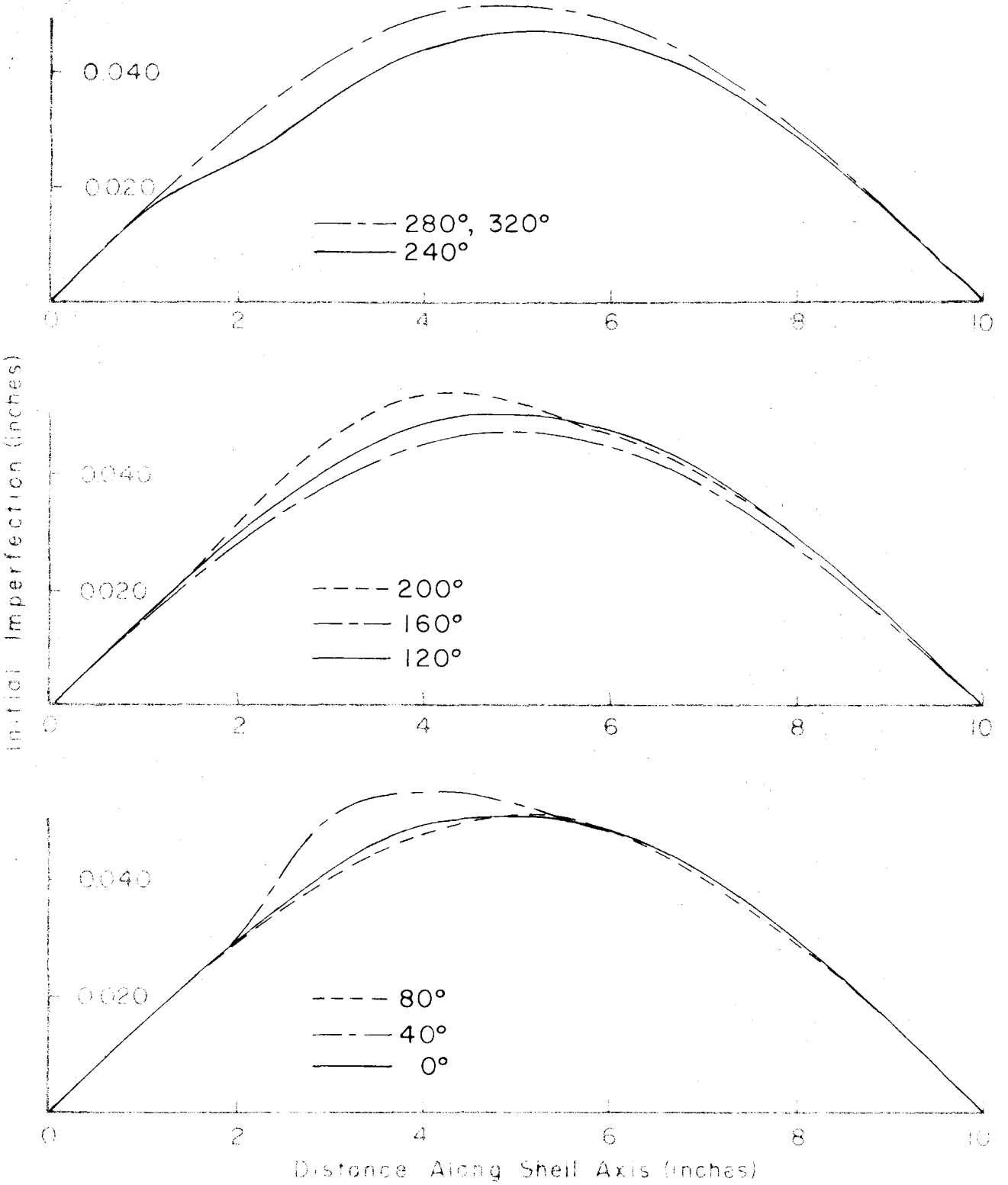

FIG. 32 SHELL I INITIAL IMPERFECTION

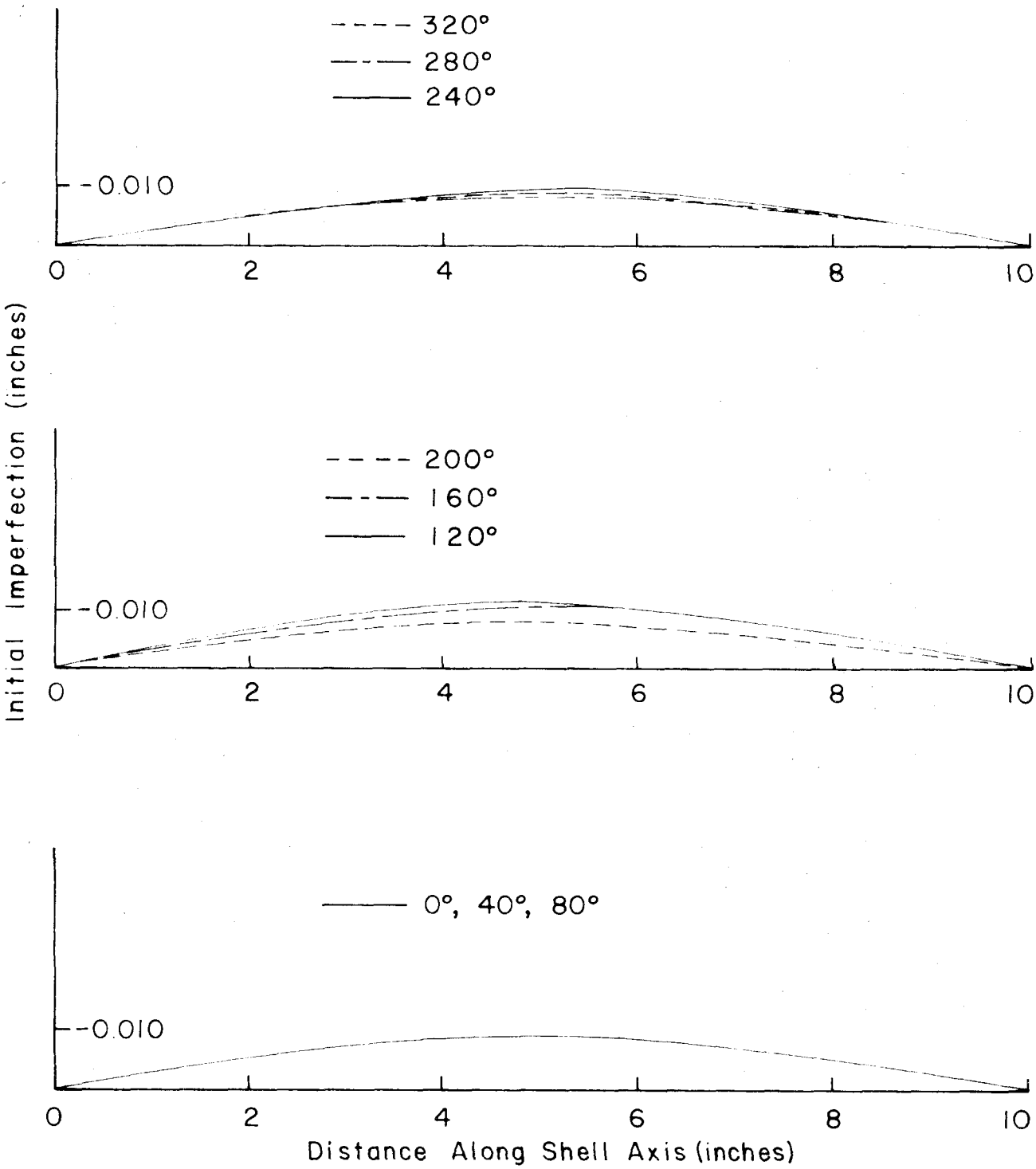

FIG. 33 SHELL AB INITIAL IMPERFECTION

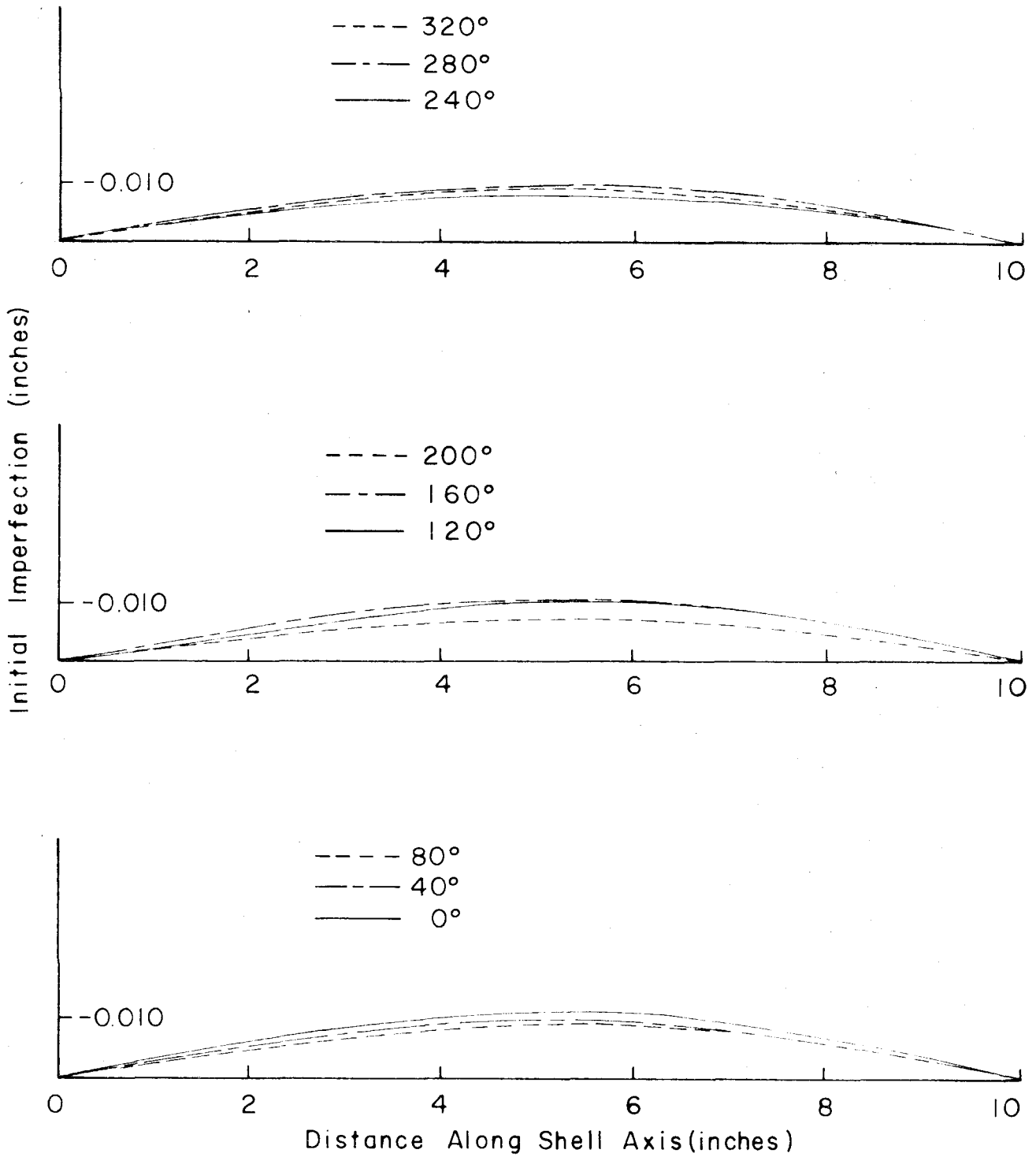

FIG. 34 SHELL AD INITIAL IMPERFECTION

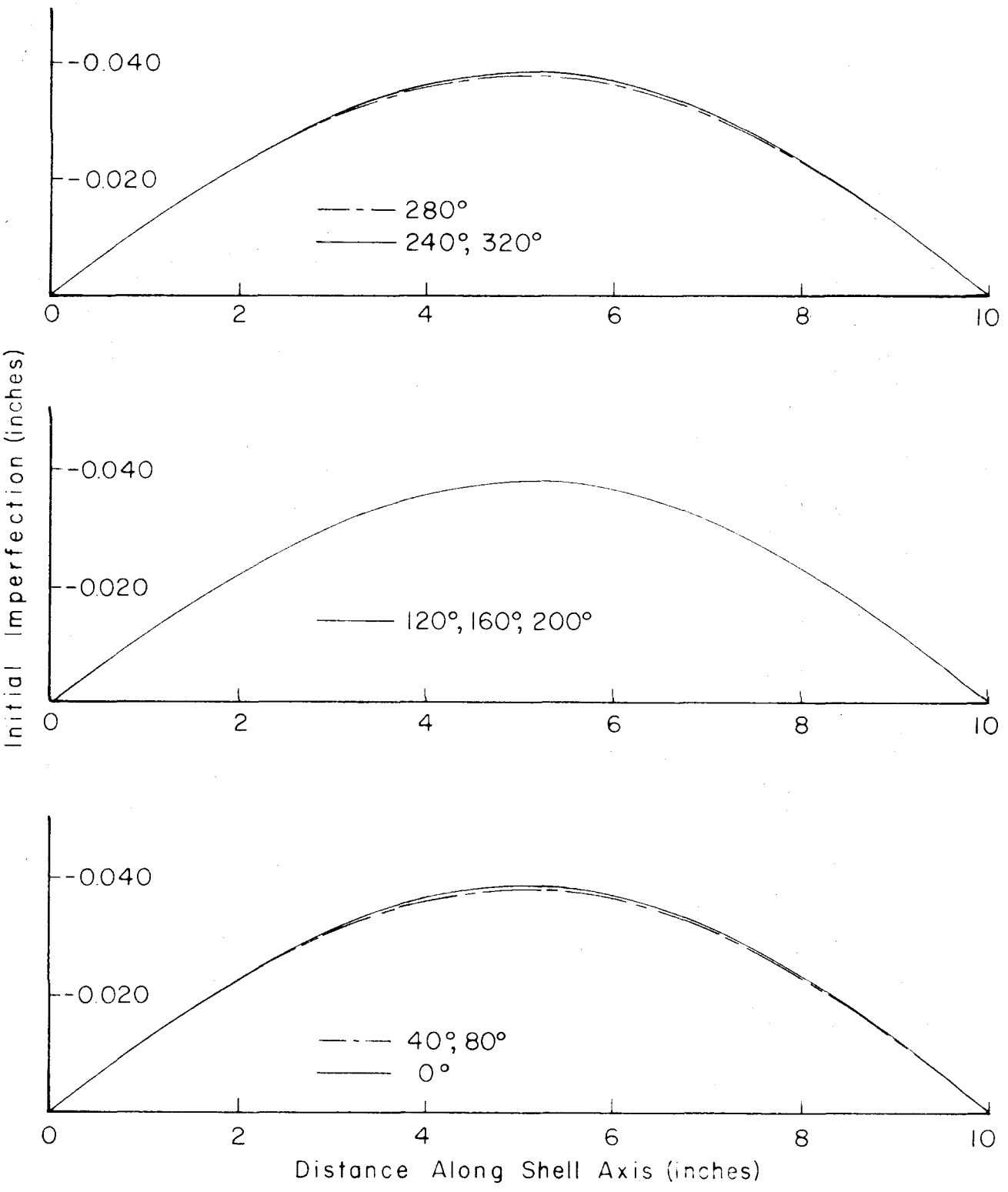

FIG. 35 SHELL S INITIAL IMPERFECTION

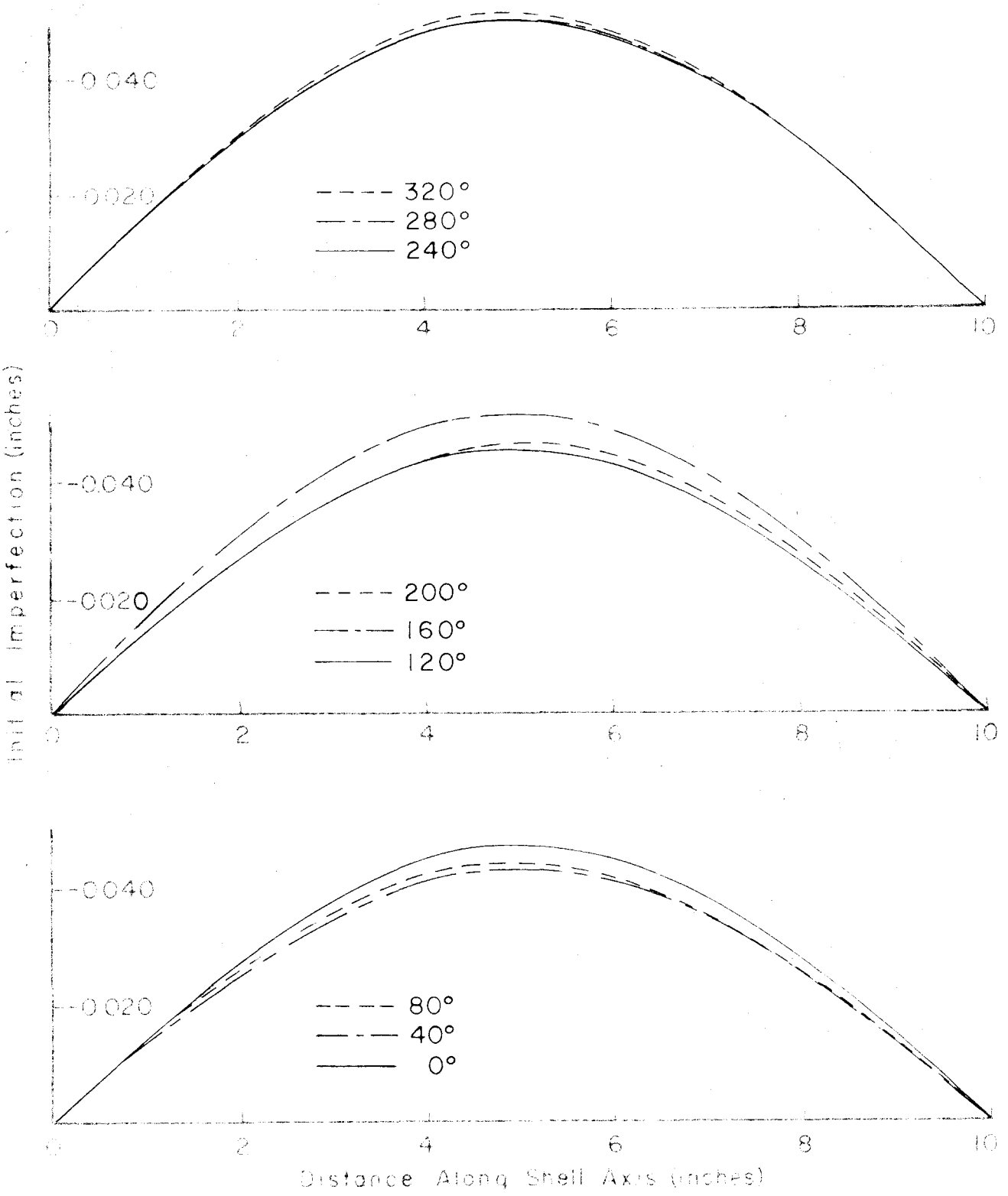

FIG. 36 SHELL P INITIAL IMPERFECTION

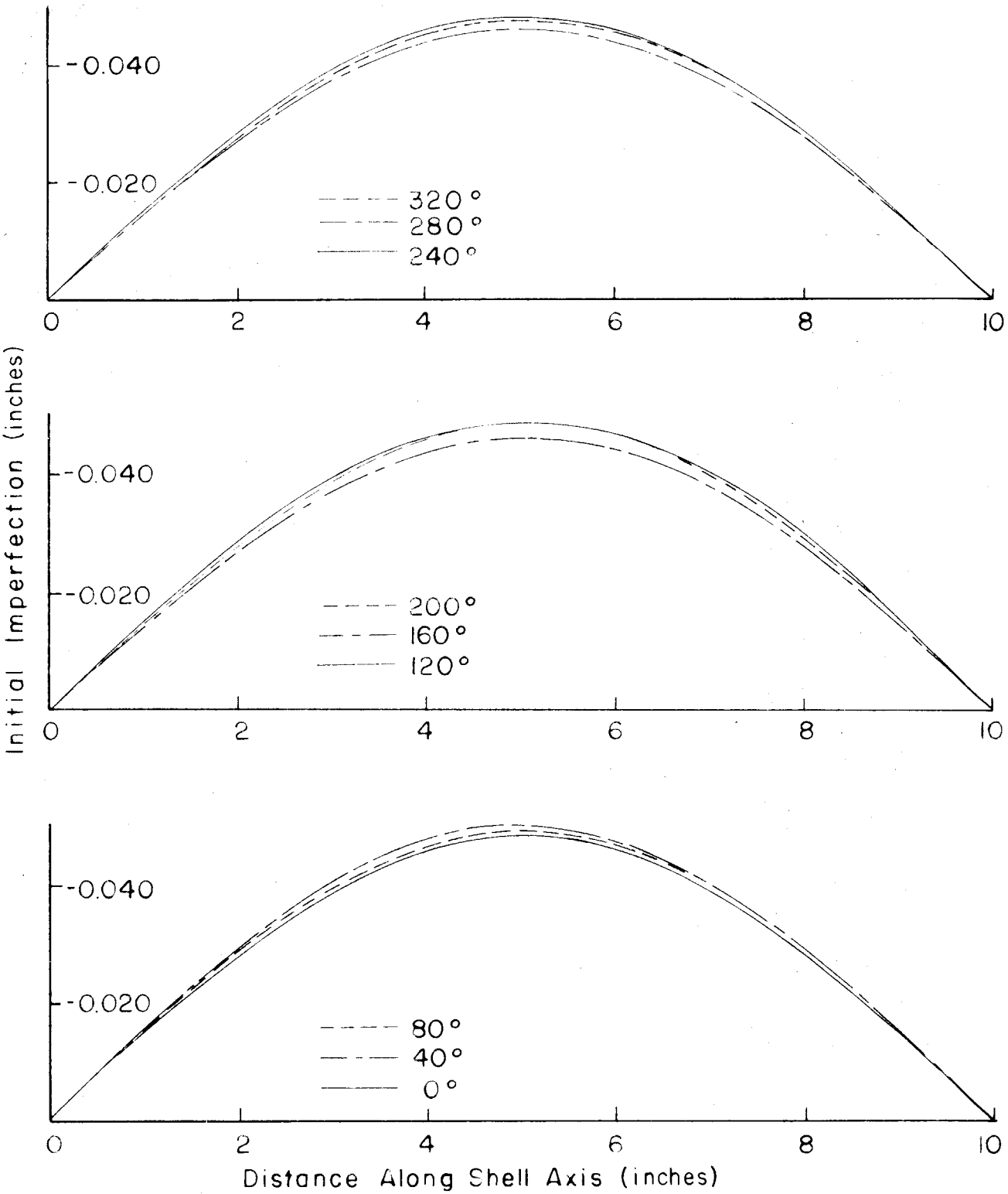

FIG. 37 SHELL R INITIAL IMPERFECTION

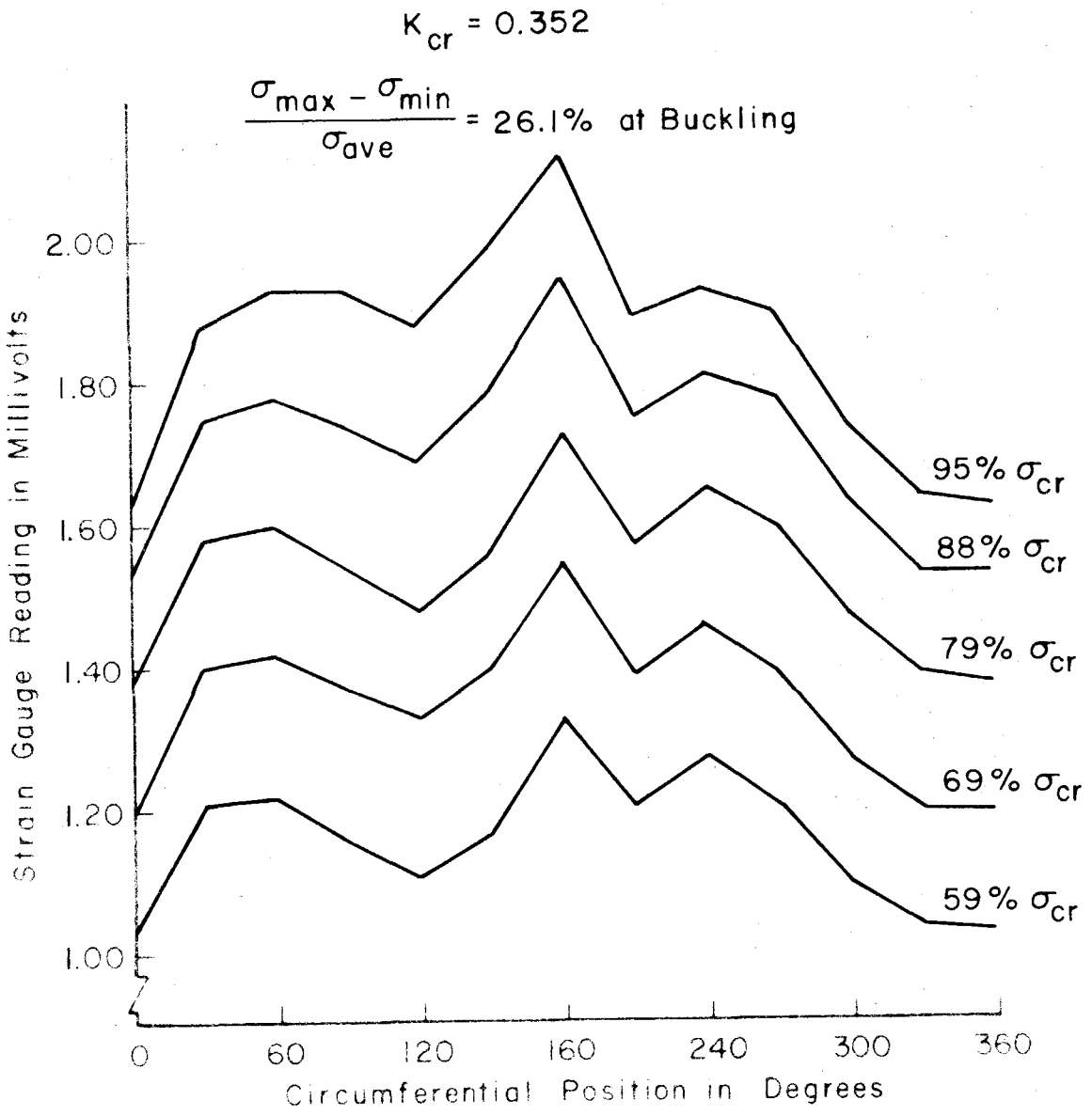

FIG. 38 SHELL W LOAD DISTRIBUTION

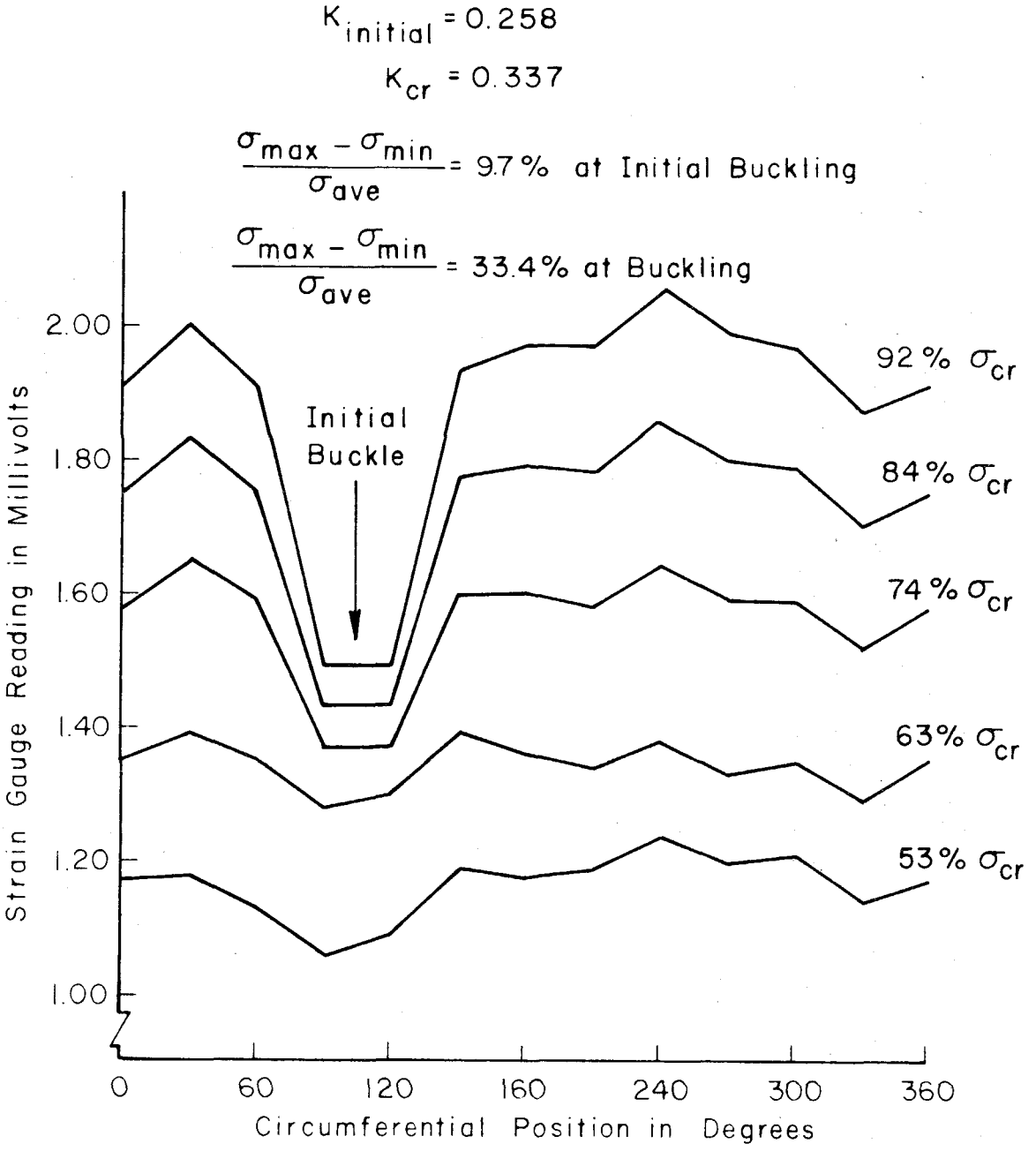

FIG. 39 SHELL X LOAD DISTRIBUTION

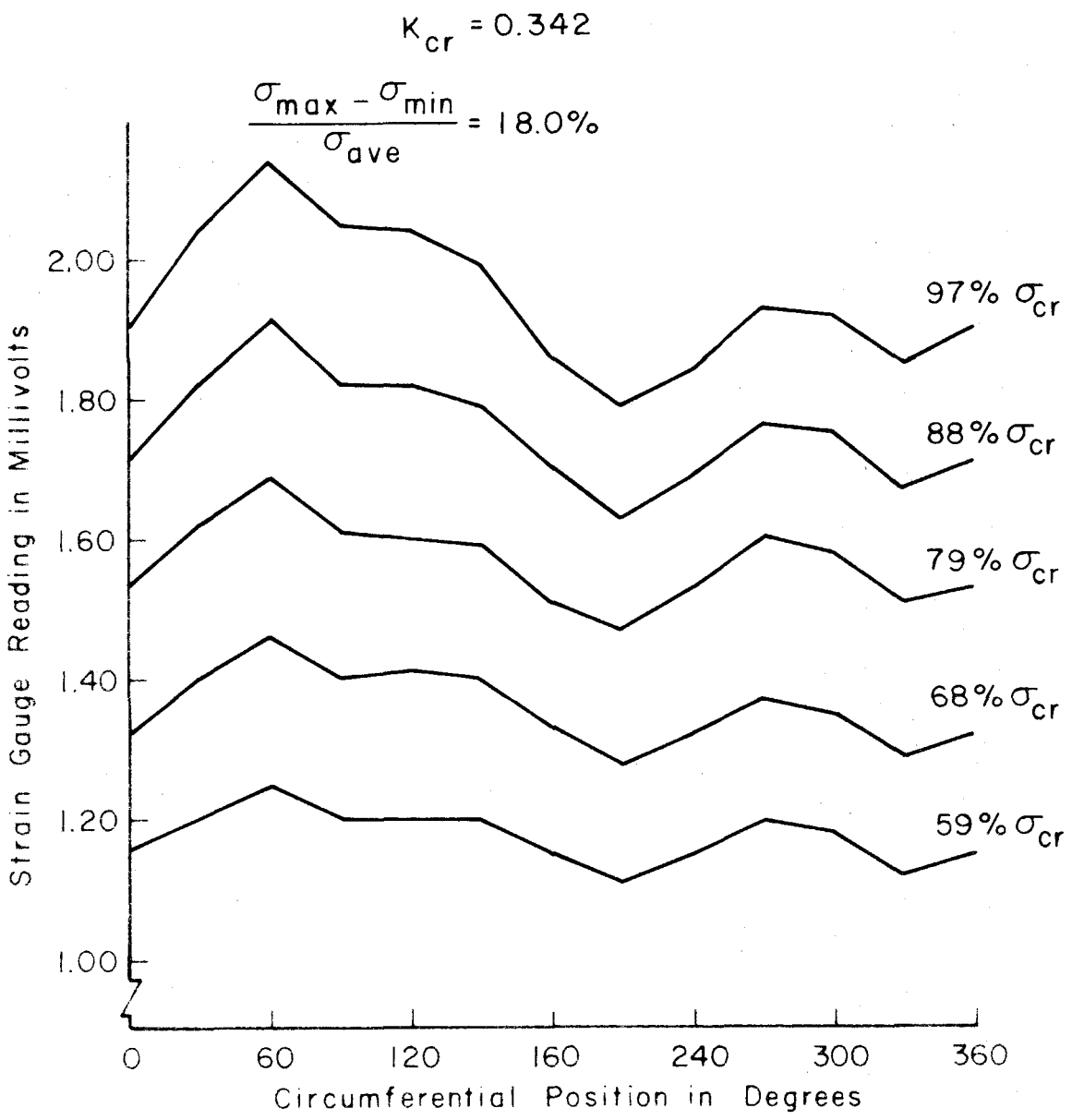

FIG. 40 SHELL N LOAD DISTRIBUTION

$K_{initial} = 0.351$

$K_{cr} = 0.377$

$\frac{\sigma_{max} \quad \sigma_{min}}{\sigma_{ave}} = 10.0\%$ at Initial Buckling

$\frac{\sigma_{max} - \sigma_{min}}{\sigma_{ave}} = 21.0\%$ at Buckling

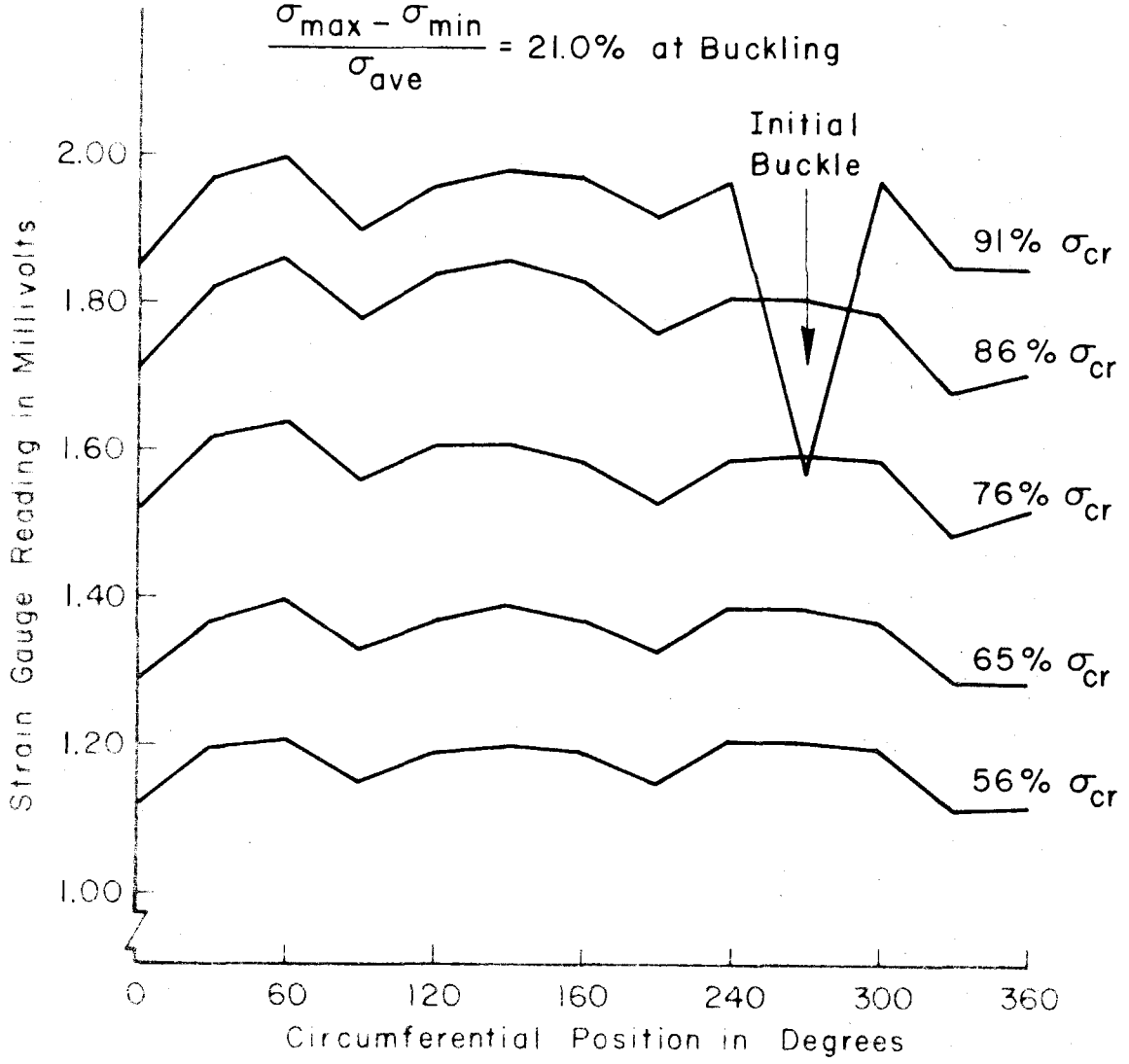

FIG. 41 SHELL O LOAD DISTRIBUTION

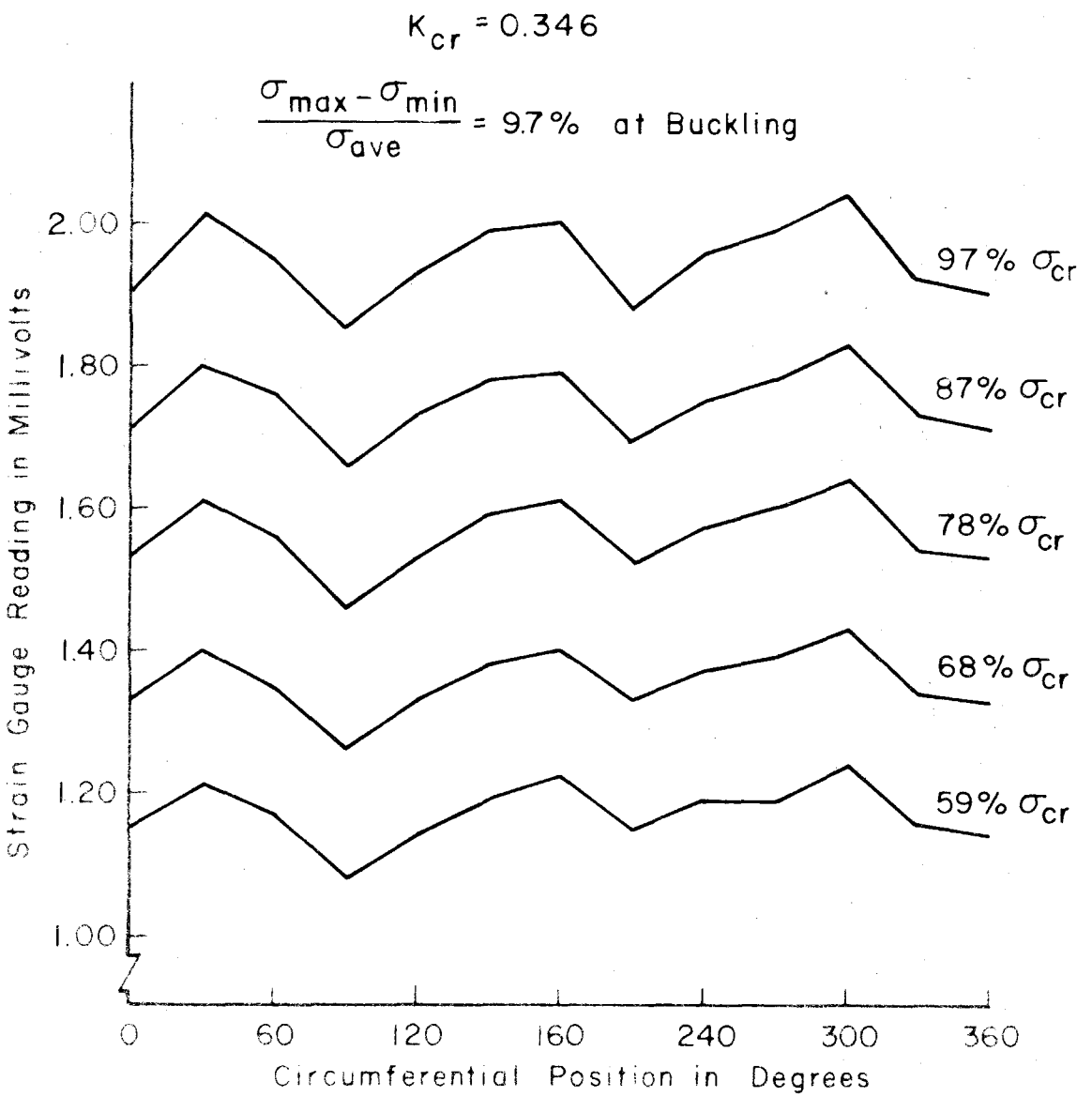

FIG. 42 SHELL K LOAD DISTRIBUTION

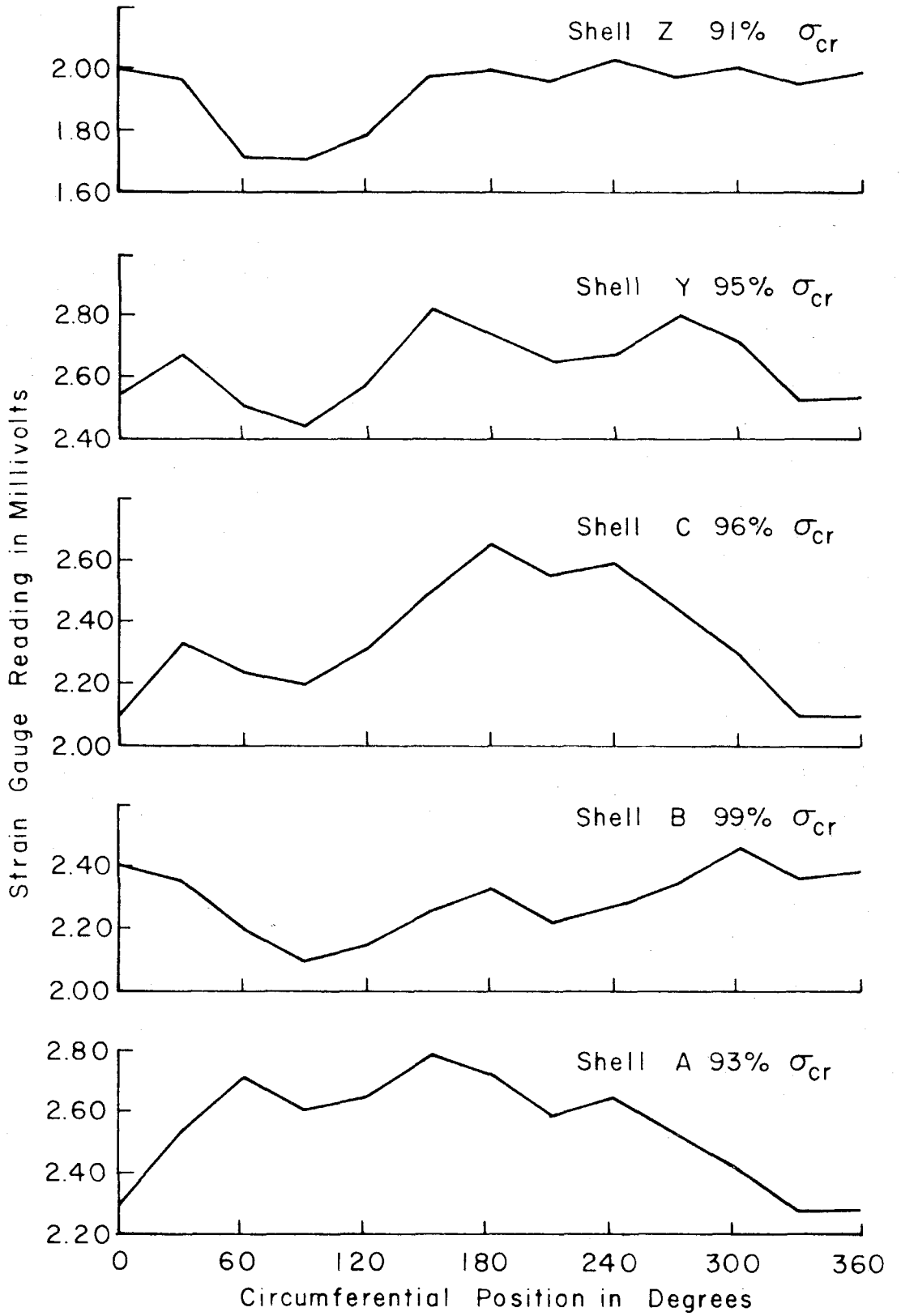

FIG. 43 LOAD DISTRIBUTION NEAR BUCKLING SHELLS A, B, C, Y, Z

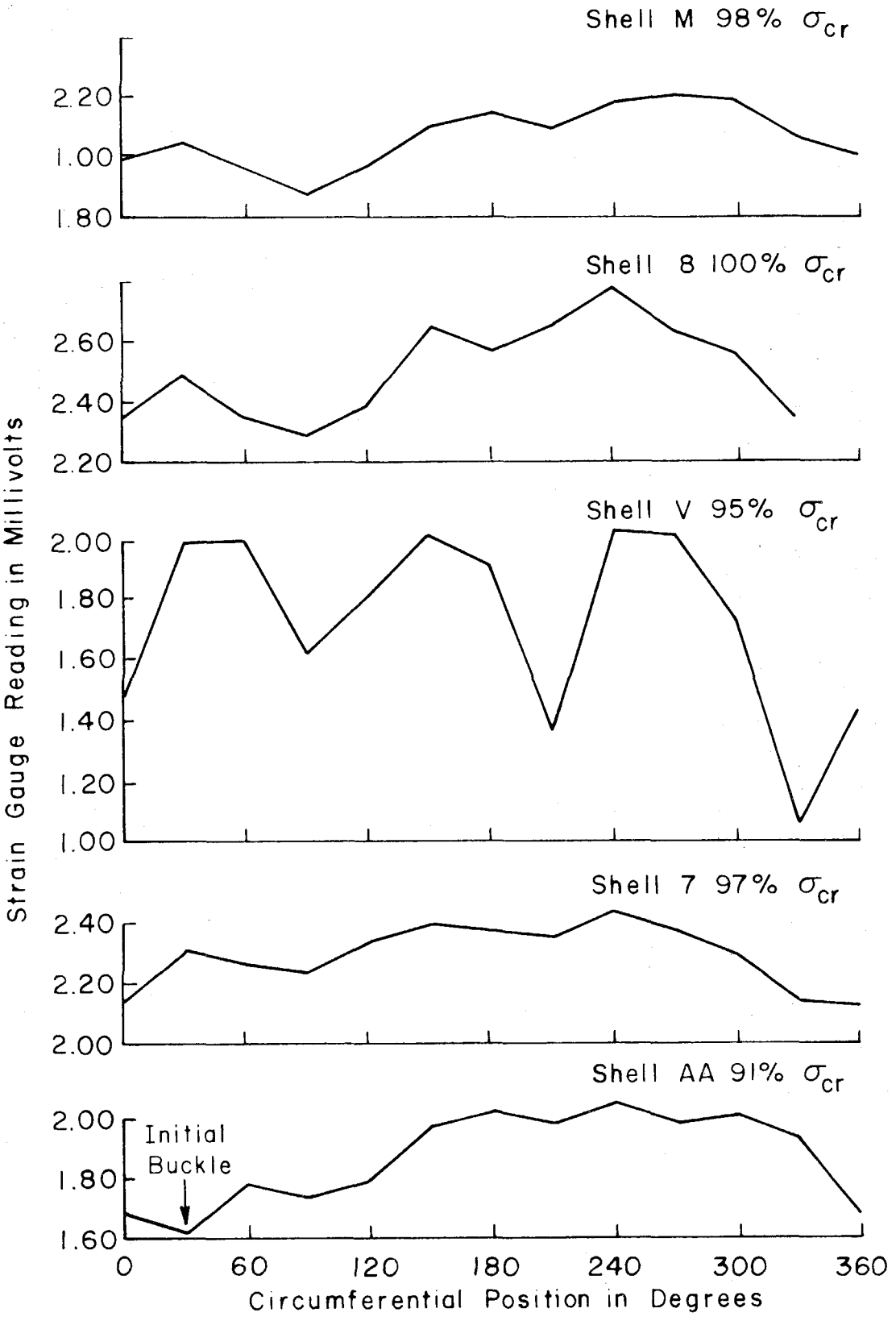

FIG. 44 LOAD DISTRIBUTION NEAR BUCKLING
SHELLS AA, 7, V, 8, M

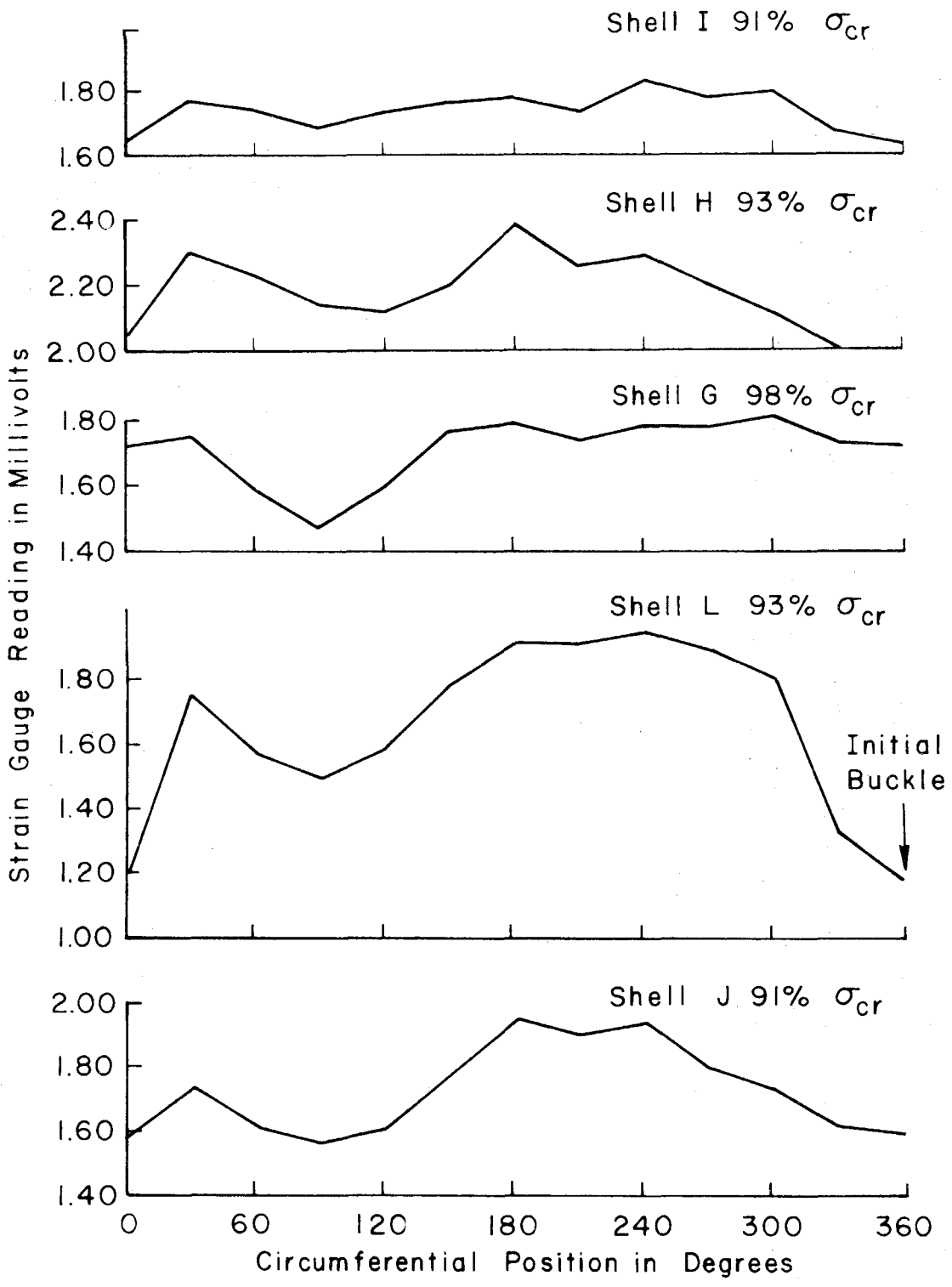

FIG. 45 LOAD DISTRIBUTION NEAR BUCKLING SHELLS J, L, G, H, I

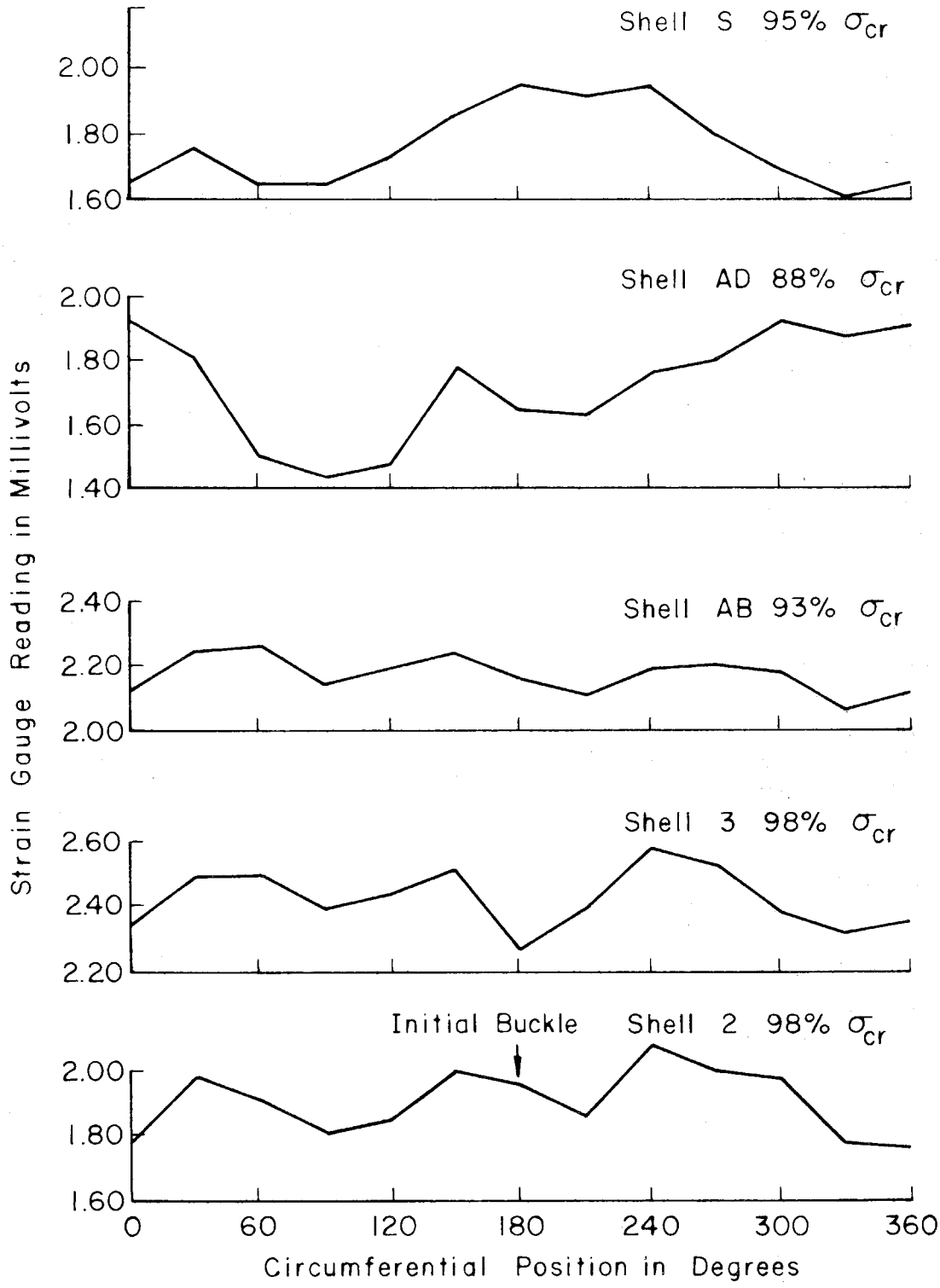

FIG. 46 LOAD DISTRIBUTION NEAR BUCKLING SHELLS 2, 3, AB, AD, S

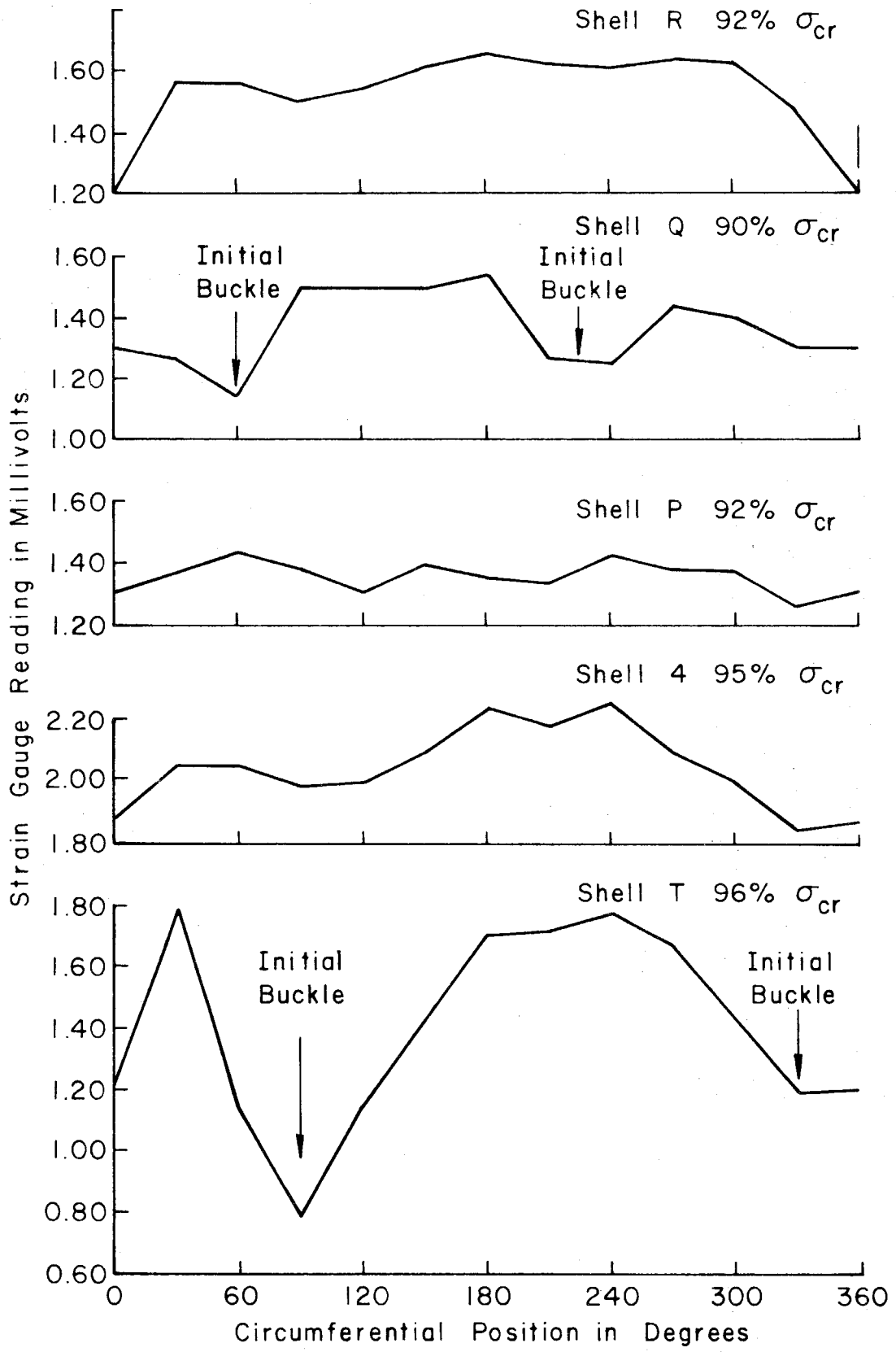

FIG. 47 LOAD DISTRIBUTION NEAR BUCKLING SHELLS T, 4, P, Q, R

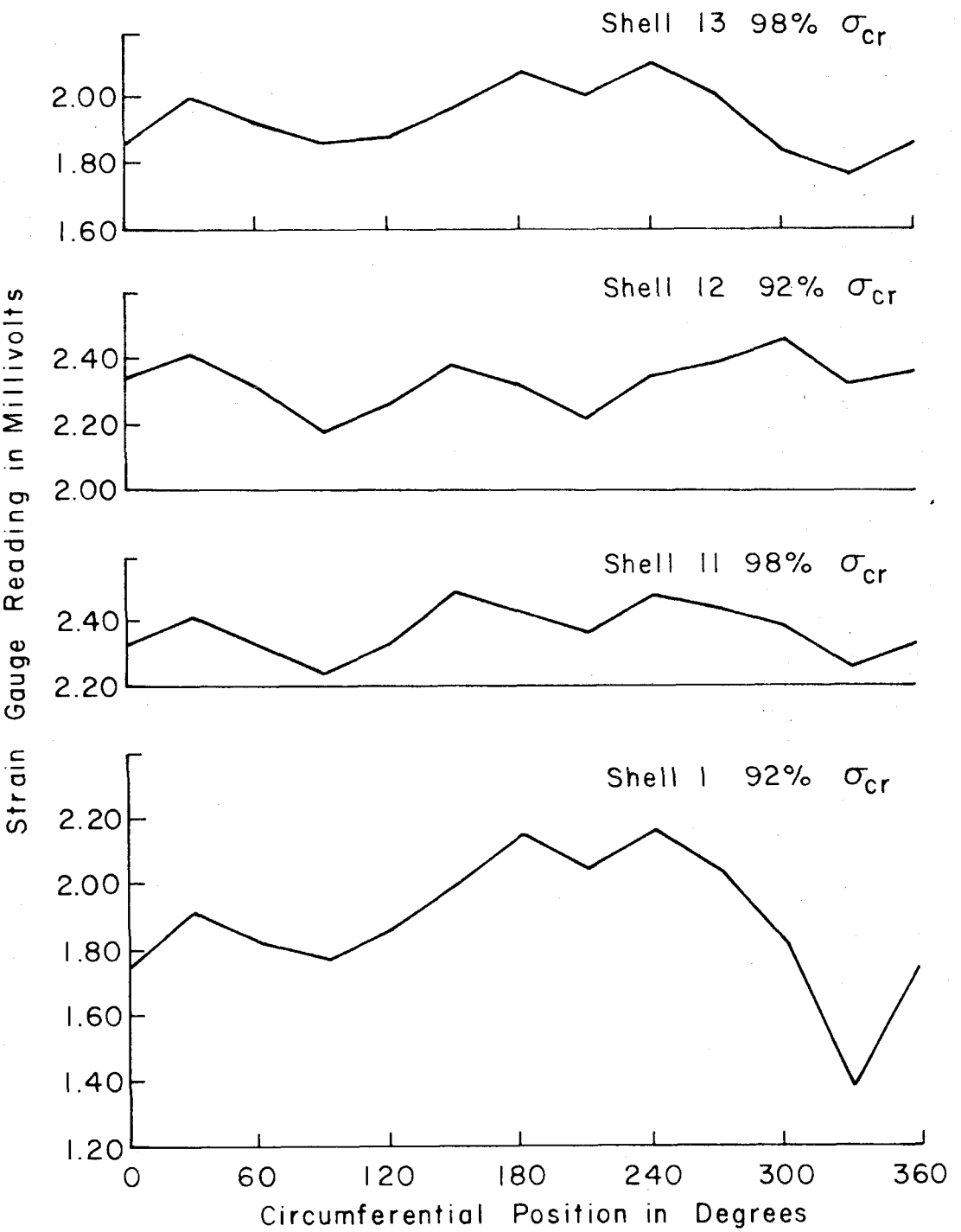

FIG. 48 LOAD DISTRIBUTION NEAR BUCKLING SHELLS 1, 11, 12, 13

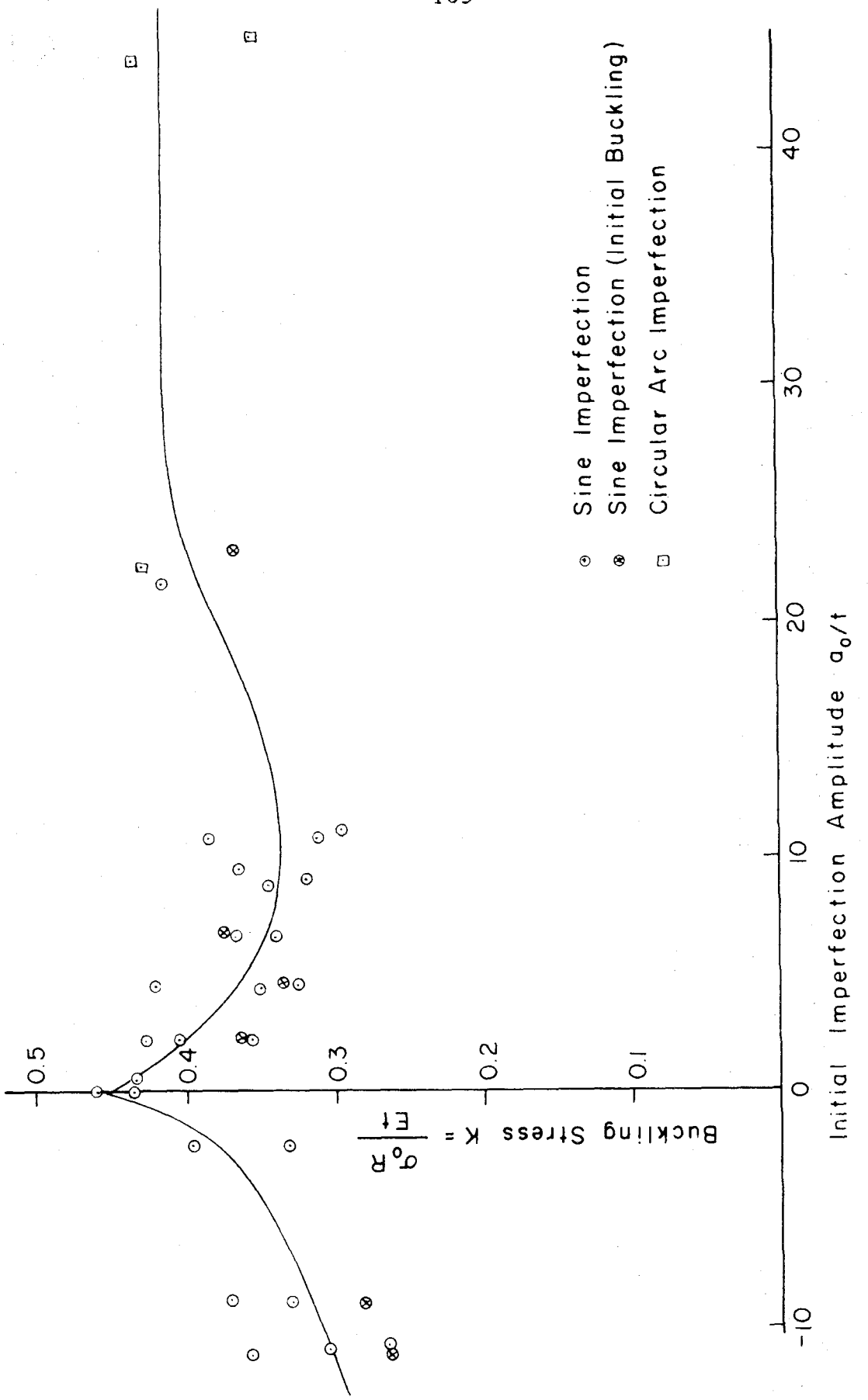

FIG. 49-VARIATION OF BUCKLING STRESS WITH INITIAL IMPERFECTION AMPLITUDE

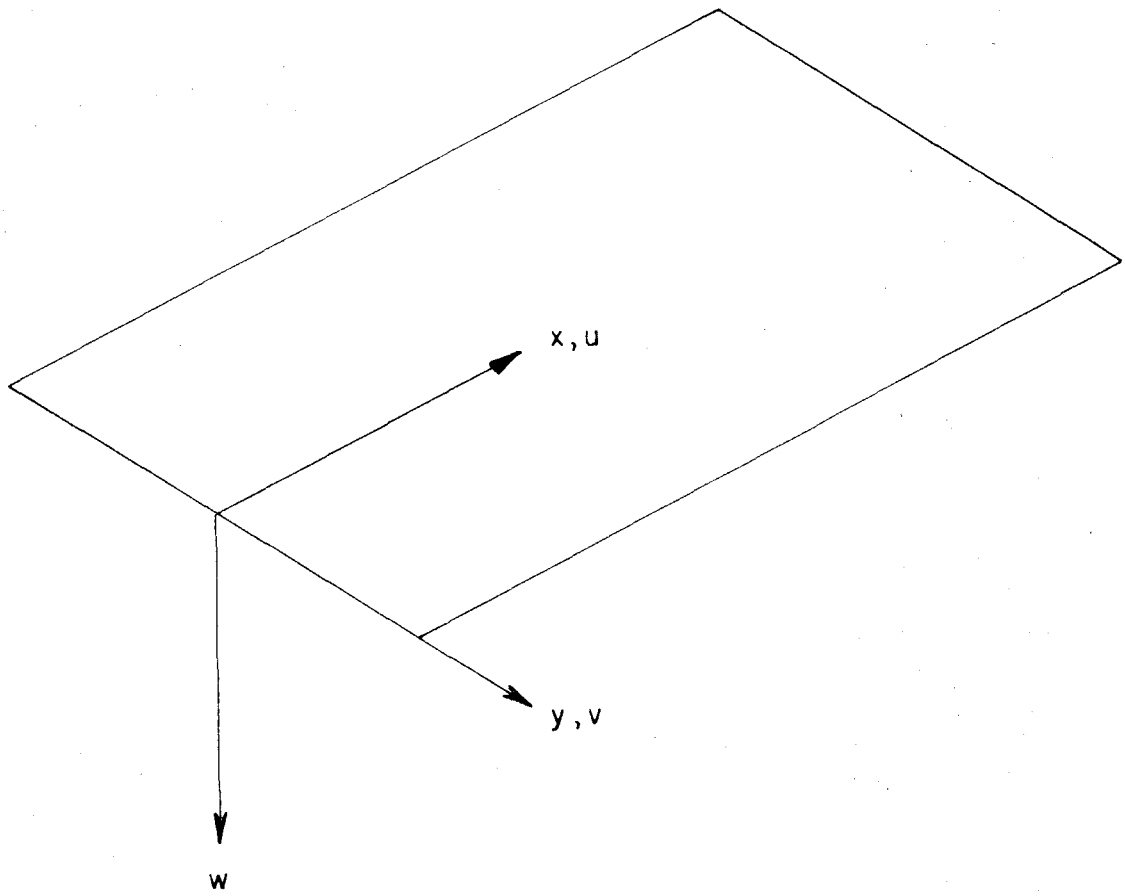

FIG. 50 - COORDINATE SYSTEM FOR SHALLOW SHELL EQUATIONS

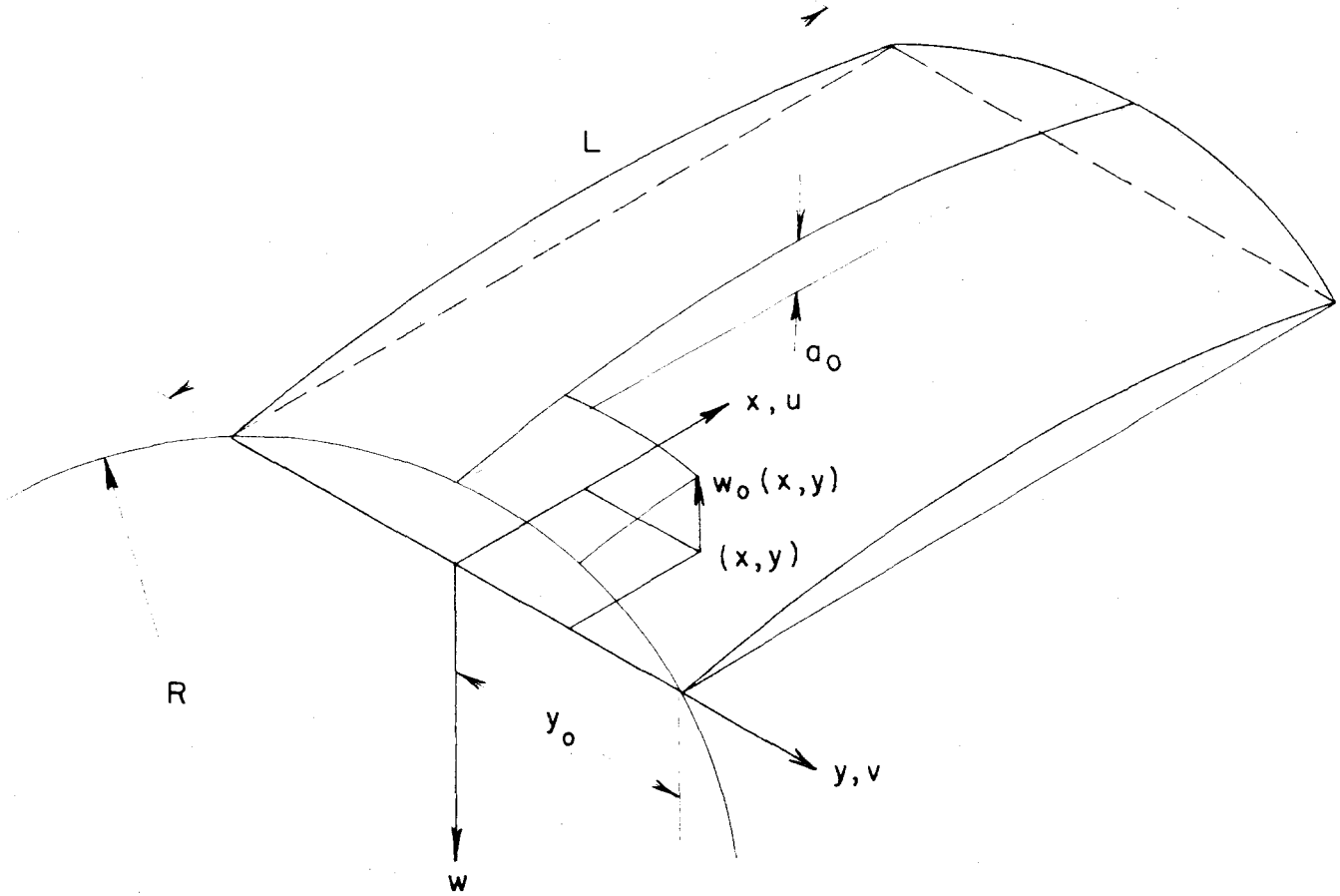

FIG. 51 - W_o FOR A CYLINDER WITH A HALF SINE WAVE INITIAL IMPERFECTION IN THE LENGTH DIRECTION

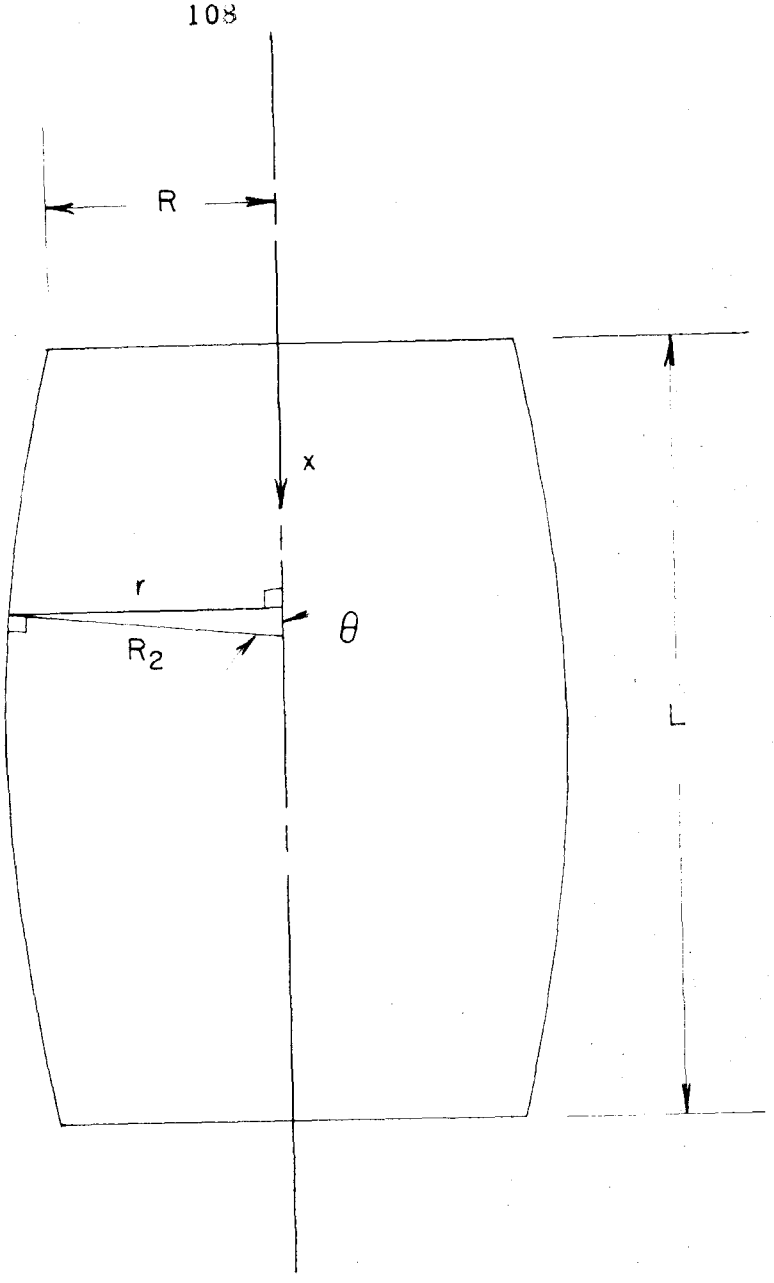

FIG. 52 - COORDINATE SYSTEM FOR MEMBRANE SOLUTION

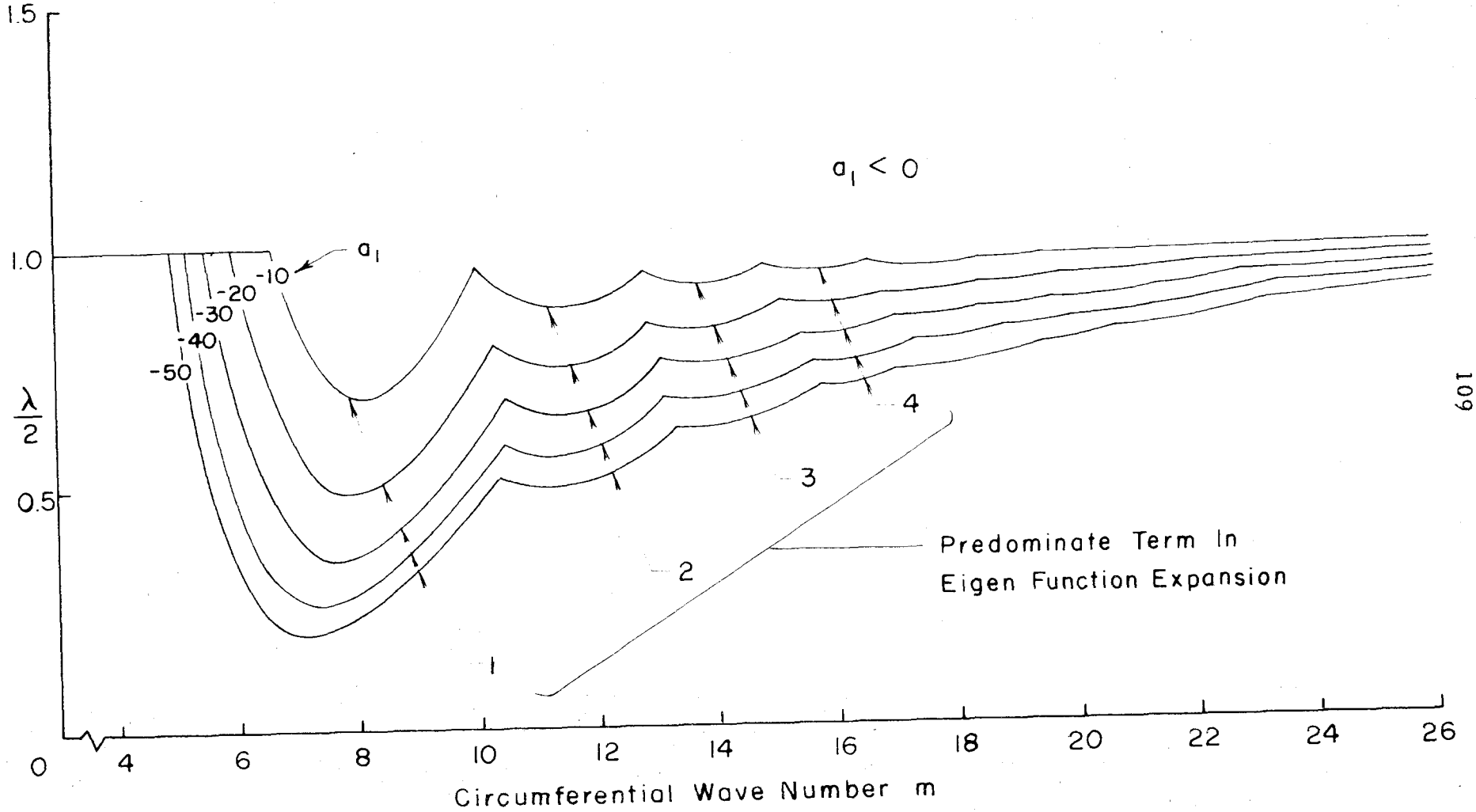

FIG. 53-MINIMUM EIGEN VALUE VARIATION WITH THE CIRCUMFERENTIAL WAVE NUMBER

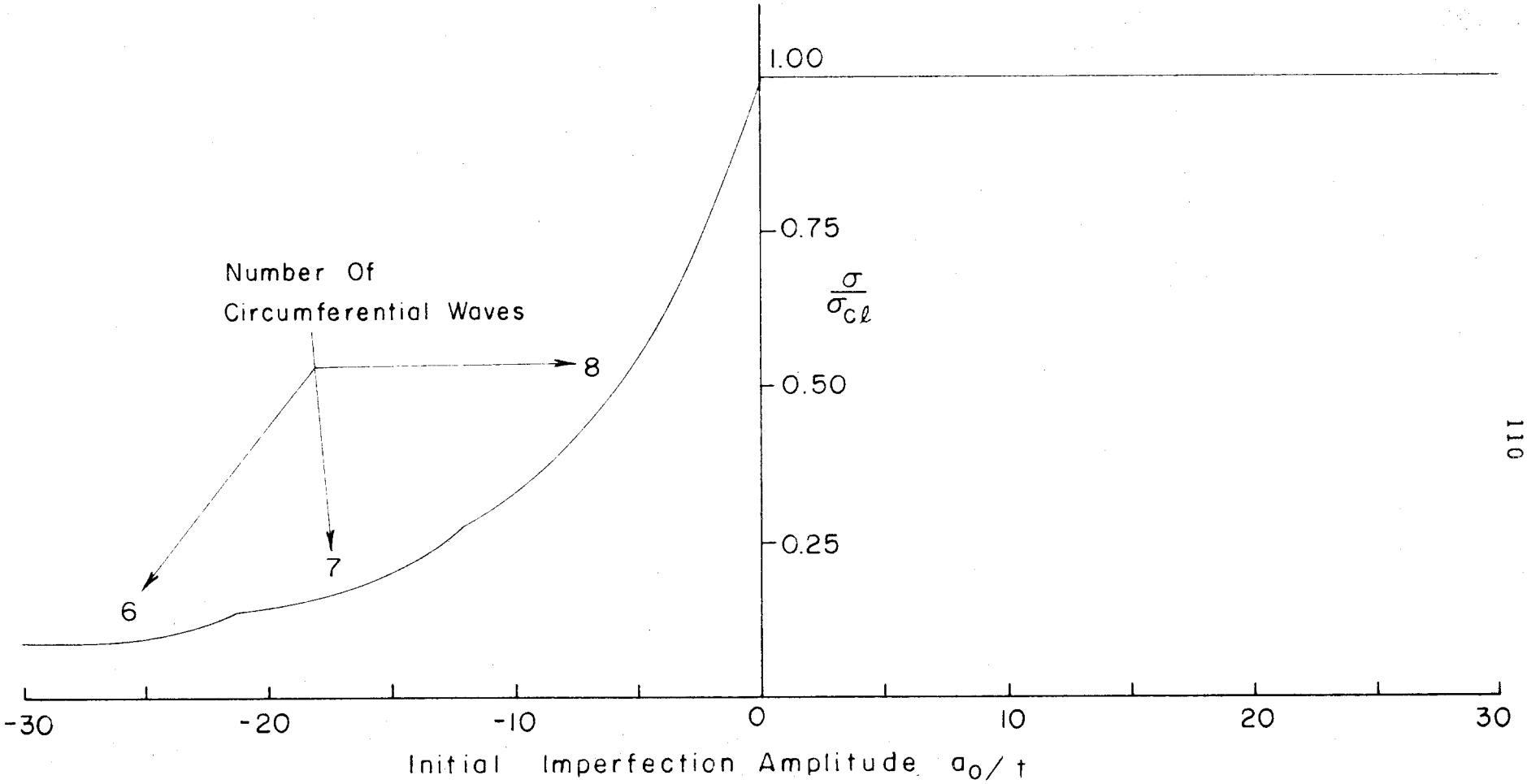

FIG. 54-BUCKLING STRESS VARIATION WITH INITIAL IMPERFECTION AMPLITUDE

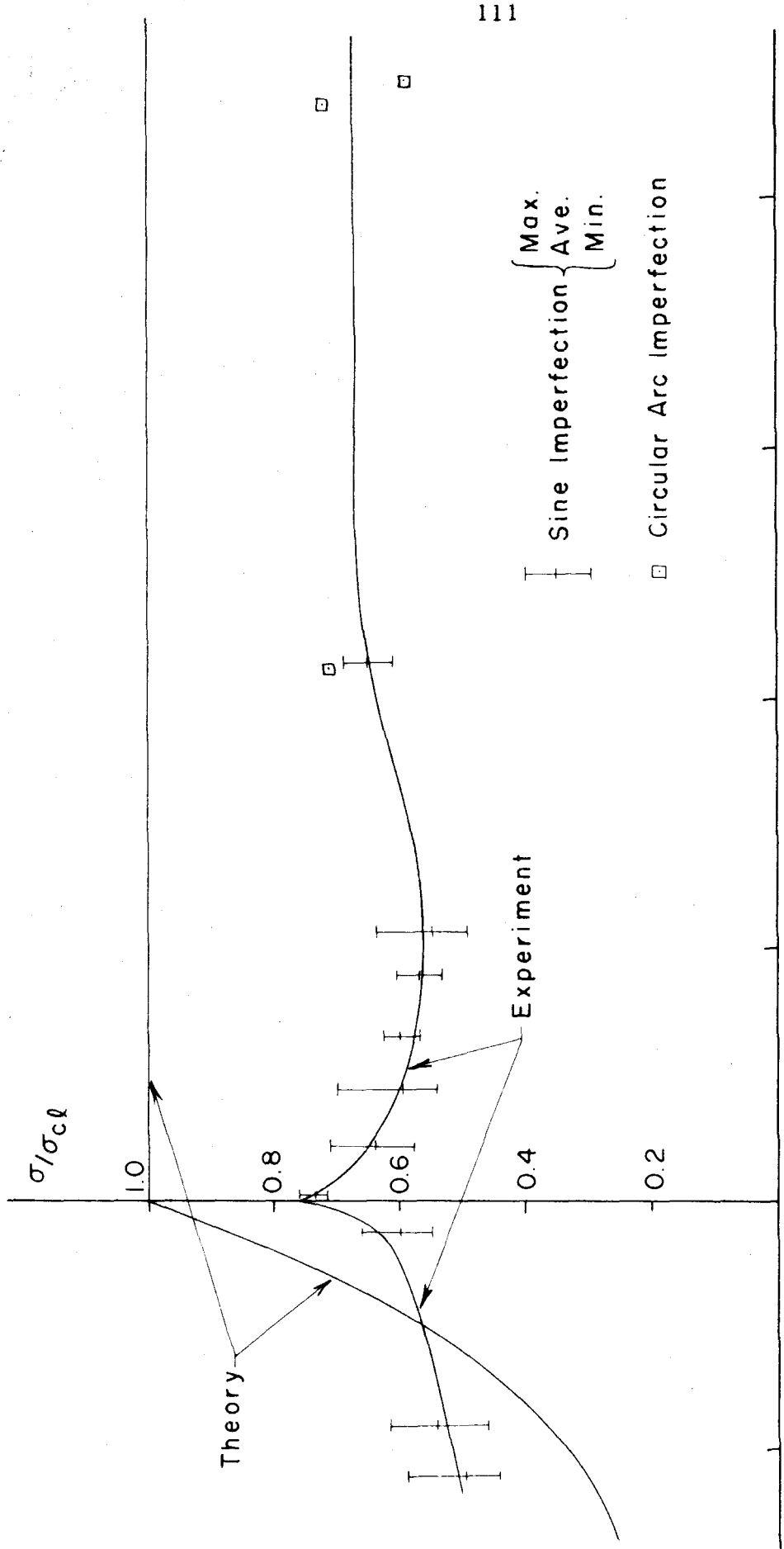

FIG. 55-COMPARISON OF THEORY AND EXPERIMENT

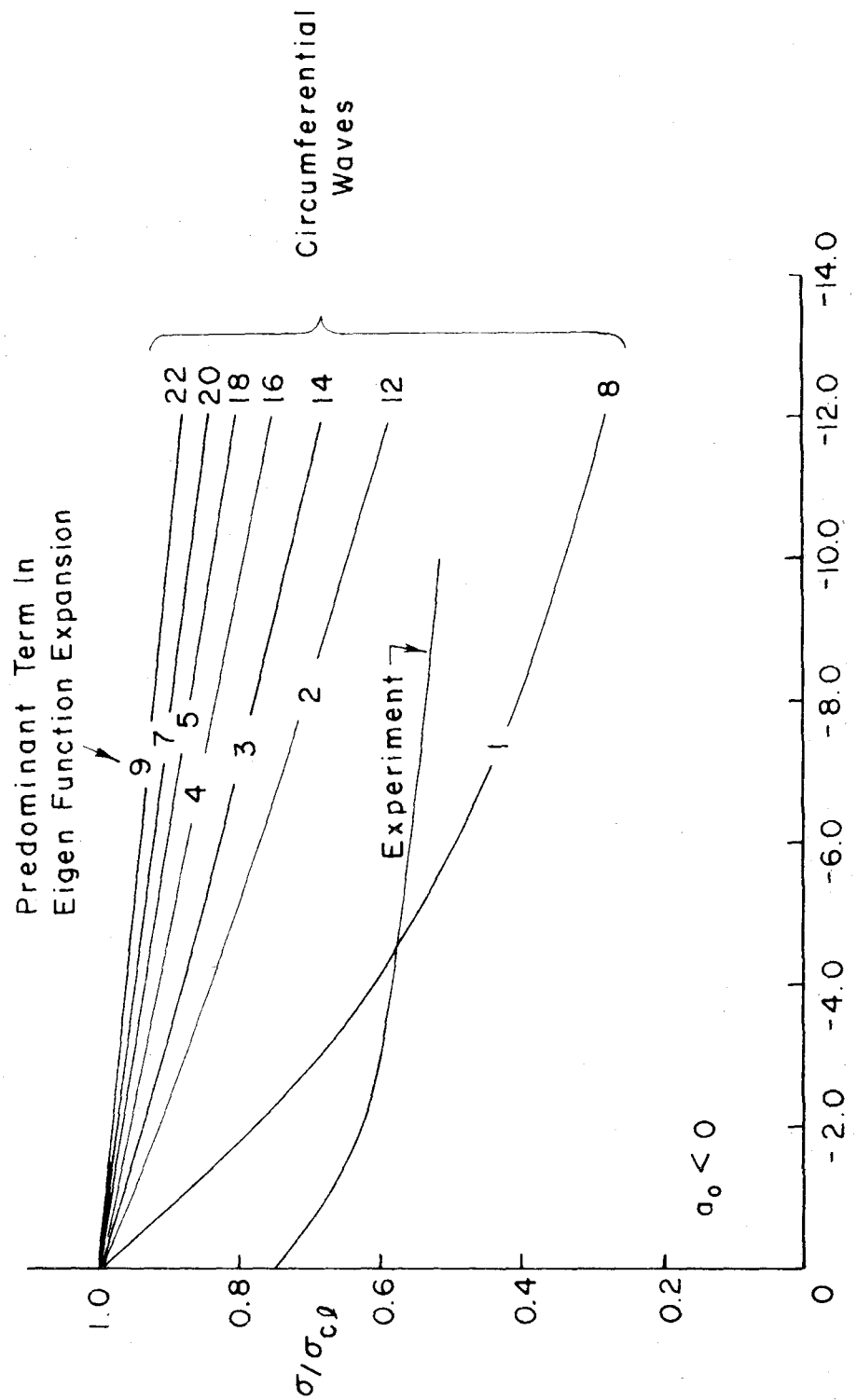

FIG. 56-VARIATION OF BUCKLING STRESS WITH INITIAL IMPERFECTION AMPLITUDE AND CIRCUMFERENTIAL WAVE NUMBER